UNIVERSIDAD NACIONAL AUTONOMA DE MÉXICO
INSTITUTO DE GEOFÍSICA
POSGRADO EN CIENCIAS DE LA TIERRA

ALGUNOS EVENTOS RECIENTES ASOCIADOS A LA BRECHA SÍSMICA DE GUERRERO: IMPLICACIONES PARA LA SISMOTECTÓNICA Y EL PELIGRO SÍSMICO DE LA REGIÓN

T E S I S

QUE PARA OBTENER EL GRADO DE:

DOCTOR EN CIENCIAS

(SISMOLOGÍA)

P R E S E N T A

ARTURO IGLESIAS MENDOZA

D I R E C T O R

DR. SHRI KRISHNA SINGH

Octubre de 2004

Para mi esposa:

Si te quiero es porque sos
mi amor mi cómplice y todo
y en la calle codo a codo
somos mucho más que dos
(M. Benedetti)

... y aunque tenga don de profecía y sepa
todos los misterios y toda la ciencia y
tenga toda la fe en forma que traslade
montañas, si no tengo amor, nada soy.
(1ª Corintios, 13)

ÍNDICE

Resumen	4
Abstract	6
Introducción	7
I. Estudio de la fuente y de la propagación del sismo del 21 de Julio de 2000, Copalillo, México(Mw=5.9): Implicaciones de los sismos intraplaca en el peligro sísmico de la Ciudad de México.	20
II. El sismo de Coyuca del 8 de Octubre del 2001, (Mw=5.8): Una falla normal sobre la brecha sísmica de Guerrero.	33
III. El sismo silencioso de 2002 en la brecha sísmica de Guerrero, México(Mw=7.6): Inversión del deslizamiento en la interfase de las placas y algunas implicaciones.	50
IV. Los sismos de trinchera en México presentan aceleraciones máximas anómalamente bajas.	60
V. El sistema de alerta sísmica para la ciudad de México: La evaluación de su desempeño y una estrategia para mejorarlo.	68
Conclusiones	91
Agradecimientos	96

RESUMEN

Trabajos previos han permitido establecer, de manera general, la situación de la sismotectónica de la brecha sísmica de Guerrero y su impacto en la estimación del peligro sísmico asociado a la región. Sin embargo, algunos eventos recientes demuestran que el panorama es más complejo de lo que se había supuesto anteriormente. En la presente tesis se presenta una serie de trabajos acerca de estos eventos, pretendiendo aportar nuevos elementos que ayuden al mejor entendimiento tanto de los procesos tectónicos como de sus implicaciones en la estimación del peligro sísmico.

El primero de ellos versa en torno al sismo de Copalillo del año 2000 (21/07/2000, Mw=5.9) localizado en el límite de los estados de Guerrero y Puebla. El sismo de Copalillo representa el temblor intraplaca más alejado de la trinchera Mesoamericana y más cercano al Valle de México que se haya registrado hasta ahora. Aparentemente, la placa de Cocos subducida pierde su identidad sísmica a distancias de la trinchera mayores y por lo tanto a profundidades más grandes. En este trabajo se analizan las principales características de la fuente sísmica y la propagación de las ondas generadas. Los resultados en este sentido indican un plano de falla buzando hacia el noreste y de naturaleza extensiva (lat=18.113°, lon=-98.974°, h=50.0 km, ϕ=305°,δ=32°, λ=-80°). El resultado de una inversión cinemática muestra que, aparentemente, la ruptura se propagó en dirección noroeste a partir del hipocentro. Regresiones distancia .vs. aceleración-máxima indican que, a diferencia de los sismos costeros, la aceleración máxima no se ve amplificada en las estaciones de Cuernavaca y Ciudad Universitaria. Usando como semilla el sismo de Copalillo, se realizaron simulaciones de sismos de mayor magnitud (hasta Mw=7.3) para estudiar las características en los registros de aceleración en la Ciudad de México. Los resultados sugieren que, para el peor escenario, algunos trabajos previos podrían haber subestimado el peligro sísmico.

El segundo trabajo muestra el análisis del sismo de Coyuca del 2001 (08/10/2001, Mw=5.8, (17.003°, -100.095°, h=8.0 km) y de la secuencia de réplicas que lo acompañó. Un análisis de la fuente sísmica muestra que el sismo se encuentra localizado en la placa continental de Norteamérica y que está asociado a un régimen extensivo (ϕ=89°, δ=42°, λ=-99°). Lo anterior revela que esta placa se encuentra en extensión, aún a menos de 80 km de la trinchera. Un proceso de relocalización de las réplicas mostró que éstas se distribuyeron en un área de ~ 15 x 10 km^2.

El siguiente trabajo está dedicado a un sismo ocurrido cerca de la trinchera Mesoamericana (18/04/2002, Mw=6.7, lat.=16.75°, lon=-101.06, ϕ=291°, δ=9°, λ=-89°). Una peculiaridad del evento consiste en que, con respecto de los sismos que ocurren en la costa, generó aceleraciones considerablemente menores en todas las estaciones que lo registraron. Siguiendo un método propuesto anteriormente, el temblor es catalogado como un "sismo de trinchera", y de acuerdo a la misma clasificación posee cierto potencial tsunamigénico. Analizando sismos, que anteriormente habían sido clasificados en la misma categoría, se concluye que, al menos para México, los "sismos de trinchera" además de tener potencial tsunamigénico presentan, consistentemente, aceleraciones máximas menores con respecto de los sismos que se localizan en la costa.

Otro de los trabajos incluidos, está dedicado al análisis de un deslizamiento asísmico registrado en los primeros meses del 2002. Durante 4 meses (enero-abril, 2002) las estaciones permanentes de GPS en el sureste de México, principalmente en el Estado de Guerrero, registraron una deformación superficial lenta. Siguiendo las expresiones cerradas, para la deformación estática en superficie debido a un deslizamiento sobre una falla, se utilizó un esquema de inversión global para invertir los datos de las estaciones GPS que registraron el fenómeno. A pesar de no ser concluyentes, los resultados muestran que el principal deslizamiento ocurrió en la interfase entre las placas de Cocos y Norteamérica y muy probablemente justo debajo de la zona acoplada. El principal deslizamiento ocurrió en un área de ~ 60 x 220 km^2, que corresponde a un temblor "silencioso" equivalente a Mw~7.4. Esta solución, además de explicar las observaciones, no contraviene la historia sísmica de la región.

Finalmente, en el último trabajo se realiza una evaluación del Sistema de Alerta Sísmica para la Ciudad de México (SAS) que desde 1994 opera continuamente para alertar a la población de esta ciudad ante un sismo importante localizado en la costa del Estado de Guerrero. La comparación de las aceleraciones máximas registradas en el Valle de México contra la historia de alertas del SAS, muestra que, independientemente de la magnitud de los sismos, los disparos de las alertas tienen poco que ver con las aceleraciones máximas registradas en el Valle de México y por lo tanto con los posibles daños en la ciudad.

A través de un análisis de registros de aceleración de estaciones localizadas en el sur del país, se presenta una alternativa basada en el cálculo del RMS para algunos segundos de la señal prefiltrada a bajas frecuencias. Esta opción permite separar de manera confiable y en pocos segundos aquellos sismos que generarán cuando menos 2 gal en el registro filtrado de una estación ubicada en la zona de roca firme del valle de México. La alternativa propuesta, junto con un arreglo modificado de sensores distribuidos en tres anillos concéntricos a la Ciudad de México, puede mejorar sustancialmente el desempeño del SAS ante falsas alertas y fallos y, potencialmente, salvar miles de vidas.

ABSTRACT

Previous works have studied the gross situation of the seismotectonics and associated seismic risk of the Guerrero Seismic gap. However, some recent seismic events show that the situation is more complex than supposed before. This thesis covers some results obtained from these events, and it tries to contribute to a better understanding of the tectonic process and its implications for the seismic hazard estimation.

The first event analyzed is the 2000 Copalillo earthquake (21/07/2000, Mw=5.9), which was located on the border of the Guerrero and Puebla states. This event is the farthest intraplate earthquake from the Middle American trench and the closest to Mexico City that has been recorded until today. Apparently, seismic signature of the subducted Cocos plate is loser for greater depths and distances. At this work I study the main features of the seismic source and wave propagation. The results show an extensive fault, dipping to northeast (lat=18.113°, lon=-98.974°, h=50.0 km, ϕ=305°,δ=32°, λ=-80°). A kinematic source inversion shows that the rupture, apparently, propagates in a northwest direction from the hypocenter. In contrast with coastal earthquakes, distance vs. peak acceleration correlations show that peak acceleration is not amplified at Cuernavaca and Ciudad Universitaria sites. In order to study the features of acceleration records in Mexico City, Copalillo earthquake was used as a seed to compute some simulations of bigger magnitude earthquakes. The results suggest, that for the worst scenario, some previous works could have underestimated seismic hazard.

The second event analyzed is the 2001 Coyuca earthquake (08/10/2001, Mw=5.8) and its aftershock sequence. The location and moment tensor solution (17.003°, -100.095°,ϕ=89°,δ=42°,λ=-99°) shows that this earthquake is located in the North American continental plate and is associated to an extensive regime. This reveals that the overriding plate is under extension even at less than 80 km from trench. Aftershock relocations show a distribution over an area of 15 x 10 km^2.

Then, I studied an earthquake located close to the Middle American trench (18/04/2002, Mw=6.7). Its main feature was its low peak accelerations at the stations that recorded it. Following a methodology presented by other authors, this earthquake was classified as a "trench earthquake" and this implied that it had a tsunamigenic potential. By analyzing previous earthquakes, classified before as trench earthquakes, is possible to conclude that although those have tsunamigenic potential, these earthquakes present low peak accelerations in comparison to coastal events.

Another part of this thesis is dedicated to the study of an aseismic slip recorded at the beginning of 2002. For 4 months (January-April, 2002), GPS permanent stations of south of Mexico, especially at Guerrero state, recorded a slow deformation of the surface. I utilize close expressions to compute static deformation due to slip over a fault plane; I use a global inversion scheme to invert data from GPS stations. The results, although not conclusive, show that the main slip occurred at the interface of the Cocos and the North American plate and below the coupled interface. The main slip occurred over an area of ~ 60 x 220 km^2, corresponding to a silent earthquake of Mw=7.4. This solution, not only fits the observations, but also agrees with the seismic history of the region.

Finally, the last part of this thesis is an evaluation of the Seismic Alert System for Mexico City (SAS), which has been in operation since 1994 in order to prevent the population of the city from possible big earthquakes located in the Guerrero coast. Comparison between peak accelerations and alert history from SAS shows that SAS-alerts are poor indicators of Amax and in consecuence of possible damage on the city.

Using acceleration records from stations located in the south of the country, I present an alternative alert, based on computation of RMS of few seconds of a low-pas filtered signal. This option permits separating for a few seconds, the earthquakes that might generate 2 gal in a station located on a hard rock site at the Valley of Mexico. This proposed alternative, together with a modified set up of sensors, distributed on three concentric rings to Mexico City, could help improving, substantially, the performance of SAS, reducing the number of false alerts and faults and, potentially, saving thousands of lives.

Introducción

El concepto de "brecha sísmica" ha motivado que algunas líneas de investigación relacionadas con la sismología y la ingeniería sísmica se concentren en regiones geográficas específicas, donde la probabilidad de ocurrencia de un temblor importante en un período de tiempo corto, es alta. Diversos autores *(P. ej. Fedotov, 1965; Kelleher et al.,1973)* han propuesto que los sitios con mayor probabilidad de generar sismos grandes, en un futuro cercano, son segmentos de los límites de placas, convergentes o transformantes, que no han generado un temblor importante en las últimas décadas. Estos segmentos son denominados brechas sísmicas.

Atendiendo a esta definición, diversos grupos de investigación han estudiado las regiones tectónicamente activas para tratar de determinar las zonas que, de acuerdo a los datos existentes, pueden ser consideradas como brechas sísmicas (*P.ej. Kelleher et al., 1973; Mc Cann et al., 1979, Singh et al., 1981*). En el caso específico de México *Nishenko y Singh (1987)* analizaron los diferentes segmentos que componen la zona de subducción mexicana con el fin de establecer probabilidades condicionales de ocurrencia de sismos en dichos segmentos. De acuerdo a estos autores, una de las regiones con mayor potencial sismogénico es la región central del estado de Guerrero, denominada como la "brecha sísmica de Guerrero".

Desde el sur del estado de Jalisco hasta el golfo de Tehuantepec los procesos tectónicos regionales están controlados por el régimen convergente entre las placas de Cocos y Norteamérica. De acuerdo al "catálogo de sismos importantes del siglo XX" (*Singh et al., 1984; Kostoglodov y Pacheco, 1999*), la brecha sísmica de Guerrero se encuentra acotada al noroeste por el área de ruptura del sismo del 14 de Marzo de 1979 (Mw=7.4) (sismo de Petatlán) (*Valdés et al., 1982*) y al sureste por los sismos del 11 y 19 de Mayo de 1962 (Mw=7.1 y Mw=7.0, respectivamente) *(Ortiz et al., 2000)*. El último temblor registrado en la "brecha sísmica" ocurrió en Diciembre de 1911 (Ms 7.8). Previo a este sismo ocurrieron los temblores de Diciembre de 1899 (Ms 7.7), Marzo de 1908 (Ms 7.8) y Julio de 1909 (Ms 7.5). La secuencia de sismos antes mencionada podría indicar que la región libera energía en eventos de magnitudes entre 7.5 y 7.8. Sin embargo, la

dimensión total de la brecha sísmica es capaz de generar un sismo de magnitud Mw=8.0 *(Nishenko y Singh, 1987)*.

El período estimado de retorno para esta región ha sido calculado como 60-70 años *(Nishenko y Singh, 1987)*, por lo que la ocurrencia de un sismo importante podría haberse retardado más de 30 años. En consecuencia, la brecha sísmica de Guerrero es una de las regiones, de la zona de subducción mexicana, con mayor probabilidad de generar un temblor importante en los próximos años.

Algunos trabajos han determinado que la zona que rompieron los sismos del 28 de Julio de 1957 y del 25 de Abril de 1989, tiene períodos de retorno de ~ 30 años (*Singh et al., 1982*), por lo que, en este contexto, esta región podría considerarse también como una brecha sísmica madura. Tomando en cuenta lo anterior la brecha sísmica podría tener una longitud de hasta 230 km, por lo que si rompiera en un solo sismo, alcanzaría una magnitud de hasta M~8.2 (*Singh y Mortera, 1991*).

La evidencia de la "madurez" de la brecha sísmica proviene de los datos de movimiento relativo entre las placas de Cocos y Norteamérica y de los registros y reportes de sismos importantes de finales del XIX y principios del siglo XX. Sin embargo, las localizaciones y magnitudes asociadas a estos temblores son, en gran medida, inciertas. De esta manera, en sentido estricto, no se tiene un registro completo del ciclo sísmico de la zona. Por esta razón toda la sismicidad asociada a la brecha y a las zonas adyacentes de la misma debe ser analizada y tomada en cuenta para el entendimiento cabal del ciclo sísmico de la zona.

El estado actual de la instrumentación sísmica permite contar hoy en día con datos de alta calidad (aun para sismos no muy grandes) que permiten llevar a cabo estudios detallados tanto de la fuente de los temblores, como de la propagación de las ondas sísmicas que estos producen. Adicionalmente, los datos recientemente generados a través de los sistemas GPS (Global Positioning System), permiten conocer detalles de la deformación superficial causada tanto por los sismos como por los procesos propios de la

subducción. En este contexto, toda la información generada deberá ser tomada en cuenta para entender mejor la tectónica regional.

El potencial de la brecha sísmica de Guerrero tiene implicaciones importantes en la estimación del riesgo sísmico de ciudades importantes como el Puerto de Acapulco y la Ciudad de México. En este último caso, la distancia de la brecha de Guerrero a la Ciudad de México es de alrededor de 300 km. Considerando los daños provocados por el sismo de Michoacán del 19 de Septiembre de 1985 (Mw 8.1), cuyo epicentro se localizó a unos 350 km de la Ciudad de México, el riesgo para dicha ciudad, ante un gran sismo en la brecha de Guerrero, podría ser muy importante (*Kanamori et al., 1993; Ordaz et al., 1995*). De hecho, la Ciudad de México cuenta, desde 1993, con un sistema de alerta temprana denominada "SAS" (Sistema de Alerta Sísmica) (*Espinosa-Aranda, 1995*), la cual está diseñada para proporcionar unos cincuenta segundos de ventaja ante la ocurrencia de un temblor importante en la costa del estado de Guerrero.

El presente trabajo tiene dos directrices principales.

- El estudio de los sismos recientes de diversa naturaleza asociados a la brecha sísmica y sus implicaciones en la sismotectónica regional.
- Algunas de las repercusiones de estos eventos en el análisis del peligro sísmico asociado.

Uno de estos temblores recientes es el sismo de Copalillo del 21 de Julio del 2000, cuyo fallamiento normal confirma que el principal mecanismo que gobierna el estado de esfuerzos en la placa de Cocos subducida es la fuerza de gravedad sobre la propia placa ("*slab-pull*"). En el trabajo titulado ***"Estudio de la fuente y de la propagación del sismo del 21 de Julio de 2000, Copalillo, México(Mw=5.9): Implicaciones de los sismos intraplaca en el peligro sísmico de la Ciudad de México."*** (capítulo I) se discuten las principales características de este temblor. El mecanismo obtenido suponiendo una fuente puntual muestra claramente que la naturaleza del temblor es extensiva, sin embargo no hay *a priori* ninguna consideración evidente que permita discriminar entre los dos planos de falla resultantes de la solución de mecanismo focal para una fuente puntual. Con el objeto

de discriminar entre ambos planos de falla, se llevó a cabo una inversión cinemática de la ruptura usando datos locales y regionales a través de un esquema propuesto originalmente por *Cotton y Campillo (1994)* y modificado para hacer una búsqueda global eficiente utilizando un esquema de recristalización simulada ("simulated annealing") (*Iglesias et al., 2001*).

Por otro lado, la ubicación geográfica de este temblor muestra que el peligro sísmico asociado a los temblores de fallamiento normal podría ser importante para algunas ciudades del Altiplano Mexicano incluyendo la propia Ciudad de México. En este trabajo se discuten algunas de las implicaciones que este tipo de temblores podría tener en la estimación del riesgo sísmico para la Ciudad de México. La existencia de temblores intraplaca de régimen extensional en territorio mexicano no es poco común. Solo la década pasada ocurrieron dos sismos de este tipo (15-Jun-99, Mw=7.0 y 30-Sep-99, Mw=7.5) los cuales causaron daños significativos en las ciudades de Puebla (*Singh et al., 1999*) y Oaxaca, respectivamente (*Singh et al., 2000, Hernández et al., 2001*).

Otro evento de especial interés ocurrió el 8 de Octubre del 2001 (Mw=5.8) muy cerca de la población de Coyuca de Benítez, Gro. Este sismo también fue asociado a un mecanismo de falla normal. Sin embargo, la profundidad hipocentral indica claramente que no ocurrió dentro de la placa de Cocos subducida, sino en la placa cabalgante de Norteamérica. El epicentro de este sismo se encuentra localizado precisamente sobre la "brecha sísmica" de Guerrero. Dada su posición con respecto a la zona acoplada (justo encima), este temblor es, probablemente, el único evento de esta naturaleza y magnitud reportado hasta ahora.

En el trabajo "***El sismo de Coyuca del 8 de Octubre del 2001, (Mw=5.8): Una falla normal sobre la brecha sísmica de Guerrero***" (capítulo II), se analizan las características principales del sismo de Coyuca y sus implicaciones en la tectónica regional. Numerosas réplicas fueron localizadas con bastante precisión gracias a una red local de estaciones portátiles desplegadas después del sismo principal. Las réplicas muestran claramente la orientación del plano de falla. Una inversión cinemática de la ruptura, usando

el esquema anteriormente mencionado, permitió conocer *a groso modo* las características generales de la ruptura.

Sí bien algunos autores (*P.ej. Singh y Pardo, 1993*) han propuesto que la placa cabalgante de Norteamérica se encuentra en un régimen tensional, hasta ahora la evidencia provenía de sismos pequeños continentales lejanos a la costa. Este régimen tensional, evidenciado por el sismo de Coyuca, podría estar relacionado al fenómeno llamado "retroceso de la trinchera" (*P.ej. Molnar y Atwater, 1978; Uyeda y Kanamori, 1979; Nakamura y Uyeda, 1980*) o al conocido como "erosión tectónica" (*P.ej. Murauchi, 1971*).

El proceso de erosión tectónica se refiere al desgaste que sufre la base de la placa cabalgante por la interacción de la placa subducida. El material que es separado de la placa cabalgante es llevado a profundidades mayores lo que provoca que se generen zonas con deficiencias de material. La deficiencia de material provoca un desequilibrio que puede reflejarse en un sistema de fallas normales. Por otro lado, el fenómeno de retroceso de la trinchera es provocado por el aumento del ángulo con que la placa subduce debajo de la placa cabalgante. Esto provoca que la línea de la trinchera retroceda y entonces la placa cabalgante puede quedar bajo un estado extensivo.

Poco después del sismo de Coyuca del 8 de Octubre, comenzó en la misma región un deslizamiento extremadamente lento y asísmico (*Kostoglodov et al., 2003*). Este deslizamiento fue registrado solamente por las estaciones permanentes GPS del Departamento de Sismología del Instituto de Geofísica de la UNAM. El deslizamiento asísmico mencionado ocurrió desde principios del mes de Enero del 2002 y tuvo una duración de al menos 4 meses. El desplazamiento tuvo lugar muy probablemente en la interfase de las placas de Cocos y Norteamérica.

En el trabajo ***"El sismo silencioso de 2002 en la brecha sísmica de Guerrero, México (Mw=7.6): Inversión del deslizamiento en la interfase de las placas y algunas implicaciones "*** (capítulo III), se presentan los resultados de la inversión de los datos de deformación (GPS) correspondientes, tanto a la parte de la carga tectónica, como a la fase

de deslizamiento asísmico. Nuevamente se utilizó un esquema de inversión global de cristalización simulada pero esta vez modificado a partir de los algoritmos propuestos por *Erickson (1986)* basados en la solución exacta de los campos de esfuerzos y deformación para un semiespacio elástico infinito propuesta por *Converse (1973)* (ver también *Okada, 1992*).

El objetivo central de estas inversiones fue determinar la zona donde ocurrió el deslizamiento asísmico pero la calidad y cantidad de los datos disponibles no permite ser concluyente al respecto. No obstante, hay razones suficientes para considerar un modelo en el cual durante el proceso intersísmico se presenta una acumulación de deformación sobre una zona acoplada ancha (~ 150 km). Por otro lado el deslizamiento asísmico o "descarga", aparentemente solo ocurre en una parte de esta zona acoplada. Los resultados obtenidos, aunados a observaciones previas (*Lowry et al., 2001; Kostoglodov et al., 2003*), sugieren que parte de la energía acumulada en la zona acoplada se libera en episodios recurrentes de deslizamientos asísmicos y otra parte se descarga a través de eventos sísmicos de subducción.

Trabajos previos consideran que el límite superior del ancho de la zona acoplada, para la zona de subducción mexicana, es menor a ~80 km. (*P.ej Singh et al.,1985, Singh y Mortera, 1991*). En contraste, el modelo propuesto en el presente trabajo considera una zona acoplada más ancha (~150 km). Debido a que parte de esta zona acoplada libera energía a través de deslizamientos asísmicos, la diferencia de tamaño de la zona acoplada no implica un incremento en la máxima magnitud esperada para un temblor, sin embargo podría tener impacto en el cálculo del período de recurrencia de los sismos en esta región.

Los resultados de las inversiones muestran, también, que la parte del modelo más cercana a la trinchera tiene un bajo grado de acoplamiento lo cual no significa que no existan sismos de pequeña o moderada magnitud en esta zona. Precisamente, el 18 de Abril del 2002 ocurrió un sismo de Mw=6.7 a unos 55 km frente a las costas del estado de Guerrero. Esta distancia lo ubica en una zona muy cercana a la trinchera mesoamericana. Por esta razón, este sismo es catalogado como un sismo de trinchera. Este tipo de sismos

merece un tratamiento especial ya que presentan características peculiares tanto en las cualidades de la fuente sísmica como en las trayectorias de propagación.

Shapiro et al. (1998) analizaron este tipo de sismos en México, encontrando que su espectro de Fourier presenta consistentemente deficiencia de amplitud en altas frecuencias con respecto a los sismos que ocurren cercanos a la costa. Diversos estudios (*P.ej. Ide et al., 1993; Kanamori y Kikcuhi, 1993*) han resaltado la relación entre este tipo de sismos y la ocurrencia del fenómeno conocido como Tsunami. Con base en lo anterior, *Shapiro et al. (1998)* propusieron la implementación de un sistema rápido de alerta de Tsunami basada en la discriminación entre un sismo de trinchera y un sismo de otra naturaleza a través de un simple análisis del espectro del temblor. En el artículo titulado ***"Los sismos de trinchera en México presentan aceleraciones máximas anómalamente bajas"*** (capítulo IV), se analizan las características del sismo del 18 de Abril catalogándolo como un sismo potencialmente tsunamigénico (utilizando el criterio antes mencionado). En este trabajo se retoman las observaciones hechas por *Shapiro et al. (1998)* acerca de la relación entre la deficiencia de amplitud en altas frecuencias y este tipo de sismos, para mostrar que las aceleraciones máximas que provocan los sismos de trinchera son consistentemente menores a las aceleraciones máximas provocadas por sismos "costeros". Esta conclusión, junto con la presentada por *Shapiro et al. (1998),* conducen al planteamiento de una paradoja; por un lado este tipo de sismos tsunamigénicos representan un peligro para las poblaciones costeras, pero por otro lado, las aceleraciones que se producen son menores a las provocadas por sismos costeros y por tanto los daños esperados en las estructuras pueden ser menores.

Otra implicación de lo mencionado antes es que, a pesar de su localización y magnitud, el sismo del 18 de Abril no generó ningún tipo alerta en el SAS. Como se mencionó anteriormente, este sistema de alerta ha sido implementado para generar una alerta rápida para la Ciudad de México ante la ocurrencia de sismos importantes en la costa de Guerrero *(Espinosa-Aranda et al., 1997)*. La idea de la alerta consiste, básicamente, en aprovechar la diferencia de velocidad entre la propagación de las ondas sísmicas con respecto a la velocidad de propagación de las ondas electromagnéticas. De esta manera,

cuando ocurre un sismo importante este es detectado inmediatamente por las estaciones acelerográficas localizadas a lo largo de la costa. La señal es analizada *in-situ* para obtener un pronóstico de la magnitud del evento. Si cumple ciertos criterios se emite una señal de radio que llega de manera casi instantánea a la Ciudad de México. Si el pronóstico es confirmado por al menos otra estación, se emite una alerta. A pesar del tiempo de transmisión y confirmación y dado que las ondas sísmicas viajan a mucha menor velocidad que las electromagnéticas, la señal de alerta es enviada ~50 segundos antes de que las ondas sísmicas de gran amplitud alcancen la Ciudad de México. De acuerdo al "Centro de Instrumentación y Registro Sísmico" (CIRES) (*Espinosa-Aranda et al., 1997),* el sistema de alerta dispara en modo restringido (solamente para algunas instituciones) con sismos de magnitud $5 \leq M < 6$ y en alerta pública (estaciones de radio) para sismos de $M \geq 6$. Sin embargo, en el caso del 18 de Abril, a pesar de que el sismo tuvo una magnitud $M \geq 6$, el SAS no disparó ni siquiera en alerta restringida. El CIRES reportó que no se detectó ninguna falla en el sistema y que la razón por lo cual no se activó la alerta se encontraba en que en ninguna de las estaciones que registro el evento, había superado el umbral para tal propósito. Esto concuerda con las conclusiones alcanzadas en el ya mencionado capítulo IV de esta tesis.

En el trabajo titulado ***"El sistema de alerta sísmica para la Ciudad de México: La evaluación de su desempeño y una estrategia para mejorarlo"*** (capítulo V) se presenta un análisis del desempeño del SAS. Este análisis fue hecho en función de los sismos que generaron tanto alerta pública como restringida y las aceleraciones máximas que provocaron en la Ciudad de México. En este sentido el SAS muestra un desempeño deficiente básicamente por dos razones:

- Cobertura limitada (diseñada únicamente para eventos provenientes de la costa del estado de Guerrero)
- El algoritmo de discriminación no parece apropiado para pronosticar las aceleraciones máximas que se registrarán en el Valle de México.

Debido a que el SAS ha sido diseñado para disparar solamente con los sismos localizados a lo largo de la costa de Guerrero, el sistema no es capaz de detectar sismos que provienen de otras zonas con alto potencial sísmico y que también pueden afectar a la Ciudad de México. Por esta razón es deseable evaluar la posibilidad de extender el sistema para abarcar la mayor parte de las regiones cuyo potencial sismogénico represente un riesgo para la Ciudad de México.

Siguiendo el esquema del actual sistema, esta tarea pudiera verse complicada tanto desde el punto de vista logístico como económico, ya que se requerirían un gran número de estaciones y, por lo tanto, un gran esfuerzo en las fases de instalación, operación y mantenimiento.

Una de las partes críticas de una alerta temprana es el método para determinar en unos cuantos segundos si el sismo puede causar daños o no. En este contexto diversos autores han trabajado en el diseño de algoritmos que en solo unos cuantos segundos pueden discriminar entre los eventos pequeños y los grandes (*p. ej . Tsuboi y Kikuchi, 2002; Allen y Kanamori,2003*).

En este trabajo se presenta una alternativa basada en el análisis de registros obtenidos principalmente por la red acelerográfica de Guerrero (GAA) operada por el Instituto de Ingeniería de la UNAM.

La tarea fundamental consistió en encontrar alguna relación entre la aceleración máxima registrada en la estación CUIP (localizada en la Ciudad Universitaria dentro del valle de México) y el registro de aceleraciones de una estación cercana al epicentro de los temblores (estación de referencia). Se encontró que, si las señales son pre-filtradas a bajas frecuencias ($0.2Hz < f < 1.0Hz$), es posible establecer una correlación entre el valor cuadrático medio (RMS) de los primeros segundos del tren de ondas S en la estación de referencia y la aceleración máxima registrada en la estación CUIP. Este filtro está basado en el hecho de que las ondas sísmicas sufren amplificación dentro del valle de México sobre esta banda de frecuencias especialmente en aquellas zonas propensas a sufrir daños.

Los resultados obtenidos muestran que es posible separar, de manera confiable, los eventos que exceden 2 gales en la estación CUIP usando el valor de RMS filtrado en la estación cercana. Este umbral parece adecuado ya que, al menos, la mayoría de las personas sentirían cualquier evento superando ese umbral.

Por otro lado esta propuesta presenta un mejor desempeño, con respecto a falsas alertas y fallos (eventos importantes para los cuales no disparó el sistema).

Siguiendo el esquema planteado, se necesitarían cerca de 40 estaciones separadas entre sí por una distancia de alrededor de 60 km y distribuidas en tres anillos concéntricos a la Ciudad de México, para alertar ante prácticamente cualquier sismo costero importante generado desde Michoacán hasta Oaxaca. Este mismo arreglo permitiría tener cobertura para muchos de los sismos de profundidad intermedia que ocurren dentro de la placa de Cocos subducida.

Referencias:

Allen R. y H. Kanamori, 2003. The potential for earthquake early warning in Southern California. *Science*. 300, 786-789.

Cotton, F. y M. Campillo,1995. Inversion of strong ground motion in the frequency domain, *J. Geophys. Res.* **100**, 3961-3975.

Converse, G., 1973. Equations for the displacements and displacement derivatives due to a rectangular dislocation in a three-dimensional elastic half-space, unpublished, U. S. Geological Survey, Menlo Park.

Erickson, L., 1986. A three-dimensional dislocation program with applications to faulting in the Earth, M.S. thesis, 167 pp., Stanford Univ., Stanford, Calif.

Espinosa Aranda, J.M:, A. Jiménez, G. Ibarrola, F. Alcantar, A. Aguilar, M. Inostroza y S. Maldonado,1995. Mexico City seismic alert system, *Seism. Res. Lett.* **66**, 42-53.

Fedotov, S.A., 1965. Regularities of the distribution of strong earthquakes in Kamchatka, the Kurile islnads and northeastern Japan, *Trans. Acad. Sci. USSR, Inst. Phys. Earth* **36**, 66-93.

Hernandez, B., N. Shapiro, S.K. Singh, J. Pacheco, F. Cotton, M. Campillo, A. Iglesias, V. Cruz, J.M. Gómez y L. Alcántara, 2001. Rupture history of Sep 30, 1999 intraplate earthquake of Oaxaca, Mexico (Mw=7.5) from inversion of strong motion data in the frequency domain, *Geophys. Res. Lett.*, **28**, 363-366.

Iglesias, A., V.M. Cruz-Atienza, N.M. Shapiro, y J.F. Pacheco, 2001. Crustal structure of south-central Mexico estimated from the inversion of surface-wave dispersion curves using genetic and simulated annealing algorithms, *Geof. Int.*, **40**, 181-190.

Ide, S, F. Imamura, Y. Yoshida y K. Abe, 1993. Source characteristics of the Nicaraguan tsunami earthquake of September 2, 1992, *Geophys. Res. Lett.* **9**, 863-866.

Kanamori, H. y M. Kikuchi, 1993. The 1992 Nicaragua earthquake: a slow tsunami earthquake associated with subducted sediments, *Nature* **361**, 714-716.

Kanamori, H., P.C. Jennings, S.K. Singh y L. Astiz, 1993. Estimation of strong ground motion in Mexico City expected for large earthquakes in the Guerrero seismic gap, *Bull Seism. Soc. Am.*, **83**, 811-829.

Kelleher, J., Sykes, L. y Oliver, J., 1973. Possible criteria for predicting earthquake locations and their applications to major plate boundaries of the Pacific and the Caribbean. *J. Geophys. Res.*, **78**, 2547-2585.

Kostoglodov, V., Larson K. M., S. K. Singh, A. Lowry, J. A. Santiago, S. I. Franco y R. Bilham, 2003. A large silent earthquake in the Guerrero seismic gap, Mexico. *Geophys. Res. Lett.* 30, 1807.

Kostoglodov V., Pacheco J. Un catálogo de sismos moderados y grandes ocurridos en México durante el siglo XX, Poster 100 años de sismicidad en México, Instituto de Geofísica, UNAM, 1999.

Lowri, A. R., Larson K. M. Kostoglodov, V. and Bilham,R., 2001. Tansient fault slip in Guerrero, southern Mexico. *Geophys, Res. Lett.* **28**, 3753-3756 .

McCann, W. R., S. P. Nishenko, L. R. Sykes y J. Krause, 1979. Seismic gaps and plate tectonics: Seismic potential for major boundaries, *Pure Appl. Geophys.* **217**, 1082-1147.

Molnar, P. y T. Atwater, 1978. Interarc spreading and cordilleran tectonics as alternates related to the age of subducted oceanic lithosphere, *Earth Planet, Sci. Lett.*. 330-340, 1978

Murauchi, S., 1971. The renewal of island arcs and the tectonics of marginal seas, 1971. En *Island Arcs and Marginal Seas*. Tokai University Press, Tokyo.

Nakamura K. y S. Uyeda, 1980. Stress gradient in arc-back arc regions and plate subduction. *J. Geophys. Res.*, 85, 6419-6428.

Nishenko, S.P. y S.K. Singh, 1987, Conditional probabilities for the recurrence of large and great interplate earthquakes along the mexican subduction zone. *Bull. Seism. Soc. Am.*, **77**, 2095-2114.

Okada,Y., 1992. Internal deformation due to shear and tensile faults in a half-space,. *Bull. Seism. Soc. Am.*, **82**, 1018-1040.

Ordaz, M. J. Arboleda y S.K. Singh, 1995. A scheme of random summation of an empirical Green's function to estimate ground motions from future large earthquakes, *Bull. Seism. Soc. Am.*, **85**, 1635-1647.

Ortiz, M., S. K. Singh, V. Kostoglodov y J. Pacheco, 2000. Source areas of the Acapulco-San Marcos, Mexico earthquakes of 1962 (M 7.1; 7.0) and 1957 (M 7.7), as constrained by tsunami and uplift records. *Geof. Int.*, **39**, 337-348.

Shapiro, N.M., S.K. Singh y J. Pacheco, 1998. A fast and simple diagnostic method for identifying tsunamigenic earthquakes, *Geophys. Res. Lett.* **25**, 3911-3914.

Singh, S. K., L. Astiz y J. Havskov, 1981. Seismic gaps and recurrence periods of large earthquakes along the Mexican subduction zone: a Reexamination. *Bull. Seism. Soc. Am.*, **71**, 827-843.

Singh, S.K., J. M. Espíndola, J. Yamamoto y J. Havskov, 1982. Seismic potential of Acapulco-San Marcos region along the Mexican subduction zone, *Geophys. Res. Lett.*, **9**, 633-636.

Singh, S.K., M. Rodríguez y J. M. Espíndola, 1984. A catalog of earthquakes of Mexico from 1900 to 1981, *Bull. Seism. Soc. Am.* **74**, 267-279.

Singh, S.K., G. Suárez y T. Domínguez, 1985. The great Oaxaca earthquake of 15 January 1931: Lithosphere normal faulting in the subducted Cocos plate. *Nature*, **317**, 56-58.

Singh, S.K. y F. Mortera, 1991. Source-time functions of large Mexican subduction earthquakes, morphology of the Benioff zone and the extent of the Guerrero gap, *J. Geophys. Res.*, **96**, 21487-21502.

Singh, S.K. y M. Pardo, 1993. Geometry of the Benioff Zone and state of stress in the overriding plate in Central Mexico. *Geophys. Res. Lett.*, **20**, 1483-1486.

Singh, S.K., M. Ordaz, J.F. Pacheco, R. Quaas, L. Alcántara, S. Alcocer, C. Gutirrez, R. Meli y E. Ovando,1999. A preliminary report on the Tehuacán, México earthquake of June 15, 1999 (Mw=7.0), *Seism. Res. Lett.* **70**, 489-504.

Singh, S.K., M. Ordaz, L. Alcántara, N. Shapiro, V. Kostoglodov, J. F. Pacheco, S. Alcocer, C. Gutierrez, R. Quaas, T. Mikumo y E. Ovando, 2000. The Oaxaca Earthquake of September 30, 1999 (Mw=7.5): A Normal-Faulting Event in the Subducted Cocos Plate, *Seism. Res. Lett.* **71**, 67-78.

Tsuboi, S.; Saito y Kikuchi, M., 2002. Real-time earthquake warning by using broadband P Waveform. *Geophys. Res. Lett.*, **29**, 1483-1486

Uyeda, S. y H. Kanamori, 1979. Back arc opening and the mode of subduction, *J. Gepohys. Res.*, **84**, 1049-1061.

Valdés, C., R.P. Meyer, R. Zuñiga, J. Havskov and S.K. Singh, 1982. Analysis of Petatlan aftershocks: Numbers energy release, and asperities, *J. Geophys. Res.*, **87**, 8519-8527.

Capítulo I

"Estudio de la fuente y de la propagación del sismo del 21 de Julio de 2000, Copalillo, México(Mw5.9): Implicaciones de los sismos intraplaca en el peligro sísmico de la Ciudad de México"

Bulletin of the Seismological Society of America, Vol. 92, No. 3, pp. 1060–1071, April 2002

A Source and Wave Propagation Study of the Copalillo, Mexico, Earthquake of 21 July 2000 (M_w 5.9): Implications for Seismic Hazard in Mexico City from Inslab Earthquakes

by A. Iglesias, S. K. Singh, J. F. Pacheco, and M. Ordaz

Abstract The Copalillo earthquake of 21 July 2000 (M_w 5.9) is the closest, well-located inslab event to Mexico City ever to be recorded. In this study, we analyze local and regional broadband and accelerometric recordings to determine the source parameters of the earthquake and the attenuation of ground motion with distance and to obtain a preliminary estimate of the seismic hazard posed to the city by such events. Our results show that the earthquake occurred at a depth of about 50 km, most probably in the subducted oceanic crust. The waveform inversion discriminates between the two nodal planes; the fault plane defined by the following: strike, 305°; dip, 32°; and rake, −80°. The rupture propagated nearly unilaterally along the strike toward northwest with a small downdip component. The observed source spectrum can be well explained by an ω^2-source model with $M_0 = 6.0 \times 10^{25}$ dyne cm and a stress drop of 360 bar. We find that high-frequency ground motion ($f > 3$ Hz), which is related to A_{max} during inslab earthquakes, is not amplified at Ciudad Universitaria (CU), a hill-zone site in the Valley of Mexico that is known to suffer amplification at low frequencies ($0.1 < f < 2.0$ Hz). Simulations using the recording at CU of the Copalillo earthquake as an empirical Green's function suggests that a M_w 7.0 event could give rise to an A_{max} value of 30–40 gal. The CU recordings indicate that the A_{max} value of 30 gal could have a return period of about 40 yr, about the same as from shallow-dipping thrust earthquakes along the Mexican subduction zone, which have been regarded as posing the highest hazard for the city. An inslab earthquake with an A_{max} value of about 40 gal could cause heavy damage to small buildings at certain locations of the city. We conclude that seismic hazard from inslab earthquakes to Mexico City has so far been underestimated.

Introduction

Inslab earthquakes in the subducted Cocos plate below south-central Mexico cease to occur at depths of less than about 80 km and well before reaching the Mexican Volcanic Belt (MVB). Indeed, no well-located inslab earthquake is known to have occurred below the MVB. The recent earthquake of 21 July 2000 (M_w 5.9; H = 50 km), henceforth called the Copalillo earthquake, is the closest, reliably located, normal-faulting inslab event to Mexico City (Fig. 1). The epicenter of the earthquake lies near the town of Copalillo, about 65 km to the northeast of Iguala and 136 km to the south of Ciudad Universitaria (CU), Mexico City. In this article, we study the characteristics of the source and the ground motions generated by this earthquake and discuss the implications for seismic hazard to the city from inslab earthquakes. There are several reasons for this endeavor. (1) Source characteristics of inslab earthquakes in the Cocos plate, while essential to understand the mechanism of generation of such events, are available for only a few earthquakes. (2) There is evidence that high-frequency ground motion from inslab events in Mexico are more intense than from interplate earthquakes (see, e.g., Singh *et al.*, 2000). This observation needs further confirmation. (3) A critical issue in the estimation of seismic hazard to Mexico City is related to inslab, normal-faulting earthquakes in the subducted Cocos plate.

The concern about the seismic hazard arises because in the past inslab earthquakes have caused significant damage to cities and towns in the Mexican altiplano. There are many recent examples. The earthquake of 15 January 1931 (M 7.8, H = 40 km) caused severe destruction to the City of Oaxaca (Barrera, 1931; Singh *et al.*, 1985); the earthquakes of 28 August 1973 (M_w 7.0; H = 82 km) and 24 October 1980 (M_w 7.0; H = 65 km) resulted in deaths and damage in the states of Veracruz, Puebla, and Oaxaca (Singh and Wyss,

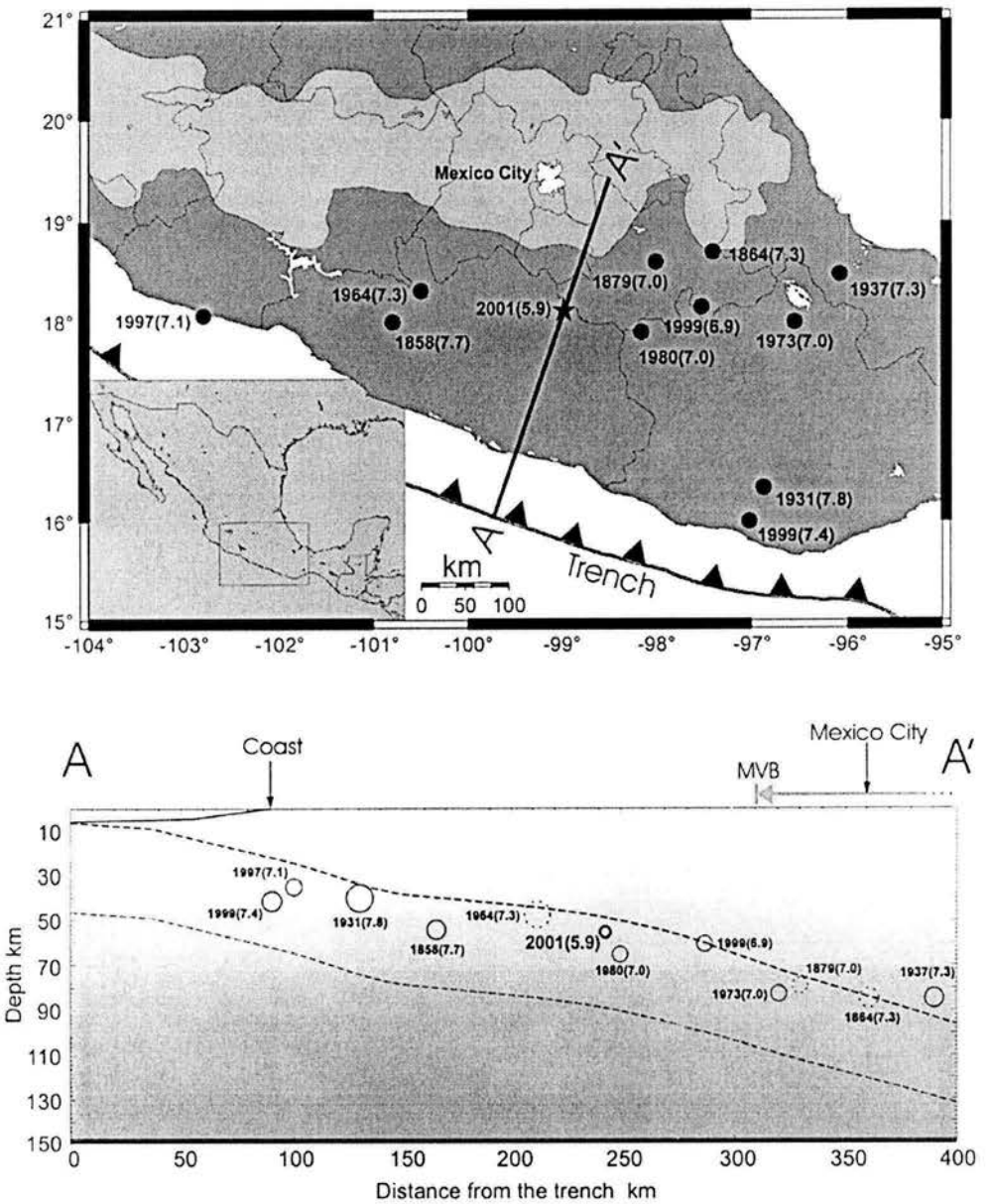

Figure 1. (Top) Epicenters of large ($M \geq 6.9$) inslab, normal-faulting, intermediate-depth earthquakes and location of Mexico City. Also shown is the 21 July, 2000 Copalillo earthquake (M_w 5.9) (star). Lightly shaded area represents the Mexican Volcanic Belt (MVB). (b) The projection of the hypocenters of the inslab events on a vertical plane AA′. The dashed lines delineate the subducted Cocos plate. The depths of the nineteenth-century earthquakes (dashed circles) have been arbitrarily assigned to fall near to the plate interface. The 1937 event lies above the plate interface probably because of the error in its depth.

1976; Lomnitz, 1982; Yamamoto *et al.*, 1984; Nava *et al.*, 1985). The recent earthquake of 15 June 1999 (M_w 6.9, H = 60 km) caused damage in the State of Puebla, especially to colonial structures in and near the City of Puebla (Singh *et al.*, 1999). The 30 September 1999 Oaxaca earthquake (M_w 7.4; H = 40 km) was damaging to the City of Oaxaca and many towns along the coast and between the coast and the city of Oaxaca (Singh *et al.*, 2000). It has been suggested that the great earthquake of 19 June 1858, which caused severe damage to inland towns in the state of Michoacan, including its capital city of Morelia, and to Mexico City, may also have been an inslab, normal-faulting event (Singh *et al.*, 1996). A list of large inslab earthquakes ($M \geq 6.9$) in the subducted Cocos plate is given in Table 1, and their epicenters are shown in Figure 1.

The closest hypocentral distance of an inslab earthquake

to Mexico City and its likely maximum magnitude are uncertain. The design spectra for the Federal District does contemplate an inslab M_w 6.5 earthquake at focal distance of 80 km from Mexico City (Rosenblueth *et al.*, 1989). The choice of the magnitude and the focal distance were based on the available data at that time and the best judgment of the authors. The expected ground motion from such an earthquake was estimated assuming an ω^2 seismic source model and application of results from random vibration theory (Boore, 1983), with little constraint from actual recordings. For these reasons, the seismic hazard to Mexico City from inslab earthquakes is subject to relatively large uncertainty.

Figure 1 shows epicenters of large ($M \geq 6.9$), inslab earthquakes in the subducted Cocos plate. It should be noted that the locations and the magnitudes of nineteenth-century events are less reliable. Figure 1 suggests that such earthquakes can reach a magnitude of 7.3 within 200 km of Mexico City. The figure also includes the location of the Copalillo earthquake. As mentioned earlier, this earthquake is the closest inslab earthquake. In view of Figure 1, an inslab M_w 7.3 earthquake may reasonably be expected to occur as close as 136 km from the city at a depth of about 50 km. It is, therefore, of interest to estimate ground motions in the Valley of Mexico from such an earthquake. We do this by using a CU recording of the Copalillo earthquake as the empirical Green's function (EGF) to simulate expected ground motion in the city from future large earthquakes in the same region. We show that the point-source approximation inherent in the EGF method is quite reasonable and the effect of source directivity on the estimation of A_{max} in CU is not significant (less than 8%) for postulated earthquakes with $M_w \leq 7.5$. We finally discuss the significance of the results in terms of seismic hazard to Mexico City from inslab earthquakes.

Data

The data used in the analysis of the Copalillo earthquake consist of recordings from the broadband (BB) seismic network of the Servicio Sismológico Nacional (SSN) of the Instituto de Geofisica (IGF) and from the stations of the accelerographic networks operated by Instituto de Ingeniería (II) and Centro Nacional de Prevención de Desastres (CENAPRED). A typical BB station of SSN consists of a STS-2 seismometer and a Kinemetrics FBA-23 accelerometer connected to a 24-bit Quanterra digitizer. Continuous velocity data, sampled at 1 and 20 Hz, are saved in a buffer memory. For triggered events both velocity and acceleration channels, sampled at 80 Hz, are saved. The accelerometric networks mostly consist of Kinemetrics K2 and ETNA digital accelerographs, equipped with 19 and 18 bit A to D converters, respectively. The time synchronization is provided by GPS receivers. The triggered events are saved at a sampling rate of 200 Hz. Descriptions of the accelerometric networks may be found in Anderson *et al.* (1994) and Quass *et al.* (1987, 1989, 1993).

Table 1
Significant Inslab Earthquakes ($M \geq 6.9$) in the Subducted Cocos Plate close to Mexico City

Event	Date (yyyymmdd)	Latitude	Longitude	Depth	Magnitude
1	18580618	18.00	−100.80	—	7.7
2	18641003	18.70	−97.40	—	7.3
3	18790517	18.60	−98.00	—	7.0
4	19310115	16.34	−96.87	40	7.8
5	19370726	18.48	−96.08	85	7.3
6	19640706	18.31	−100.50	55	7.3
7	19730828	18.00	−96.55	82	7.0
8	19801024	17.90	−98.15	65	7.0
9	19970111	18.06	−102.79	34	7.1
10	19990615	18.15	−97.52	60	6.9
11	19990930	16.00	−97.02	40	7.4

Source Parameters

The location of the event, determined from local and regional data, and the source parameters, obtained from the moment tensor (MT) inversion of regional waveforms, are given in Table 2. The MT solution was obtained from the inversion of the bandpass-filtered (between 20 and 50 sec) BB regional seismograms. The procedure of Randall *et al.* (1995) was followed in the inversion. The details of the method, as applied to the analysis of BB data of the Mexican network, are given by Pacheco and Singh (1998). The crustal structure used in the location and the waveform modeling is given in Table 3. The source parameters reported in the Harvard centroid moment tensor (CMT) catalog are included in

Table 2
Source Parameters of the 21 July 2000, Copalillo Earthquake

Source	Latitude (°N)	Longitude (°E)	Depth (km)	M_0 dyne cm	Strike	Dip	Rake
Regional*	18.113	−98.974	50.0	4.1×10^{24}	305°	32°	−80°
Regional†	—	—	—	6.0×10^{24}	—	—	—
CMT‡	18.28	−98.77	58.4	7.9×10^{24}	310°	39°	−75°

*Epicentral location and depth from local/regional data; other source parameters from regional waveform inversion (see text).
†Seismic moment from *S*-wave spectra, local/regional data (see text).
‡Preliminary Harvard CMT solution.

Table 3
Crustal Structure Used in Locating and Modeling the Copalillo Earthquake

Layer Thickness (km)	*P*-Wave Speed (km/sec)	*S*-Wave speed (km/sec)	Density (gm/cm^3)
7.7	5.60	3.20	2.56
12.0	6.00	3.41	2.69
23.3	6.90	3.92	2.98
36.7	8.10	4.67	3.36
∞	8.40	4.85	3.46

Table 2. We note that the regional MT and the Harvard CMT focal mechanisms are similar, but the seismic moments differ by a factor of 2.

Slip Distribution on the Fault

We inverted the bandpass-filtered (0.1–0.5 Hz) near-source displacement records to retrieve the rupture history of the Copalillo earthquake. The inversion was performed in the frequency domain to obtain slip, rise time, and rupture velocity using a simulated annealing inversion technique adopted from the nonlinear least-squares inversion scheme developed by Cotton and Campillo (1995). We chose the focal mechanism retrieved from the regional MT inversion for our inversion—nodal plane 1: strike, 305°; dip, 32°; rake, −80°; nodal plane 2: strike, 113°; dip, 59°; rake, −96°.

In order to discriminate between the fault plane and the auxiliary plane, we performed separate inversion for each nodal plane. The expected rupture area of a magnitude 5.9 earthquake is about 100 km^2 (e.g., Singh *et al.* 1980). There is, *a priori*, no reason to expect that the rupture was bilateral. To allow for possible directivity, we took a larger fault model: 20 km along the strike and 20 km along the dip. It was divided in 10 × 10 subfaults. Figure 2 shows the surface projection of the nodal plane 1 as the fault plane and stations whose recordings were used in the inversion. Figure 3 (central frames) shows the fault plane, where the star indicates the rupture initiation point. Synthetic seismograms for each pair of subfault and station were computed using Bouchon's discrete wavenumber algorithm (Bouchon, 1982). We considered two starting models: in one we assigned zero slip on the fault plane, and in the other we assigned a constant slip of 1.5 m to the two subfaults nearest the hypocenter and a slip of zero elsewhere. A rise time of 1.5 sec was assigned for each subfault. In the inversion, the rupture velocity was chosen to lie between 3.3 and 3.6 km/sec. The slip and the rise time on each subfault were allowed to vary between 0 and 1.5 m and 0 and 1.5 sec, respectively. We found that the results of the inversion were insensitive to the initial slip distribution.

The rupture history is shown in Figure 3. The left frames correspond to the inversion with nodal plane 1 as the fault plane, whereas the right frames show the corresponding results with nodal plane 2 as the fault plane. Visually, the fit to the observed waveforms are about the same for the two nodal planes, although a quantitative measure of the misfit (Cohee and Beroza, 1994) suggests that model 1 is a slightly better choice for the causative fault than model 2. On the other hand, slip distribution for model 2 (Fig. 3, right) shows three patches of slip: one near the hypocenter and the other two above and below it, separated by about 16 km. The largest slip occurs on the patch located at depth close to the limit of the model. This relative location and the separation of the slip patches suggest that this solution is unrealistic. Taken together, we find a preference for nodal plane 1 as the fault plane, although the evidence is admittedly weak.

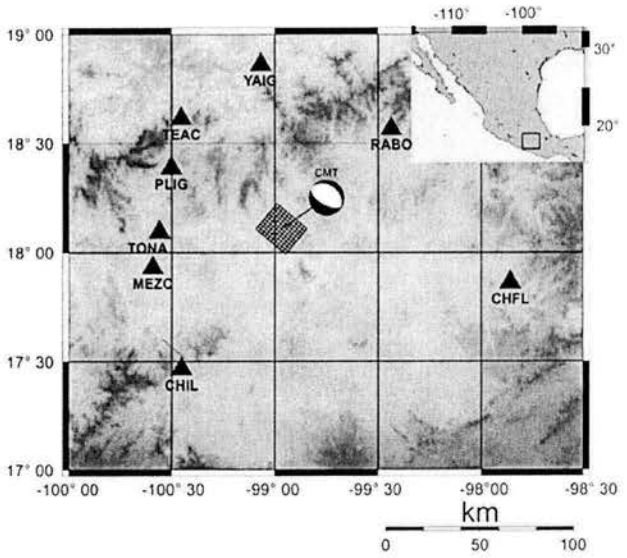

Figure 2. Location of the Copalillo earthquake and stations whose data were used in the inversion. Surface projection of the rectangular fault plane (nodal plane 1: strike, 305°; dip, 32°; rake, −80°) is indicated by a straight line.

We note from the left frames (nodal plane 1) that the rupture unilaterally propagates along the strike toward northwest with a small downdip component. The rupture velocity is about 3.5 km/sec. Most of the slip occurs over a 6 × 4 km area. The bottom frames in Figure 3 show the smoothed rise times. The smoothing was performed by requiring the rise times to be zero (irrespective of the result of the inversion) over areas with slip less than or equal to 1 cm. We tested the sensitivity of the inversion by fixing the rise time to 0.5 sec. This yielded a slip distribution very similar to the previous case, which suggests that the rise time is not well resolved.

Although detailed rupture histories are available for only a few recent inslab earthquakes in Mexico, all of these events show a component of rupture propagation that is downdip (e.g., Cocco *et al.*, 1997; Hernandez *et al.*, 2001). It will be interesting to know whether this is a common feature of most inslab, normal-faulting earthquakes in the Cocos plate.

Source Spectrum and Seismic Moment from Spectral Analysis of Near-Source Data

The source spectrum of the Copalillo earthquake has been estimated from horizontal components of *S* waves recorded at stations PLIG, RABO, MEZC, CHFL, CHIL, and YAIG (Fig. 2). The far-field Fourier acceleration spectral amplitude of the intense part of the ground motion, $A_i(f, R_i)$, at station i, which is located at a distance R_i from the source, can be written as

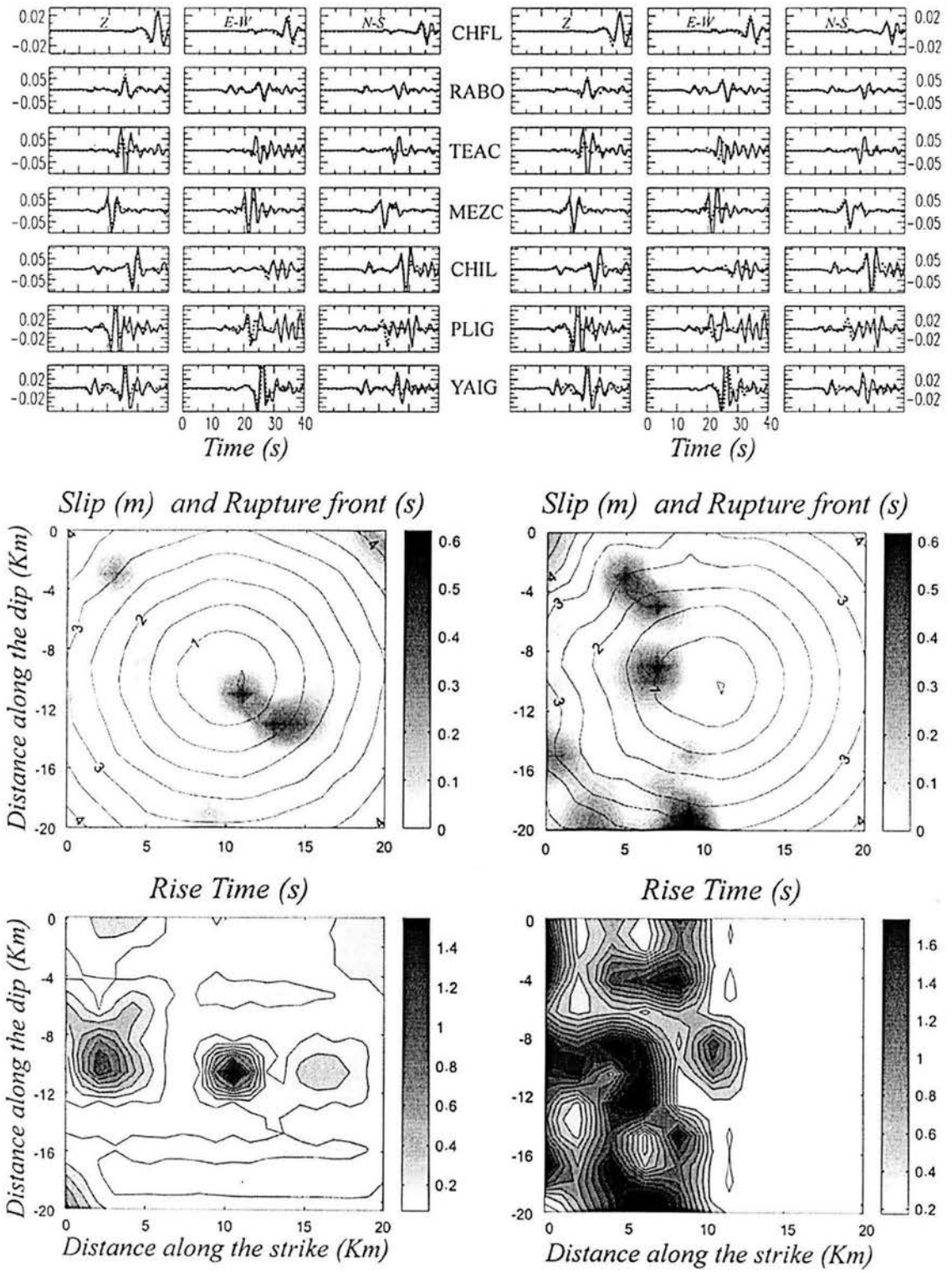

Figure 3. Results from the inversion of near-source bandpassed-filtered (between 0.05 and 0.5 Hz) displacement records. (Left) The chosen fault plane: strike, 305°; dip, 32°; rake, −80°. (Right) The chosen fault plane: strike, 113°; dip, 59°; strike, −96° (Top) Observed and synthetic seismograms. (Middle) Slip distribution on the fault and isochrons. (Bottom) Smoothed rise time (see text).

$$A_i\ (f,\ R_i)\ =\ C\ f^2\ \mathring{M}_0\ (f)\ e^{-\pi f R i/\beta Q(f)}/G(R_i), \qquad (1)$$

where

$$C\ =\ R_{\theta\varphi}\ FP(2\pi)^2/(4\pi\rho\beta^3), \qquad (2)$$

and $\mathring{M}_0(f)$ is the moment-rate (or source displacement) spectrum. In the limit, $\mathring{M}_0(f)$ tends to M_0, the seismic moment, as f approaches 0. For an ω^2-source model,

$$S(f)\ =\ f^2 f_c^2\ M_0/(f^2\ +\ f_c^2). \qquad (3)$$

For Brune's model (Brune, 1970), f_c, the corner frequency, is given by

$$f_c\ =\ 4.9\ \times\ 10^6\ \times\ \beta\ (\Delta\sigma/M_0)^{1/3}. \qquad (4)$$

In the previous equations, R_i is the hypocentral distance of the ith station, β is the shear-wave velocity, ρ is the density, $Q(f)$ is the quality factor, $R_{\theta\phi}$ is the average radiation pattern (0.55), F is the free-surface amplification (2.0), and P takes into account the partitioning of energy in the two horizontal components ($1/\sqrt{2}$). $G(R)$ in equation (1) is the geometrical spreading term, which may be taken as $G(R) = R$ for $R \leq R_x$ and $G(R) = (RR_x)^{1/2}$ for $R > R_x$. This form of $G(R)$ implies dominance of body waves for $R \leq R_x$ and of surface waves for $R > R_x$. For the Copalillo earthquake, we took β = 4.2 km/sec, ρ = 3.2 gm/cm^3, $Q(f) = 273f^{0.66}$ (Ordaz and Singh, 1992), and R_x = 100 km.

Figure 4 shows the source displacement and acceleration spectra, $\mathring{M}_0\ (f)$ and $f^2\ \mathring{M}_0\ (f)$. At low frequencies, $\mathring{M}_0\ (f)$ approaches a seismic moment of about 6.0×10^{24} dyne cm. The figure also shows that the data can be fit by an ω^2-source model, with $M_0 = 6.0 \times 10^{24}$ dyne cm and corner frequency, f_c, of 0.806 Hz. This yields, via equation (4), a Brune stress drop, $\Delta\sigma$, of 360 bars for the earthquake.

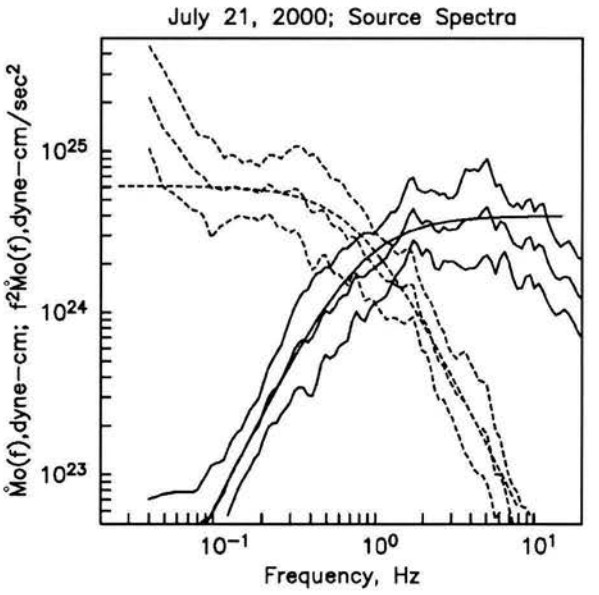

Figure 4. Average source displacement spectra, $\mathring{M}_0(f)$ (dashed lines) and acceleration spectra, $f^2\mathring{M}_0(f)$ (continuous lines) from local/regional data. The smooth curves correspond to an ω^2-source model, with $M_0 = 6.0 \times 10^{24}$ dyne cm and corner frequency, f_c = 0.806 Hz.

Attenuation of Ground Motion from the Copalillo Earthquake

Figure 5 shows a plot of horizontal peak ground acceleration, A_N and A_E, recorded at hard sites as a function of focal distance, R. In this plot we have included CU and Cuernavaca, although these sites, which lie on volcanic rocks, are known to suffer significant site effects between 0.1 and 4 Hz during coastal events (Ordaz and Singh, 1992; Singh *et al.*, 1995). The figure includes the predicted value of A_{max} based on a regression analysis of 10 inslab earthquakes of Mexico ($5.4 \leq M_w \leq 7.4$; $40 \leq H \leq 65$ km; $R \leq 400$ km), which relates horizontal A_{max} (in gal), M_w, and R (in km) by:

$$\log A_{max}\ =\ -0.148 + 0.623\ M_w\ -\ \log\ R\ -\ 0.0032R, \qquad (5)$$

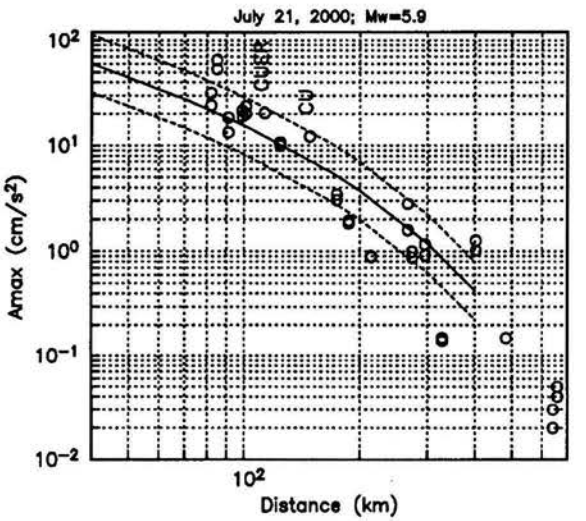

Figure 5. Peak horizontal peak acceleration, A_N and A_E, recorded at hard sites (including CU and Cuernavaca) as a function of focal distance, R. The predicted and $\pm$ one standard deviation curves, based on a regression analysis of 10 inslab earthquakes of Mexico ($5.4 \leq M_w \leq 7.4$; $40 \leq H \leq 65$ km; $R \leq 400$ km) are also shown.

where $A_{max} = [((A_N)^2 + (A_E)^2)/2]^{1/2}$. In equation (5) the standard deviation, σ, of log A_{max} is 0.273. The regression fits Copalillo data fairly well. It is interesting to note that, although the regression excluded data recorded both at CU and Cuernavaca stations to avoid possible contamination from site amplification, it also fits CU and Cuernavaca data quite well for this earthquake. To investigate whether site effect at CU is important for A_{max} from inslab earthquakes or not, in Figure 6 we plot observed and predicted values of A_{max} for 16 events listed in Table 4.

For these 16 recordings, we obtain a bias of only -0.013 and a standard error of 0.25 for log A_{max}, which shows that site effect at CU is not important for inslab earthquake, at least for A_{max}. This result, which at first glance appears surprising, is in fact in accordance with the observation of Ordaz and Singh (1992), Singh *et al.* (1995), and Pacheco and Singh (1995) that amplitudes at CU at high frequencies do not seem to be affected by site effect.

Recently, it was reported by Shapiro *et al.* (2000) that seismic waves that pass below the Popocatepétl volcano before reaching the Valley of Mexico (corresponding to events in sector 1, Fig. 7) are diminished by a factor of about one-third at values of f greater than 1 Hz as compared to those that do not cross the volcano (events from sector 2). The high attenuation was attributed to the presence of magma and partial melting of rocks below the volcano. One implication of the high attenuation is a decrease in the seismic hazard to low-rise buildings in the valley from earthquakes that originate in sector 1. The Copalillo earthquake provides a further check on this observation. The location of the event with respect to Popocatépetl (Fig. 7, bottom) shows that the waves reaching CUIG do not cross the volcano. Thus, the seismic waves from this earthquake, just like the waves from the events of sector 2, should not be abnormally diminished before reaching the valley. Indeed, as seen in Figure 7 (top), the spectral ratios, CUIG/YAIG and CUIG/PLIG, for the Copalillo earthquake, after equalizing the spectra to the common distance of CUIG (see Shapiro *et al.*, 2000, for details), confirm this.

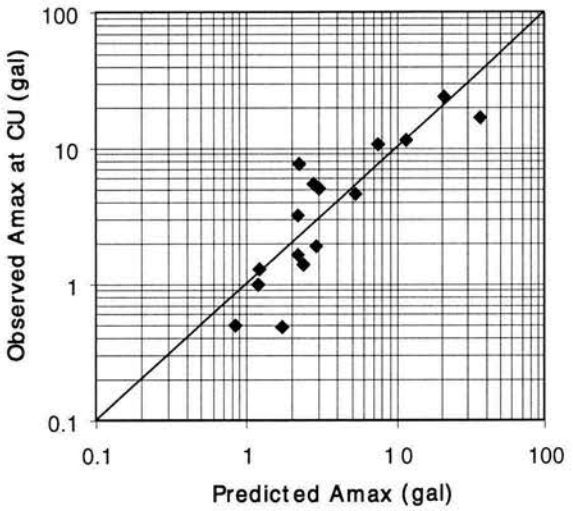

Figure 6. Observed and predicted A_{max} at station CU from inslab earthquakes. The predicted A_{max} is computed from equation (5); which was derived excluding CU data.

Table 4
Peak Accelerations Recorded at CU during Inslab Earthquakes in the Subducted Cocos Plate

Date (yyyymmdd)	Latitude (°N)	Longitude (°E)	Depth (km)	M_w	R (km)	A_{max} (N) (gal)	A_{max} (E) (gal)	A_{max} (Z) (gal)
19640706	18.310	−100.500	55	7.3	179	18.30	15.70	12.00
19730828	18.250	−96.550	82	7.0	301	(19.52)*	(17.54)*	(12.87)*
19801024	18.030	−98.270	65	7.0	173	25.30	23.50	12.50
19930805	17.429	−98.337	54	5.2	229	0.54	0.46	0.35
19940223	17.750	−97.270	75	5.8	267	1.04	0.95	0.62
19940506	18.390	−97.980	57	5.2	163	0.44	0.54	0.40
19940523	18.020	−100.570	50	6.2	206	5.00	4.30	2.90
19941210	17.982	−101.517	49	6.4	288	5.40	5.50	2.60
19970111	18.340	−102.580	40	7.1	374	4.20	5.90	3.10
19970403	18.510	−98.100	52	5.2	145	1.20	2.00	1.20
19970522	18.370	−101.820	54	6.5	298	1.70	2.10	1.70
19980420	18.350	−101.190	64	5.9	238	1.30	1.50	1.20
19990615	18.130	−97.540	60	6.9	218	11.90	11.40	7.50
19990621	18.150	−101.700	53	6.3	296	3.10	3.40	1.60
19990930	16.030	−96.960	40	7.4	435	7.80	7.70	5.10
19991229	18.000	−101.630	50	5.9	297	1.19	1.38	0.73
20000721	18.120	−98.970	49	5.9	136	12.21	9.35	5.80

*The earthquake was not recorded at CU, so it was not used in the analysis. The peak values listed here correspond to station Palacio de los Deportes.

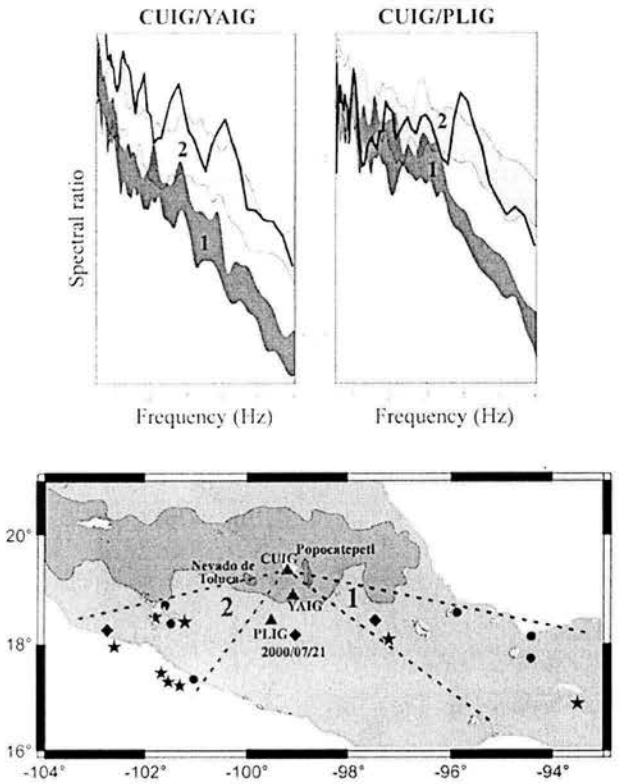

Figure 7. (Top) The spectral ratios, CUIG/YAIG and CUIG/PLIG, show that the seismic waves from events which occur in sector 1 are more diminished at CUIG than from events that occur in sector 2 (see Shapiro *et al.*, [2000] for details). As expected the spectral ratios of the Copalillo earthquake (shown by thick curves) are similar to sector 2 events. (Bottom) Earthquakes used in establishing abnormally high attenuation of seismic waves that pass below Popocatépetl. The location of the Copalillo earthquake has been added. Dots, stars, and diamonds indicate events recorded at YAIG, PLIG, and at both stations, respectively.

Estimation of Ground Motion in the Valley of Mexico during Future Earthquakes

We have used a random summation technique (Ordaz *et al.*, 1995) to synthesize expected ground motions at CU from future inslab earthquakes in the Copalillo region. The recording of the Copalillo earthquake has been used as the EGF. It is sufficient to predict the ground motions in CU because the ground motions at other sites in the Valley of Mexico can be estimated from the Fourier acceleration spectrum (FAS) at CU. The method consists of estimating FAS at these sites (from FAS at CU and the known transfer functions of these sites with respect to CU), and application of results from random vibration theory (Ordaz *et al.*, 1988; Singh *et al.*, 1988a, b; Reinoso and Ordaz, 1999).

The random summation model used in this article obeys the ω^2-source scaling law at all frequencies and produces time histories whose envelopes are realistic. The method requires specification of the seismic moments and the stress drops of the EGF and the target event. The details of the method are given in Ordaz *et al.* (1995). If only peak ground motion parameters are desired, then the computation of the time histories is bypassed; the Fourier spectrum, along with an estimation of duration (T_R) of the intense part of the ground motion, and application of results from random vibration theory (RVT) suffices (see Appendix B of Ordaz *et al.*, [1995] for relevant formulas).

In the synthesis, we take $\Delta\sigma = 360$ bar for both the EGF and the target event. The duration T_R in sec is given by $T_R = f_c^{-1} + 0.05R$, where f_c is the corner frequency (equation 4) and R is the hypocentral distance in km (Hermann, 1985). The results of the synthesis are shown in Figure 8. We note that for a M_w 7.0 earthquake in the Copalillo region (and probably also in any other region at similar focal distance from CU, except in sector 1), the expected peak acceleration (A_{max}), velocity (V_{max}), and displacement (D_{max}) at CU are about 35 gal, 7 cm/sec, and 4 cm, respectively. The corresponding values for a M_w 7.3 earthquake are about 50 gals, 10 cm/sec, and 7 cm, respectively. The predicted A_{max} as function of M_w based on regression analysis (equation 5) is also shown in Figure 8 (straight line). The predicted A_{max} from the EGF technique and the regression analysis are in very good agreement. Figure 9 illustrates samples of time histories (north–south component). Note that the waveforms are quite realistic.

We recall that the previous synthesis is based on a point-source approximation. For this approximation to be valid, L and λ should be smaller than R, where L is the source dimension, R is the hypocentral distance, and λ is the wavelength of interest. In our case, $R = 145$ km, and $\lambda \sim 20$ km. Let us assume that the rupture area, A, is square in shape. A, in km^2, is related to M_w by the following relation: $\log A = M_w - 4.0$ (e.g., Wyss, 1979; Singh *et al.*, 1980). It follows that L is about 32 km, 45 km, and 56 km for M_w 7.0, 7.3, and 7.5 earthquakes, respectively. These estimations suggest that for $M_w \leq 7.5$ events, which are of interest in this study, the point-source approximation may be valid. We further tested the validity of this approximation by using finite-source stochastic model of Beresnev and Atkinson (1997, 1998, 1999, 2001). The method requires the fault plane to be divided in subfaults whose size, Δl, in km, is given by $\log \Delta l = 0.4\ M_w - 2.0$. The subfaults are stochastic ω^2 sources. The subevent time history at a site is generated following the procedure of Boore (1983). The rupture propagates radially from a specified hypocenter, and the randomness is introduced in the subevent rupture times. A standard technique sums the contribution from each subfault. A stress parameter, which relates subfault moment and its size, is fixed at 50 bars. A free parameter, called the strength factor, sfact, which controls the level of high-frequency radiation, needs to be specified (see Beresnev and Atkinson, 1997, 1998). Other required parameters are the same as used in the estimation of the source spectrum. The azimuth of the fault

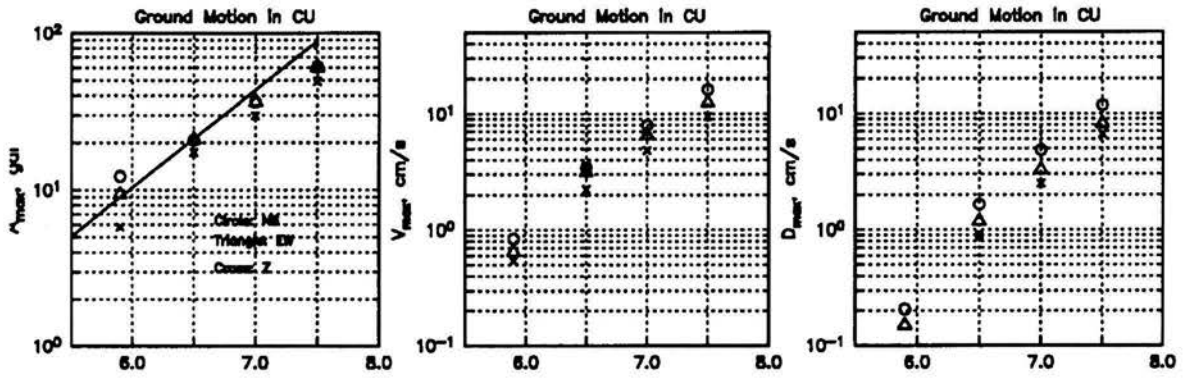

Figure 8. Expected peak ground motions at CU from postulated future large earthquakes in the region of Copalillo. The Copalillo earthquake recording has been used as empirical Green's function (EGF). A stress drop of 360 bars has been taken for both the EGF and the target event. The straight line in the left frame is the predicted A_{max} value based on regression relation given in equation (5).

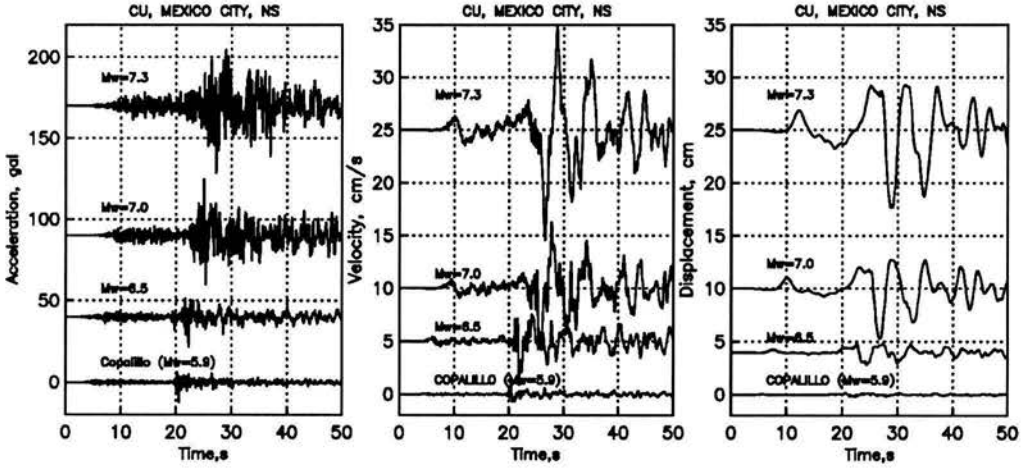

Figure 9. Samples of simulated peak ground-motions at CU (north–south component) at CU from M_w 6.5 and 7.0 earthquakes. The Copalillo recordings, used as EGF, are also shown.

and its dip were taken as 305° and 32°, respectively (Table 2). We fixed the depth of the upper edge of the fault to 50 km. We first estimated the radiation strength parameter, sfact, to be 2 by requiring that the predicted values of A_{max} for M_w 7.0 from point-source EGF method and finite-source stochastic method (with hypocenter located in the center of the rupture area) be the same. This value of sfact is reasonable in view of the large Brune's stress drop, 360 bars, for the Copalillo event. We estimated A_{max} using the finite-source model for postulate earthquakes of M_w 7.3 and 7.5 and found these values were almost identical with those predicted by the point-source EGF method. This further lends weight to the validity of the point-source approximation. Finally, we estimated the effect of the source directivity on A_{max} at CU. This effect is not included in the results of EGF simulation. To accomplish this goal, we again used the finite-source stochastic model and simulated ground motions at CU with different hypocentral locations. As expected, the largest A_{max} at CU occurs when rupture initiates at the southeast edge of the fault and propagates northwest, along the strike. However, the A_{max} values at CU are less that 8% greater than for the case of radial propagation of the rupture or, equivalently, the estimation from the point-source EGF method. These checks show that our estimations of ground motion at CU using the point-source EGF method is justified.

Figure 10 shows pseudoacceleration response spectra (5% damping), *Sa*, for the Copalillo event and postulated earthquakes of M_w 6.5, 7.0, 7.3, and 7.5 using the EGF method.

The *Sa* curve corresponding to a M_w 6.5 earthquake at a focal distance of 80 km, used in developing the design spectrum for the Federal District (Rosenblueth *et al.*, 1989, henceforth referred to as ROSS89), is shown in the Figure

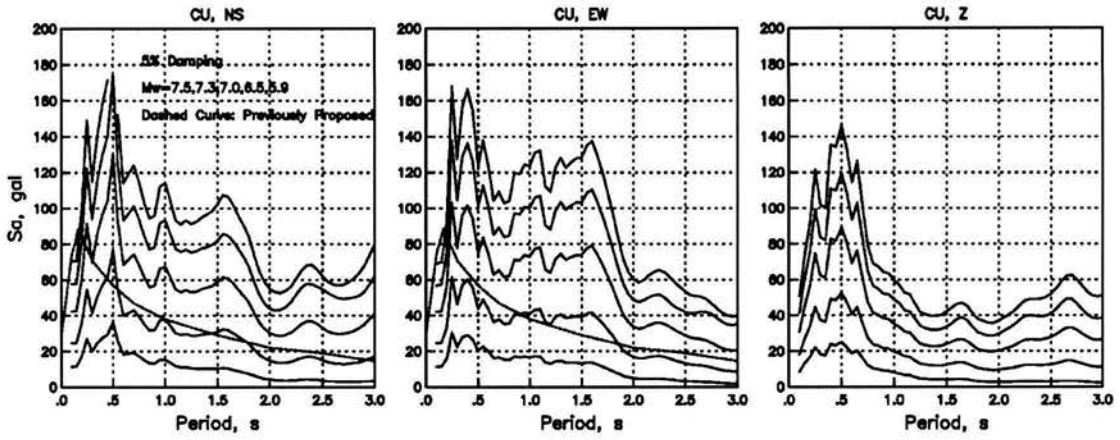

Figure 10. Expected pseudoresponse spectra (5% damping) from postulated M_w 6.5, 7.0, and 8.0 earthquakes and the computed spectra for the Copalillo earthquake at CU site. Dotted curves show the spectrum used in elaborating the design spectra for Mexico City (Rosenblueth *et al.*, 1989).

10 along with predicted *Sa* for M_w 6.5, 7.0, 7.3, and 7.5. Except at short periods (<0.5 sec), the spectra are similar for M_w 6.5 earthquakes. At short periods, *Sa* for a M_w 6.5 earthquake, computed with the recordings of the Copalillo earthquake as the EGF, are smaller than the one in ROSS89, most probably because of greater focal distance of the Copalillo earthquake. The *Sa* for $M_w \geq 7.0$ is higher at all periods as compared with the *Sa* in ROSS89.

It is of importance to know how frequently the level of A_{max} of 28 gal, contemplated in ROSS89 from inslab earthquakes, could be exceeded at CU. We note that there is no mention of this return period in ROSS89. Since a full-fledged probabilistic hazard estimation is beyond the scope of this article, we concern ourselves with a simple empirical hazard estimation.

Table 4 lists inslab earthquakes in the subducted Cocos plate that have been recorded by accelerographs in CU (except for the 1973 earthquake, which was not recorded in CU but is included in the table for completeness). The recordings are much more abundant since 1993 because of improvements in the instrumentation that were made in 1991. Figure 11 shows annual frequency of exceedance versus A_{max} based on the data from two subcatalogs: the first, complete for A_{max} values greater than or equal to 17 gal from 1964 to 1990, consists of only two earthquakes; the second, from 1991 to 2000, is believed to be complete for A_{max} values greater than or equal to 1 gal.

We note that the empirical hazard curve flattens out for A_{max} values less than 5 gal. This may be due to incompleteness of the catalog and/or due to the fact that inslab earthquakes cease to occur well before reaching the Mexican Volcanic Belt, within which Mexico City is located. The extrapolation of the straight line fit to the data for A_{max} values greater than 5 suggests that the A_{max} value of about 30 gals used in ROSS89 for this type of earthquakes could have a return period of about 40 yr. This return period of A_{max} values above 30 gal is about the same as from shallow-dipping thrust earthquakes along the Mexican subduction zone, which have been regarded as the ones posing the highest hazard for the city (Ordaz and Reyes, 1999). We are aware that the characteristics of ground motions would be different for subduction zone earthquakes as compared with an inslab earthquake with the same A_{max}, and so would be the damage patterns. However, as illustrated by Singh *et al.* (1996), inslab earthquakes with A_{max} values of about 40 gal could cause heavy damage to small buildings at certain locations of the city.

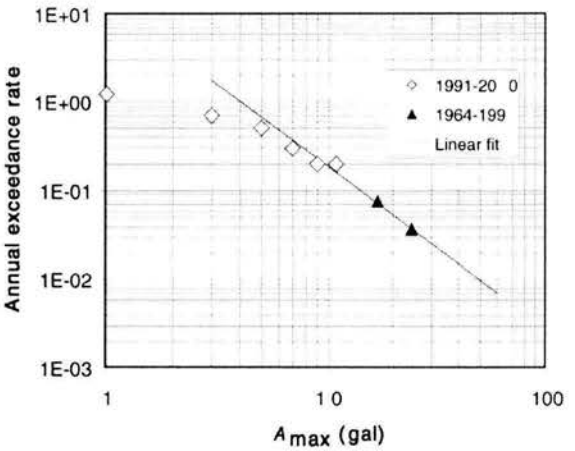

Figure 11. Empirical annual rate of exceedance vs. A_{max} at station CU from inslab earthquakes. Open symbols: data from 1991 to 2000, probably complete for $A_{max} \geq 1$ gal. Close symbols: data from 1964 to 1990, complete for $A_{max} \geq 17$ gal.

These results suggest that seismic hazard from inslab earthquakes to Mexico City has so far been underestimated, and a careful revaluation is called for.

Conclusions

1. The Copalillo earthquake occurred at a depth of about 50 km. Since the Moho in the region is probably 45-km depth, the earthquakes may have been confined to the subducted oceanic crust.
2. The inversion of near-source waveforms suggests that the northeast dipping nodal plane is the fault plane. The rupture propagated unilaterally toward northwest along the strike with a slight downdip component. The rupture velocity was about 3.5 km/sec, and much of the slip occurred over an area of 6 km $\times$ 4 km.
3. The observed source spectrum can be well explained by an ω^2-source model with $M_0 = 6.0 \times 10^{25}$ dyne cm and stress drop of 360 bars.
4. The observed A_{max} as a function of hypocentral distance is in accordance with the predicted values from a regression relationship.
5. The high-frequency ground motion ($f > 3$ Hz), as reflected by A_{max} during inslab earthquakes, is not amplified at CU, a hill-zone site in the Valley of Mexico. This is in contrast with relatively low-frequency ground motion ($f < 3$ Hz), as reflected by A_{max} from shallow, subduction-zone earthquakes, which is known to be amplified at hill-zone sites in the valley.
6. It has recently been reported that the amplitude of high-frequency ($f > 3$ Hz) seismic waves that pass through Popocatépetl Volcano is diminished by a factor of 3 before reaching Mexico City. Thus, Popocatépetl provides as a shield to Mexico City from some earthquakes. Since the wavepath from Copalillo earthquake to the city does not cross the volcano, the diminution of amplitude is neither expected nor found in the recordings.
7. Simulations using the recording at CU of the Copalillo earthquake as an EGF suggests that a M_w 7.0 event could give rise to A_{max} value of 30 to 40 gal. The pseudoacceleration response spectra (5% damping), *Sa*, from such an earthquake would exceed the *Sa* contemplated in the current design spectra for Mexico City. The A_{max} value of 30 gal could have a return period of about 40 yr at CU. This return period of A_{max} values above 30 gal is about the same as from shallow dipping thrust earthquakes along the Mexican subduction zone, which have been regarded as the ones posing the highest hazard for the city. An inslab earthquakes with A_{max} values of about 40 gal could cause heavy damage to small buildings at certain locations of the city. These results suggest that seismic hazard from inslab earthquakes to Mexico City has so far been underestimated and needs a careful revision.

Acknowledgments

We thank Igor Beresnev for providing us with his finite-source stochastic simulation program. The research was partially funded by DGAPA, UNAM Project IN109598 and CONACyT Projects 25403-A and 26185-T.

References

Anderson, J. G., J. N. Brune, J. Prince, R. Quaas, S. K. Singh, D. Almora, P. Bodin, M. Oñate, R. Vásquez, and J. M. Velasco (1994). The Guerrero accelerograph network, *Geofis. Internacional* **33,** 341–372.

Barrera, D. T. (1931). El temblor del 14 de enero de 1931, Reporte Instituto de Geologia, Universidad Nacional Autónoma de México, 40 pp.

Beresnev, I. A., and G. Atkinson (1997). Modelling finite fault radiation from the ω^n spectrum, *Bull. Seism. Soc. Am.* **87,** 67–84.

Beresnev, I. A., and G. Atkinson (1998). FINSIM: a Fortran program for simulating stochastic acceleration time histories from finite faults, *Seism. Res. Lett.* **69,** 27–32.

Beresnev, I. A., and G. Atkinson (1999). Generic finite-fault model for ground motion prediction in eastern North America, *Bull. Seism. Soc. Am.* **89,** 608–625.

Beresnev, I. A., and G. Atkinson (2001). Subevent structure of large earthquakes: a ground-motion perspective, *Geophys. Res. Lett.* **28,** 53–56.

Boore, D. M. (1983). Stochastic simulation of high-frequency ground motions based on seismological models of radiated spectra, *Bull. Seism. Soc. Am.* **73,** 1865–1884.

Bouchon, M. (1982). The complete synthetics of crustal seismic phases at regional distances, *J. Geophys. Res.* **87,** 1735–1741.

Brune, J. N. (1970). Tectonic stress and the spectra of seismic shear waves from earthquakes, *J. Geophys. Res.* **75,** 4997–5009.

Cocco, M., J. F. Pacheco, S. K. Singh, and F. Courboulex (1997). The Zihuatanejo, Mexico earthquake of December 10, 1994 (M 6.6): source characteristics and tectonic implications, *Geophys. J. Intern.* **131,** 135–145.

Cohee, B. P., and G. C. Beroza (1994). Slip distribution of the 1992 Landers earthquake and its implications for earthquake source mechanism, *Bull. Seism. Soc. Am.* **84,** 692–712.

Cotton, F., and M. Campillo (1995). Inversion of strong ground motion in the frequency domain, *J. Geophys. Res.* **100,** 3961–3975.

Hermann, R. B. (1985). An extension of random vibration theory estimates of strong ground motion at large distances, *Bull. Seism. Soc. Am.* **75,** 1447–1533.

Hernandez, B., N. Shapiro, S. K. Singh, J. F. Pacheco, F. Cotton, M. Campillo, A. Iglesias, V. Cruz, J. M. Gómez, and L. Alcántara (2001). Rupture history of September 30, 1999 intraplate earthquake of Oaxaca, Mexico (Mw = 7.5) from inversion of strong-motion data, *Geophys. Res. Lett.* **28,** 363–366.

Lomnitz, C. (1982). Direct evidence of a subducted plate under southern Mexico, *Nature* **296,** 235–238.

Nava, F. A., V. Toledo, and C. Lomnitz (1985). Plate waves and the 1980 Huajuapan de Leon, Mexico earthquake, *Tectonophysics* **112,** 463–492.

Ordaz, M., and C. Reyes (1999). Earthquake hazard in Mexico City: observations vs. computations, *Bull. Seism. Soc. Am.* **89,** 1379–1383.

Ordaz, M. and S. K. Singh (1992). Source spectra and spectral attenuation of seismic waves from Mexican earthquakes, and evidence of amplification in the hill zone of Mexico City, *Bull. Seism. Soc. Am.* **82,** 24–43.

Ordaz, M., J. Arboleda, and S. K. Singh (1995). A scheme of random summation of an empirical Green's function to estimate ground motions from future large earthquakes, *Bull. Seism. Soc. Am.* **85,** 1635–1647.

Ordaz, M., S. K. Singh, E. Reinoso, J. Lermo, J. M. Espinosa, and T. Domínguez (1988). Estimation of response spectra in the lake bed zone of the valley of Mexico during the Michoacan earthquake, *Earthquake Spectra* **4,** 815–834.

Pacheco, J. F., and S. K. Singh (1995). Estimation of ground motions in the Valley of Mexico from normal-faulting, intermediate-depth earthquakes in the subducted Cocos plate, *Earthquake Spectra* **11,** 233–248.

Pacheco, J. F., and S. K. Singh (1998). Source parameters of two moderate earthquakes estimated from a single-station, near-source recording,

and from MT inversion of regional data: a comparison of results, *Geofis. Intern.* **37,** 95–102.

Quaas, R., J. G. Anderson, and D. Almora (1987). La red acelerografica de Guerrero para registro de temblores fuertes, in *Memoria VII Congreso Nacional de Ingeniería Sísmica*, Queretaro, Mexico, 19–21 November, B40–B54.

Quaas, R., J. G. Anderson, and D. Almora (1989). La red acelerografica de Guerrero, 4 años de operación, *Ingeniería Sísmica* **36,** 53–68.

Quaas, R., J. A. Otero, S. Medina, J. M. Espinosa, H. Aguilar, and M. González (1993). *Base Nacional de Datos de Sismos Fuertes, Catálogo de Estaciones Acelerográficas 1960–1992*, Soc. Mex. Ingeniería Sísmica, A. C., Mexico, 310 pp.

Randall, G. E., C. J. Ammon, and T. J. Owens (1995). Moment tensor estimation using regional seismograms from a Tibetan plateau portable network deployment, *Geophys. Res. Lett.* **22,** 1665–1668.

Reinoso, E., and M. Ordaz (1999). Spectral ratios for Mexico City from free-field recordings, *Earthquake Spectra* **15,** 273–296.

Rosenblueth, E., M. Ordaz, F. J. Sánchez-Sesma, and S. K. Singh (1989). Design spectra for Mexico's Federal District, *Earthquake Spectra* **5,** 273–292.

Shapiro, N., S. K. Singh, A. Iglesias-Mendoza, V. Cruz-Atienza, and J. F. Pacheco (2000). Evidence of low Q below Popocatépetl, and its implication to seismic hazard in Mexico City, *Geophys. Res. Lett.* **27,** 2753–2756.

Singh, S. K., and M. Wyss (1976). Source parameters of the Orizaba earthquake of August 28, 1973, *Geofis. Internacional* **16,** 165–184.

Singh S. K., E. Bazan, and L. Esteva (1980). Expected earthquake magnitude from a fault, *Bull. Seism. Soc. Am.* **70,** 903–914.

Singh, S. K., J. Lermo, T. Domínguez, M. Ordaz, J. M. Espinosa, E. Mena, and R. Quaas (1988a). A study of relative amplification of seismic waves in the valley of Mexico with respect to a hill zone site (CU), *Earthquake Spectra* **4,** 653–674.

Singh, S. K., E. Mena, and R. Castro (1988b). Some aspects of source characteristics of 19 September 1985 Michoacan earthquake and ground motion amplification in and near Mexico city from the strong motion data, *Bull. Seism. Soc.* **78,** 451–477.

Singh, S. K., M. Ordaz, L. Alcántara, N. Shapiro, V. Kostoglodov, J. F. Pacheco, S. Alcocer, C. Gutierrez, R. Quaas, T. Mikumo, and E. Ovando (2000). The Oaxaca earthquake of September 30, 1999 (Mw = 7.5): a normal-faulting event in the subducted Cocos Plate, *Seism. Res. Lett.* **71,** 67–78.

Singh, S. K., M. Ordaz, J. F. Pacheco, R. Quaas, L. Alcántara, S. Alcocer, C. Gutirrez, R. Meli, and E. Ovando (1999). A preliminary report on the Tehuacán, México earthquake of June 15, 1999 (Mw = 7.0), *Seism. Res. Lett.* **70,** 489–504.

Singh, S. K., M. Ordaz, and L. E. Pérez-Rocha (1996). The great Mexican earthquake of 19 June 1858: expected ground motions and damage in Mexico City from a similar future event, *Bull. Seism. Soc. Am.* **86,** 1655–1666.

Singh, S. K., R. Quaas, M. Ordaz, F. Mooser, D. Almora, M. Torres, and R. Vásquez (1995). Is there truly "hard" site in the Valley of Mexico? *Geophys. Res. Lett.* **22,** 481–484.

Singh, S. K., G. Suárez, and T. Domínguez (1985). The great Oaxaca earthquake of 15 January 1931: lithosphere normal faulting in the subducted Cocos plate, *Nature* **317,** 56–58.

Wyss, M. (1979). Estimating maximum expectable magnitude of earthquakes from fault dimensions, *Geology* **7,** 336–340.

Yamamoto, J., Z. Jimenéz, and R. Mota (1984). El temblor de Huajuapan de Leon, Oaxaca, Mexico, del 24 de Octubre de (1980), *Geofis. Internacional* **23,** 83–110.

Instituto de Geofísica
UNAM, Ciudad Universitaria
04510 México
D.F., Mexico
(A.I., S.K.S., J.F.P.)

Instituto de Ingeniería
UNAM, Ciudad Universitaria
04510 México
D.F., Mexico
(S.K.S., M.O.)

Manuscript received 21 March 2001.

Capítulo II

"El sismo de Coyuca del 8 de Octubre del 2001, (Mw5.8): Una falla normal sobre la brecha sísmica de Guerrero"

El sismo de Coyuca del 8 de Octubre del 2001, (Mw=5.8): Una falla normal sobre la brecha sísmica de Guerrero.

A. Iglesias, J.F. Pacheco y S. K. Singh

Instituto de Geofisica, Universidad Nacional Autónoma de México, México, D. F. México

Introducción

El 8 de Octubre del 2001, un sismo de magnitud moderada (Mw=5.8) fue registrado cerca de la población de Coyuca de Benítez en el estado de Guerrero. Esta población está localizada cerca de la costa y justo encima de la brecha de Guerrero (figura 1). La profundidad reportada para este sismo es de ~ 8 Km. La interfase entre las placas de Norteamérica (NOAM) y la placa de Cocos subducida se encuentra a unos 20 Km de profundidad, por lo que el sismo de Coyuca se sitúa en la placa cabalgante de Norteamérica (figura 2).

El último temblor de subducción importante en la zona ocurrió en 1911 (16 de diciembre de 1911, M=7.5) y, dado que el periodo de recurrencia de la región ha sido estimado entre 60 y 70 años para sismos de magnitud 7.7 (*Nishenko y Singh 1987*), la ocurrencia de un temblor en la región podría haberse retardado por más de 30 años. Por esta razón esta zona es considerada como una brecha sísmica madura.

La colisión entre las dos placas y el estado en el ciclo sísmico, sugieren que la zona se encuentra en un régimen compresivo. Sin embargo sorprende que la solución del mecanismo focal para el sismo de Coyuca corresponda a una falla asociada a un régimen extensivo.

Algunos autores (*p. ej. Singh y Pardo, 1993*) han propuesto que la placa cabalgante de Norteamérica se encuentra en un régimen tensional, pero hasta ahora la evidencia provenía de sismos pequeños continentales lejanos a la costa. Dada su posición con respecto a la zona acoplada (justo encima), este temblor es probablemente el único evento de esta naturaleza y magnitud reportado hasta ahora, no solamente a escala local sino también a escala global.

Por otro lado, el sismo de Coyuca generó un gran número de réplicas, algunas de las cuales pudieron ser bien localizadas y permitieron restringir adecuadamente el plano de falla. En este trabajo se presenta el análisis de algunos aspectos relevantes de la fuente sísmica del temblor mencionado, así como de la distribución de sus réplicas.

Marco tectónico

La figura 1 muestra los principales rasgos tectónicos de la región central del estado de Guerrero. En la figura se observa que la denominada "brecha sísmica de Guerrero" está acotada al noroeste por el área de ruptura del sismo del 14 de Marzo de 1979 (*Valdés et al., 1981*) y al sureste por la zona de ruptura del sismo del 14 de Septiembre de 1995 (Mw=7.3).

Existe gran incertidumbre en la localización y tamaño de los sismos que ocurrieron en la zona a finales del siglo antepasado y principios del pasado, sin embargo, de acuerdo a los reportes de estos sismos la brecha sísmica podría "romper" en múltiples eventos de magnitudes en el rango de 7.5-7.8. Por otro lado, la dimensión total indica que la región puede romper en un gran evento de magnitud hasta M=8.2 (*Singh y Mortera, 1991*). En la figura 1, también se muestra la posición y el mecanismo focal del sismo de Coyuca (que se discute en una sección posterior), localizado justo encima de la brecha sísmica. La figura 2 muestra un esquema de una sección perpendicular a la trinchera donde se puede apreciar que, mientras que el sismo no tuvo una profundidad mayor a 10 Km, la interfase entre las placas de Cocos y Norteamérica se encuentra a unos 20 Km de profundidad. Por otro lado, se muestra la posición relativa (proyectada) del sismo (de trinchera) del 18 de Abril de 2002 (*Iglesias et al., 2003*) y de un deslizamiento asísmico registrado por estaciones GPS (*Kostoglodov, 2003)*. Las zonas marcadas como ~0% y ~100% acopladas y la región nombrada como de transición fueron trazadas con base en los resultados de una inversión del deslizamiento asísmico para el evento de 2002, a partir de las observaciones registradas en estaciones GPS (*Iglesias et al., 2004*).

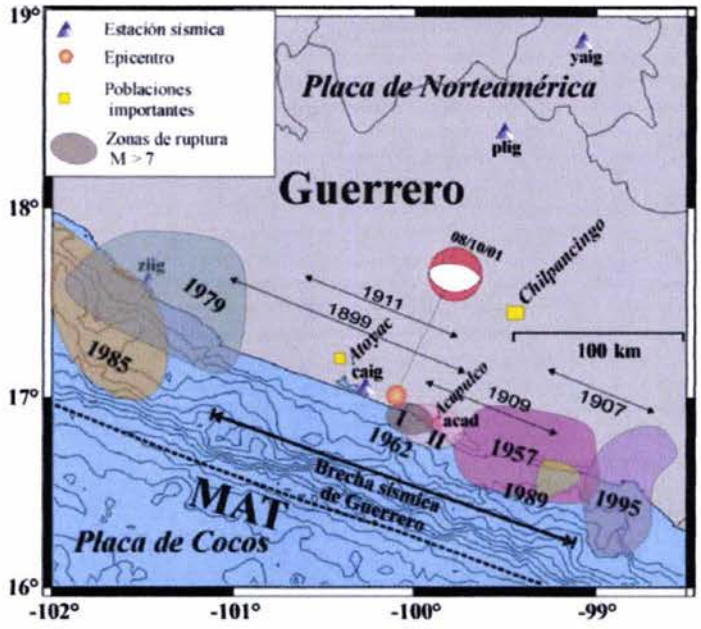

Figura 1. Rasgos tectónicos de la región central de Guerrero (ver leyenda en la figura). Con línea discontinua se muestra la posición de la trinchera mesoamericana (MAT). Las flechas dobles indican la extensión aproximada de la ruptura de los sismos de 1899,1907,1909 y 1911 (Kostoglodov et al., 2003).

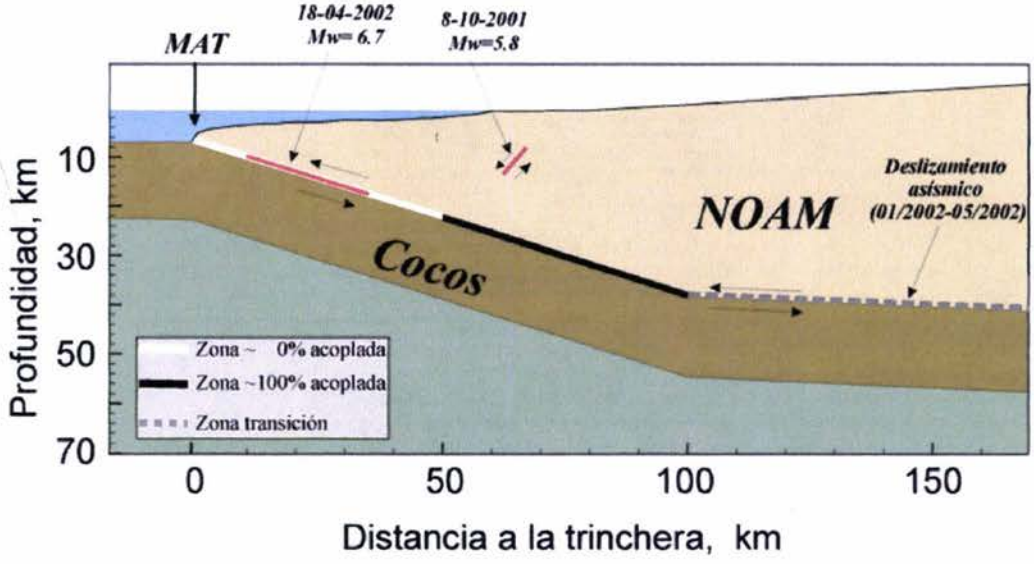

Figura 2. Esquema de una sección perpendicular a la trinchera mostrando la geometría de las placas de Cocos y Norteamérica. Se muestra la posición relativa de los sismos de Coyuca, del 18-04-2002 y del deslizamiento asísmico de principios del 2002.
Las líneas blanca, negra y discontinua muestran los diferentes grados de acoplamiento de la interfase entre las dos placas, de acuerdo con Iglesias et al. (2004) (ver texto).

Parámetros de la fuente e inversión cinemática

Las localizaciones y mecanismos focales correspondientes al sismo principal y a las cuatro réplicas más grandes, ocurridas durante los dos meses siguientes al sismo, fueron obtenidas utilizando registros de la red de banda ancha del Servicio Sismológico Nacional (SSN) y registros de movimientos fuertes de la "red acelerográfica de Guerrero" (GAA) operada por el Instituto de Ingeniería de la UNAM (I.I.) y el Centro Nacional de Prevención de Desastres (CENAPRED). La solución del tensor de momentos fue obtenida usando un esquema de inversión propuesto por *Randall et al. (1995;* ver también *Pacheco y Singh, 1998*).

Los sismogramas regionales fueron filtrados entre 10 y 50 segundos e invertidos a través de un método lineal para determinar el tensor de momentos. Con el fin de restringir la estimación para la profundidad, la inversión se lleva a cabo suponiendo diferentes profundidades. La figura 3 muestra los ajustes obtenidos para la mejor solución en la inversión del sismo principal.

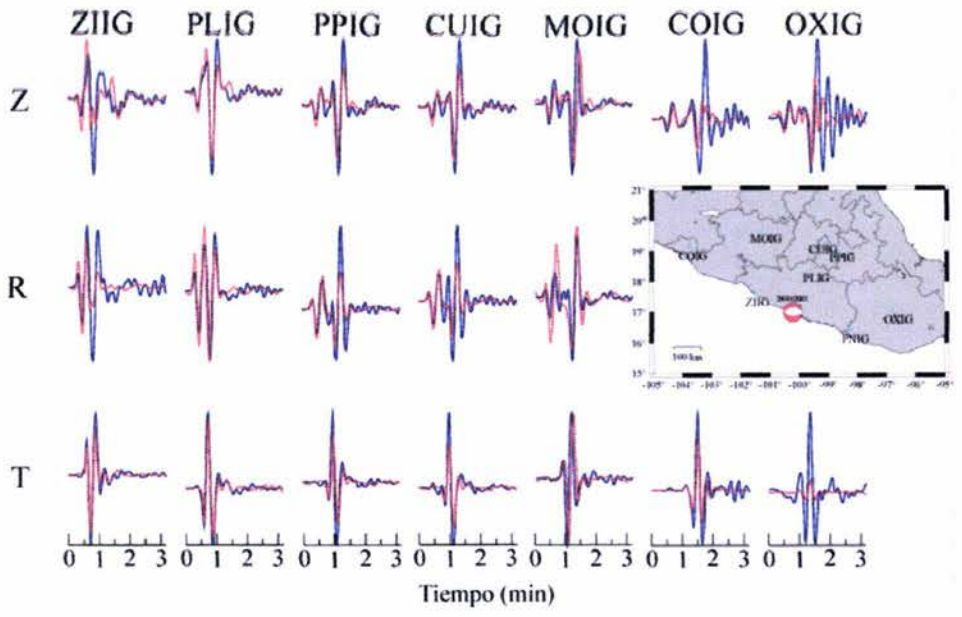

Figura 3. Ajustes obtenidos para la solución del tensor de momentos para el sismo principal

(azul: observado, rojo: sintético)

La tabla 1 muestra las localizaciones y mecanismos focales para el evento principal y las cuatro réplicas más grandes. En ella se puede observar que las réplicas también corresponden a fallas normales con orientaciones similares.

Tabla 1. Parámetros de la fuente del sismo principal y las cuatro réplicas más grandes.

Fecha	Hora	Fuente	Lat.	Lon.	Prof.	Azimut φ	Echado δ	"Rake" λ	Mw
2001-10-08	03:39:20	Regional	17.003	-100.095	8.0	281/89	49/42	-82/-99	5.8
	03:39:26	CMT	17.320	-99.890	15.0	263/105	39/53	-107/-77	5.8
2001-10-08	07:16:00	Regional	17.067	-100.095	5.0	257/99	55/37	-103/-72	4.5
2001-10-09	00:34:22	Regional	17.062	-100.088	8.0	274/97	51/39	-92/-88	4.4
2001-10-29	05:23:12	Regional	17.100	-100.135	5.0	263/95	39/52	-99/-83	5.0
	05:23:18	CMT	17.490	-99.440	15.0	240/91	44/51	-116/-67	5.0
2001-11-23	06:41:37	Regional	17.058	-100.161	8.0	258/61	54/37	-80/-103	4.6

Con el fin de determinar el patrón de deslizamiento sobre el plano de falla, se llevó a cabo una inversión en el dominio de la frecuencia utilizando datos locales. El esquema propuesto por *Cotton y Campillo (1995)*, fue modificado para emplear la técnica de inversión conocida como cristalización simulada (*Iglesias et al., 2002*). El método consiste en dividir el plano de falla en celdas de menor dimensión, para cada una de las cuales son calculadas funciones de transferencia para todas las estaciones consideradas. El cálculo de las funciones de transferencia es realizado empleando el método del número de onda discreto, propuesto por *Bouchon (1982)*. Estas funciones de transferencia son convolucionadas con una función temporal de fuente cuyos parámetros son el tiempo de inicio de la ruptura, el tiempo de ascenso (tiempo que tarda en alcanzar el máximo desplazamiento) y el deslizamiento para cada subfalla. Finalmente se suman las contribuciones de cada subfalla en el dominio de la frecuencia, con objeto de construir sismogramas sintéticos. Este cálculo de sismogramas sintéticos es empleado como problema directo dentro del esquema de inversión denominado cristalización simulada, con

el propósito de estimar los parámetros de tiempo de ruptura, tiempo de ascenso y dislocación.

En este trabajo, dedicado al estudio del sismo de Coyuca, el plano de falla fue dividido en una malla de 6 x 8 subfallas de 4 Km^2 de área. De esta forma, estudiamos un plano de falla de 12 Km a lo largo del rumbo y 16 Km a lo largo del echado. La orientación del plano de falla fue estimada a través de la inversión del tensor de momentos empleando datos locales y regionales (ϕ=281, 89; δ=49, 42, λ=–82,–99°). La distribución de las réplicas (que se discutirá adelante) muestra claramente que el plano de falla buza hacia el sur. Por esta razón, se eligió la solución correspondiente (ϕ=89°, δ=42°, λ=-99°) para la inversión.

Se utilizaron los registros de la estación CAIG de banda ancha del SSN; de las estaciones COYC, OCLL, ATYC, VNTA y ACAP de la red de acelerógrafos operados por el Instituto de Ingeniería (I. I.). Estos acelerogramas fueron integrados numéricamente dos veces, para obtener desplazamientos, y filtrados en una banda de frecuencias entre 0.1 y 0.5 Hz. Como modelo inicial se asignó un deslizamiento homogéneo de 0.1m. Los límites del tiempo de ruptura fueron calculados empleando como velocidades de propagación extremas 2.2 y 3.2 Km/s.

La figura 4 muestra la ubicación de las estaciones, así como la proyección horizontal del plano de falla utilizado para la inversión.

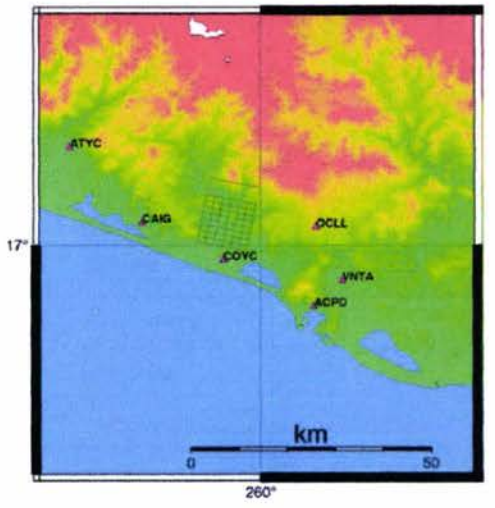

Figura 4. Mapa mostrando la localización de las estaciones, así como la proyección horizontal del plano de falla.

En la figura 5 se muestran los ajustes obtenidos a través de la inversión, mientras que en la figura 6 se muestran las distribuciones de dislocaciones, tiempos de ruptura y tiempos de ascenso (*rise time*). La figura 6 (cuadro central) muestra que la ruptura se propagó hacia la parte superior de la falla, ocurriendo el máximo deslizamiento en profundidades más someras que 10 Km. Este deslizamiento es de ~ 2 m y parece ocurrir ~5 segundos después del inicio del sismo. El tiempo de ascenso no presenta una distribución clara, evidenciando que al menos para este sismo no se tiene suficiente resolución para una buena estimación de este parámetro. El tiempo de ruptura muestra que la ruptura comienza a propagarse rápidamente hasta la zona donde ocurre el máximo desplazamiento y luego la velocidad disminuye de manera importante.

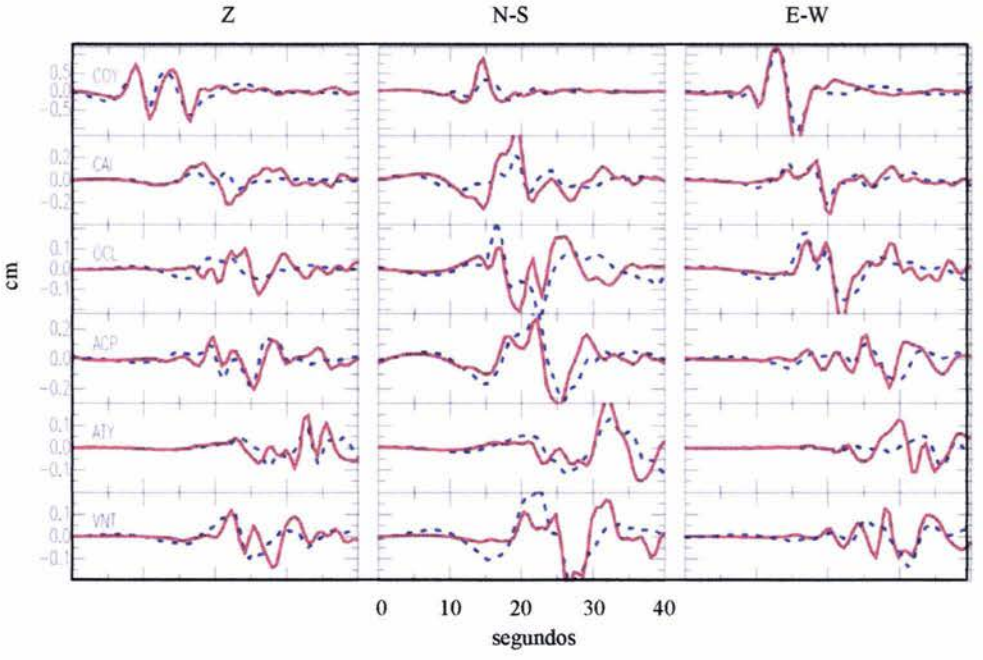

Figura 5. Ajustes obtenidos a través de la inversión cinemática. En línea continua roja se muestran los sismogramas observados y en línea discontinua azul los sintéticos.

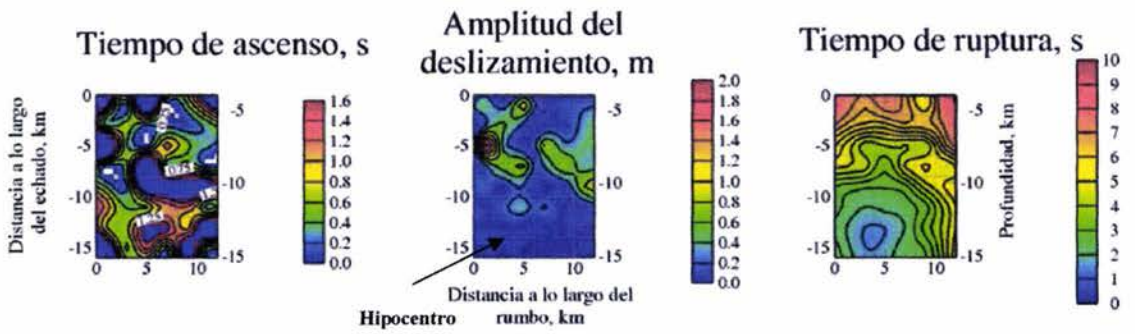

Figura 6. Modelo cinemático obtenido a través de la inversión para el plano nodal 1 (ϕ=89°, δ=49°, λ=–82°).

Análisis de la secuencia de réplicas

El sismo de Coyuca generó una larga secuencia de réplicas. Debido a la gran actividad en esta zona, se instaló una red de estaciones temporales que operó entre el 30 de octubre y el 14 de diciembre del 2001. Solamente en este período, el SSN reportó 202 réplicas asociadas al sismo de Coyuca (entre 16.75- 17.15 N y 100.5-100 W). La figura 7 muestra las localizaciones obtenidas a partir de la red de estaciones del SSN. Por otro lado la red de estaciones temporales consistió de 4 estaciones portátiles distribuidas alrededor del epicentro (figura 7). Cada una de las estaciones instaladas consistió de un sismómetro triaxial de banda ancha (Guralp, CMG-40T) y un registrador "Reftek".

La red temporal registró mas de 3000 eventos, 562 de los cuales pudieron ser localizados (registrados al menos por 3 estaciones). La figura 8 muestra la localización de los eventos registrados con la red temporal. Las localizaciones fueron llevadas a cabo usando el programa "Seisan" (*Haskov y Ottemoller, 1999*) y considerando el modelo de velocidades propuesto por *Campillo et al., 1996*. La tabla 2, muestra el modelo de velocidades usado para la localización.

Tabla 2 . Modelo de velocidades usado en el proceso de localización

Vp (km/s)	5.60	5.90	6.70	7.95
Vs (km/s)	3.23	3.41	3.87	4.59
h (km)	5.0	12.0	28.0	∞

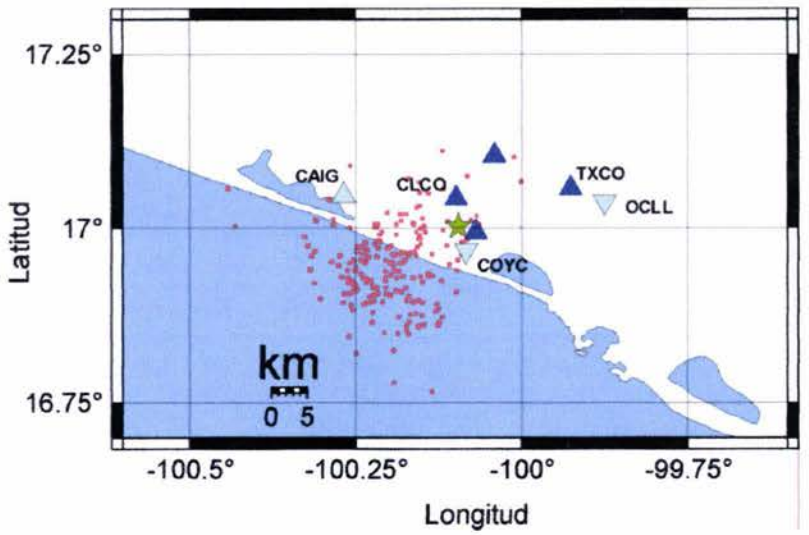

Figura 7 Localización (SSN) de las réplicas del sismo del 08 de Octubre de 2001(cuadros rojos). También se muestra la ubicación de las estaciones portátiles colocadas después del sismo de Coyuca (triángulos azul marino) y las estaciones del I.I. y del SSN (azul claro, invertido y normal, respectivamente).La localización del sismo de Coyuca es mostrada con una estrella verde.

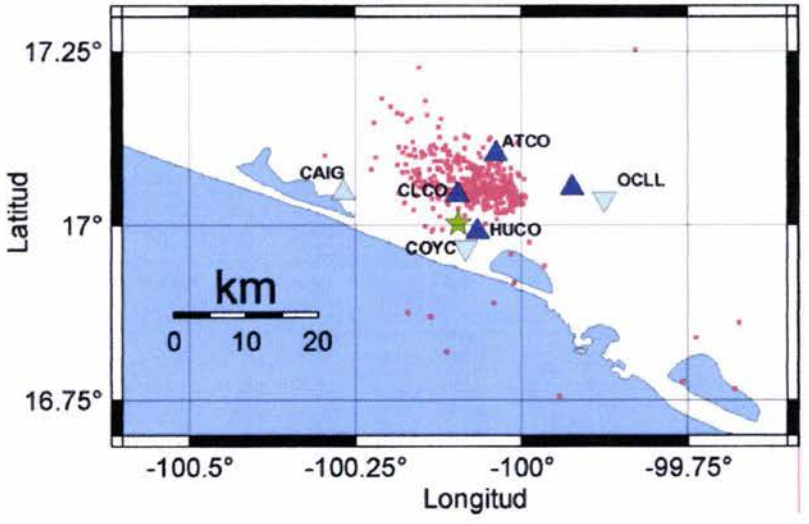

Figura 8 Localización de las réplicas del sismo del 08 de Octubre de 2001 utilizando los datos de la red de estaciones portátiles

La tabla 3 muestra el error promedio de las localizaciones usando los datos del SSN contra las localizaciones de los datos de la red temporal.

Tabla 3 . Comparación de los errores promedio de las localizaciones usando ambas redes

	err. lat. (km)	err. lon. (km)	err. prof. (km)
Datos SSN	5.68	4.87	4.55
Datos red portátil	1.91	1.64	3.5

Comparando las figuras 7 y 8 se observa que los sismos localizados con la red temporal se concentran ligeramente al norte del epicentro, mientras que las localizaciones originales del SSN son más dispersas y están localizadas en general al sur del epicentro. La tabla 1 y la distribución de las réplicas muestran que la distribución de las estaciones portátiles permite llevar a cabo localizaciones con una mayor precisión.

La distribución de estaciones de la red temporal, junto con las estaciones permanentes del I.I y del SSN, así como la distribución de las réplicas, permitieron aplicar el método de doble diferencia conocido como "HypoDD" (*Waldhauser y Ellsworth, 2001*). El método *HypoDD* localiza simultáneamente pares de eventos, utilizando tanto la diferencia de tiempos de arribo absolutos, como valores de la diferencia de tiempos relativos obtenidos a través de la correlación cruzada. El método consiste en "aparejar" eventos con tiempos de viaje similares desde el hipocentro hasta las diferentes estaciones de la red. Estos eventos, a su vez, pueden formar nuevas parejas con otros eventos, de tal manera que al final de este proceso, se tiene una red interconectada de parejas.

El problema se puede plantear mediante la expresión:

$$\frac{\partial t_k^{ij}}{\partial \mathbf{m}} \Delta \mathbf{m}^{ij} = dr_k^{ij}$$

donde:

$\Delta \mathbf{m}^{ij} = \left(\Delta dx^{ij}, \Delta dy^{ij}, \Delta dz^{ij}, \Delta d\tau^{ij}\right)$ es la diferencia entre los parámetros del sismo i con respecto del sismo j,

$\frac{\partial t_k^{ij}}{\partial \mathbf{m}}$ es la matriz de derivadas parciales del tiempo de viaje relativo (evento j - evento i) de la fase k con respecto al vector de parámetros **m**.

$dr_k^{ij} = (t_k^i - t_k^j)^{obs} - (t_k^i - t_k^j)^{cal}$ es el residual de la diferencia de tiempos entre los sismos i,j teóricos y calculados, para la fase k.

La anterior expresión corresponde a un sistema sobredeterminado, que es resuelto a través del método de mínimos cuadrados o del método de descomposición en valores singulares (SVD). El método requiere que los tiempos de viaje de los sismos sean suficientemente parecidos para formar grupos de eventos. En la secuencia de réplicas registradas algunos sismos no cumplen con este criterio y, por lo tanto, fueron descartados en el proceso de relocalización. Por esta razón se utilizaron únicamente 468 eventos, de un total de 562, a lo largo del proceso. La figura 9 muestra una comparación de las localizaciones originales y las resultantes del proceso de relocalización. Se puede notar que las réplicas relocalizadas se concentran un poco más y presentan un alineamiento Sureste-Noroeste, aparentemente. Sin embargo, el resultado más claro de la relocalización se muestra en la figura 10, donde se presentan las localizaciones de las réplicas proyectadas sobre la sección A-A'.

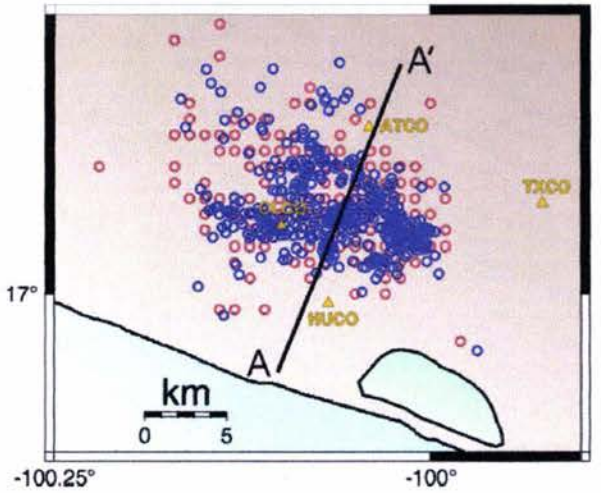

Figura 9. Relocalizaciones utilizando el método de doble diferencia (azul).

Localizaciones originales (rojo).

Después de la relocalización (figura 10, lado derecho), se observa que la franja de sismicidad sigue siendo ancha, pero es posible definir el plano de falla. Otro punto importante en esta figura es la alineación (área sombreada) de sismos que difiere de la principal, que podría asociarse con posible actividad en una falla conjugada a la falla donde ocurrió el sismo principal. Para poder determinar si esto es posible, sería necesario analizar los registros de esta zona para encontrar posibles diferencias en el mecanismo de falla.

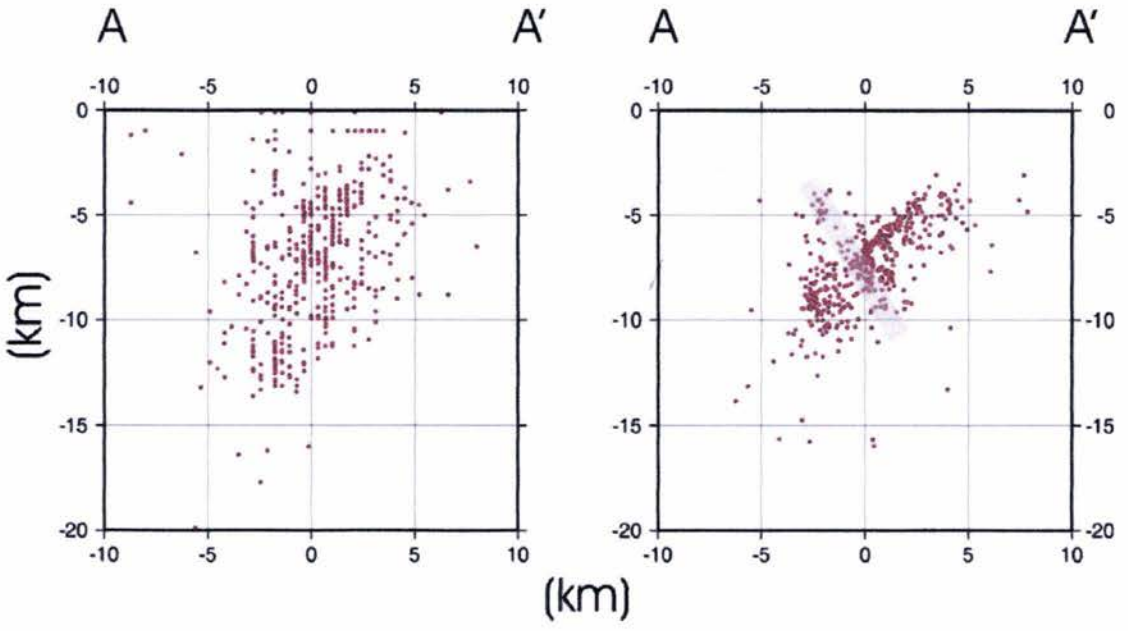

Figura 10. Sección perpendicular al plano de falla (A-A' de la figura 9).

Sismos localizados con la red temporal usando "seisan" (izquierda).

Sismos relocalizados con el método de doble diferencia (derecha).

Después de la relocalización (figura 10, lado derecho), se observa que la franja de sismicidad sigue siendo ancha, pero es posible definir el plano de falla. Otro punto importante en esta figura es la alineación (área sombreada) de sismos que difiere de la principal, que podría asociarse con posible actividad en una falla conjugada a la falla donde ocurrió el sismo principal. Para poder determinar si esto es posible, sería necesario analizar los registros de esta zona para encontrar posibles diferencias en el mecanismo de falla.

Discusión y Conclusiones

La solución del tensor de momentos muestra que el principal deslizamiento ocurrió a una profundidad somera (5-8 Km). Esto sitúa al sismo de Coyuca dentro de la placa continental de Norteamérica. Las réplicas registradas en la red temporal de estaciones de banda ancha muestran claramente que el plano de la falla buza esencialmente hacia el sur. El número de réplicas generadas por el sismo de Coyuca fue especialmente grande con respecto de la cantidad de réplicas que generan los sismos de subducción en México. Un análisis detallado de la distribución espacial y temporal de las réplicas será necesario para conocer si hubo alguna migración de la sismicidad o algún cambio sustancial en los mecanismos focales.

Existe suficiente evidencia de que la placa de Norteamérica, al menos en el centro y sur de México, se encuentra en tensión (*p. ej. Singh y Pardo, 1993; Pasquaré et al., 1988*). Sin embargo, el sismo de Coyuca es quizá la única evidencia de esfuerzos tensionales actuando sobre esta placa a menos de 80 Km. de la trinchera. Dos posibles escenarios podrían explicar este estado:

- Retroceso de la trinchera

El fenómeno del retiro o retroceso de trinchera es observado cuando el propio peso de la placa provoca que ésta se hunda y, por lo tanto, aumente el ángulo de subducción. Al aumentar este ángulo la línea de trinchera retrocede. En una zona acoplada, el desplazamiento relativo de la línea de trinchera provoca extensión en la placa cabalgante.

Las condiciones ideales para que ocurra este fenómeno incluyen una placa subduciendo con un ángulo pronunciado. Sin embargo, esta solución es poco plausible en este caso ya que la zona de subducción mexicana se caracteriza por una subducción de muy bajo ángulo (subhorizontal).

- Erosión tectónica.

El proceso de subducción implica un "desgaste" en la zona de contacto. La placa que subduce provoca que parte del material de la zona de contacto, perteneciente a la placa cabalgante, sea desgastado y acarreado a mayor profundidad. Esto induce un aumento en la pendiente del arco frontal cercano a la trinchera. La deficiencia de material en esta zona se traduce en un sistema de fallas normales y en un retroceso del frente de la placa continental.

Parece no haber ejemplos de sismos recientes de fallamiento normal en la placa cabalgante debido a este proceso. Sin embargo, existen estudios en el norte de Chile (*Delouis et al., 1998)* y en Centroamérica *(Ranero y von-Huene, 2000; Vanneucchi et al., 2001)* donde han sido observadas fallas normales, no necesariamente activas, en la placa cabalgante, que han sido atribuidas al proceso de erosión tectónica. Si bien, los procesos de erosión tectónica más evidentes se encuentran asociados a fenómenos como la subducción de montañas submarinas (lo cual no sucede en la zona de Guerrero), recientemente la zona de subducción mexicana ha sido catalogada como un margen erosivo (*p. ej. Clift y Vannucchi, 2004*) evidenciado por la falta de un prisma de acreción importante.

Una tercera posibilidad, aún no estudiada, es que el alto grado de acoplamiento entre las placas de Cocos y Norteamérica provoque lóbulos de esfuerzo tensional en zonas localizadas en los límites de la zona sellada.

En primera instancia, ninguna de las tres posibilidades puede ser descartada. Sin embargo, no existe más evidencia de sismos de fallamiento normal, al menos recientes, localizados en la placa cabalgante sobre la zona de contacto fuertemente acoplada en la brecha de Guerrero.

Por otro lado, no se puede perder de vista el deslizamiento asísmico registrado en la zona de la brecha de Guerrero. El inicio del denominado "sismo lento", a finales del 2001, guarda gran coincidencia temporal con el sismo de Coyuca. Es probable que su principal deslizamiento esté localizado justo debajo de la zona acoplada (*Iglesias et al., 2004*). Si bien es difícil establecer una correspondencia obvia entre ambos eventos, la coincidencia temporal y espacial induce a establecer una posible relación (*Kostoglodov et al., 2003*).

Por otro lado, la presencia del sismo de Coyuca sugiere la existencia de fallas normales en otras regiones costeras que pudieran generar sismos con las mismas características que el sismo de Coyuca y afectar a algunas ciudades importantes como lo son el Puerto de Acapulco.

Referencias

Bouchon, M. (1982). The complete synthetics of crustal seismic phases at regional distances, *J. Geophys. Res.* **87**, 1735-1741.

Campillo, M., S. K. Singh, N. Shapiro, J. Pacheco, y R. B. Hermann (1996). Crustal structure of the Mexican volcanic belt, based on group velocity dispersion. *Geof. Inter.*, **35**, 361-370.

Clift, P. y P. Vannucchi (2004). Controls on tectonic accretion versus erosion in subduction zones: implication for the origin and recycling of the continental crust. *Rev. Geophys.*, **42**, 1-31.

Cotton, F. y M. Campillo (1995), inversion of strong ground motion in the frequency domain, *J. Geophys. Res.* **100**, 3961-3975.

Haskov, J., y L. Ottemoller (1999). Seisan earthquake analysis software, *Seism. Res. Lett.*, **70**, 532-534.

Hernandez, B., N., Shapiro, S.K. Singh, J.F. Pacheco, F. Cotton, M. Campillo, A. Iglesias, V. Cruz, J. M. Gómez, y L. Alcántara (2001). Rupture history of September 30, 1999 intraplate earthquake of Oaxaca, Mexico (Mw=7.5) from inversion of strong-motion data, *Geophys. Res. Lett.,* **28**, 363-366

Iglesias, A., S.K. Singh, J.F. Pacheco y M. Ordaz (2002).A Source and Wave Propagation Study of the Copalillo, Mexico Earthquake of July 21, 2000 (Mw=5.9): Implications for Seismic Hazard in Mexico City from Inslab Earthquakes, *Bull. Seism. Soc. Am.,* **92,** 2, 1060-1071.

Iglesias A., S.K. Singh, J.F. Pacheco, L. Alcántara, M. Ortiz y M. Ordaz (2003). Near-Trench Mexican Earthquakes Have Anomalously Low Peak Accelerations, *Bull. Seism. Soc. Am.,* **93**, 3, 953-959,.

Iglesias A., S.K. Singh, A. Lowry, M. Santoyo, V. Kostoglodov, K. M. Larson y S.I. Franco-Sánchez . The silent earthquake of 2002 in the Guerrero seismic gap, Mexico (Mw=7.6): inversion of slip on the plate interface and some implications, *Geof. Int.*, **43**, 3, 309-317

Kostoglodov, V., Larson K. M., S. K. Singh, A. Lowry, J. A. Santiago, S. I. Franco y R. Bilham (2003). A large silent earthquake in the Guerrero seismic gap, Mexico, *Geophys. Res. Lett*. **30**, 1807.

Nishenko, S.P. y S.K. Singh (1987). Conditional probabilities for the recurrence of large and great interplate earthquakes along the mexican subduction zone, *Bull. Seism. Soc. Am.*, 77, 2095-2114.

Ortiz, M., S. K. Singh, V. Kostoglodov y J. Pacheco (2000). Source areas of the Acapulco-San Marcos, Mexico earthquakes of 1962 (M 7.1; 7.0) and 1957 (M 7.7), as constrained by tsunami and uplift records, *Geof. Int.*, **39**, 337-348.

Pacheco, J.F. y S.K. Singh (1998). Source parameters of two moderate earthquakes estimated from a single-station, near-source recording, and from MT inversion of regional data: a comparison of results, *Geof. Intern.*, **37**, 95-102, 1998.

Pasquar`e, G., V. H. Garduño, A. Tibaldi, y M. Ferrari (1988). Stress pattern evolution in the central sector of the MexicanVolcanic Belt, T*ectonophys.*, 146, 352–364, 1988.

Randall, G. R., C. J. Ammon y T. J. Owens, Moment-tensor estimation using regional seismograms from a Tibetan Plateau portable network deployment, *Geophys. Res. Lett.*, **22**, 1665-1668, 1995.

Ranero, C. y R. von Huene (2000). Subduction erosion along the Middle America Convergent Margin, Nature, **404**, 13, 748-752.

Singh, S.K. y F. Mortera (1991). Source-time functions of large Mexican subduction earthquakes, morphology of the Benioff zone and the extent of the Guerrero gap, *J. Geophys. Res.*, **96**, 21487-21502.

Singh, S.K. y M. Pardo (1993). Geometry of the Benioff Zone and state of stress in the overriding plate in Central Mexico. *Geophys. Res. Lett.*, **20**, 1483-1486.

Valdés, C., R.P. Meyer, R. Zuñiga, J. Havskov y S.K. Singh, 1982. Analysis of Petatlan aftershocks: Numbers energy release, and asperities, *J. Geophys. Res.*, **87**, 8519-8527.

Waldhauser y Ellsworth (2000). A double-difference earthquake location algorithm: Method and application to the northern Hayward Fault, California, *Bull. Seism. Soc. Am.*, **90**, 1353-1368.

Capítulo III

"El sismo silencioso de 2002 en la brecha sísmica de Guerrero, México(Mw=7.6): Inversión del deslizamiento en la interfase de las placas y algunas implicaciones"

Geofísica Internacional (2004), Vol. 43, Num. 3, pp. 309-317

The silent earthquake of 2002 in the Guerrero seismic gap, Mexico (Mw=7.6): Inversion of slip on the plate interface and some implications

A. Iglesias[1], S.K. Singh[1], A. R. Lowry[2], M. Santoyo[1], V. Kostoglodov[1], K. M. Larson[3] and S. I. Franco-Sánchez[1]

[1] *Instituto de Geofísica, Universidad Nacional Autónoma de México, México, D.F., México*

[2] *Department of Physics, University of Colorado, Boulder, Colorado, USA*

[3] *Department of Aerospace Engineering Science, University of Colorado, Boulder, Colorado, USA*

Received: February 10, 2004; accepted: March 15, 2004

RESUMEN

Con el fin de determinar la distribución de deslizamientos debida a un sismo lento que ocurrió en la interfase de las placas en la zona de la brecha sísmica de Guerrero, llevamos a cabo una inversión de los datos de posición obtenidos a través de estaciones GPS. Este sismo lento, con duración aproximada de 4 meses, fue registrado por 7 estaciones permanentes de GPS localizadas en un área de ~550x250 km^2. El mejor modelo obtenido, considerando algunas restricciones físicamente razonables, muestra que el deslizamiento ocurrió en la zona de transición a una distancia de entre 100 y 170 km de la trinchera. El deslizamiento promedio obtenido fue de alrededor de 22.5 cm (Mo~2.97 x10^{27} dyna-cm, Mw=7.6). Nuestro modelo implica un aumento en los esfuerzos de corte en la zona acoplada que se encuentra adyacente a la de transición. Esta zona acoplada es la parte sismogénica de la interfase, por lo que este modelo implica un incremento en el peligro sísmico en la región. Los resultados obtenidos para escenarios similares en otras zonas de subducción favorecen también la elección de este modelo. Sin embargo, con los datos disponibles, no es posible descartar un modelo que requiere que el deslizamiento lento invada también la zona sismogénica. Un mayor número de estaciones de GPS, así como un monitoreo más prolongado de la deformación, proporcionaría la información necesaria para discriminar entre ambos modelos.

PALABRAS CLAVE: Sismo lento, brecha sísimica de Guerrero, GPS.

ABSTRACT

We invert GPS position data to map the slip on the plate interface during an aseismic, slow-slip event, which occurred in 2002 in the Guerrero seismic gap of the Mexican subduction zone, lasted for ~4 months, and was detected by 7 continuous GPS receivers located over an area of ~550x250 km^2. Our best model, under physically reasonable constraints, shows that the slow slip occurred on the transition zone at a distance range of 100 to 170 km from the trench. The average slip was about 22.5 cm (Mo~2.97 x10^{27} dyne-cm, Mw=7.6). This model implies an increased shear stress at the bottom of the locked, seismogenic part of the interface which lies updip from the transition zone, and, hence, an enhanced seismic hazard. The results from other similar subduction zones also favor this model. However, we cannot rule out an alternative model that requires slow slip to invade the seismogenic zone as well. A definitive answer to this critical issue would require more GPS stations and long-term monitoring.

KEY WORDS: Slow earthquake, Guerrero seismic gap, GPS.

INTRODUCTION

Recent continuous geodetic observations, made possible by widespread deployment of GPS receivers, have revealed that slow slip events or silent earthquakes on plate interfaces are a relatively common phenomenon (e.g. Heki *et al.*, 1997; Dragert *et al.*, 2001; Ozawa *et al.*, 2001; Miller *et al.*, 2002). Such observations promise to revolutionize our understanding of the earthquake source process, interface coupling, the earthquake cycle, and the rheology of the plate interface.

Two silent earthquakes have been reported in the Guerrero seismic gap (Lowry *et al.*, 2001; Kostoglodov *et al.*, 2003). This gap is located along the Mexican subduction zone. It extends from 99.2°W to 101.2°W (Figure 1). No large subduction thrust earthquakes have occurred in the NW part of the gap since 1911 (Singh *et al.*, 1981). The region SE of Acapulco, up to 99.2°W, has experienced only relatively small (Mw≤7.1) earthquakes since 1957. The entire gap is about 200 km in length. If the gap were to rupture in a single earthquake, it would give rise to an event of magnitude Mw of 8.1-8.4 (Singh and Mortera, 1991). Because such an event poses great seismic hazard to Acapulco, the state of Guerrero, and to Mexico City, this region has been instrumented with seismographs, accelerographs, and GPS receivers. Figure 1 shows the 7 permanent, continuous GPS receivers that were in operation in the region in January 2003.

The first silent earthquake occurred in 1998. It was detected by the continuous GPS receiver at CAYA (Figure 1), the only station in operation at the time (Lowry *et al.*, 2001). The most active phase of the second, much larger, slow earthquake began in January 2002, and lasted for about four months (Kostoglodov *et al.*, 2003). It was recorded by seven continuous GPS receivers located over an area of ~550x250 km^2 (Figure 1). The data and a preliminary interpretation based on two-dimensional forward modeling were presented in a previous work (Kostoglodov *et al.*, 2003). In that work the authors conclude that the data could be interpreted by one of two extreme models. One model implies increased seismic hazard in the Guerrero gap (slip occurring only over the transition zone), while the second model points to diminished hazard (slip extending over the seismogenic zone). In this study, we formally invert the data, adding physical constraints, to map the slip on the plate interface. Our goal is to resolve which of the two scenarios, increased or diminished hazard, is better supported by the data. Clearly, the issue is of critical importance because of its tectonic and seismic hazard implications.

TECTONIC SETTING AND THE GEOMETRY OF THE BENIOFF ZONE

Figure 1 shows the tectonic setting of the Guerrero seismic gap. The oceanic Cocos plate subducts below continental Mexico, a part of the North American (NOAM) plate. The rate of Cocos motion relative to NOAM is ~5.6 ± 0.21 cm/yr in the direction N35°E (NUVEL-1A model, DeMets *et al.*, 1994).

Several studies deal with the geometry of the Benioff zone below Guerrero (e.g., Suárez *et al.*, 1990; Singh and Pardo, 1993). The results of these studies share a common feature: the oceanic Cocos plate enters below Mexico with a small dip (~15°), begins unbending at a distance of 100 km from the trench, and becomes subhorizontal at a distance of about 150 km. Figure 1 (bottom) shows an idealized cross section based on the locations of small and moderate earthquakes and their focal mechanisms (J. Pacheco, personal communication, 2003). In this idealization, the subducted Cocos plate enters below Mexico with a dip of 17° up to a distance of 100 km from the trench and then becomes almost horizontal (dip 2°). We will use this geometry in the inversion of the GPS data.

DATA

Kostoglodov *et al.* (2003) presented the time series of positions, relative to McDonald Observatory (MDO), Texas; of each of the seven GPS sites. These data exhibit all sites moving NE before January 2002. At this time, the sense of motion reversed and continued to do so for ~4 months. In May 2002, the motion resumed its pre-January 2002 direction at all sites. As an example, Figure 2 shows the time series of position for station CAYA during the interval January 1997 – July 2002. Silent events, one at the beginning of 1998 and another at the beginning of 2002, are highlighted in the figure.

To determine the change in the position of the sites, we took the coordinate time series relative to MDO, subtracted the difference in NUVEL1a velocities of the North American plate at MDO and each site, and inverted, via weighted least squares, for a best-fit line superimposed by a hyperbolic tangent function. Table 1 and Figure 1 summarize the resulting estimates of steady-state velocity and anomalous displacement. The motion during the slow slip was not perfectly opposite to that during the steady-state phase, instead it had a significantly less strike-parallel component of motion.

INVERSION FOR SLIP

To invert for slip on the plate interface, we use the fault geometry shown in Figure 1. The strike of the fault is chosen to coincide with the middle America trench (azimuth ϕ=289°). The length of the fault along strike is 600 km. The horizontal projection of the fault has a width of 350 km (Figure 1). The fault is subdivided into 3x4 elements, three along strike and four in the down-dip direction. A larger number of elements is not warranted in view of the small number of observations. We denote the elements by (i,j), i=1 to 3 and j=1 to 4. The elements $(2,j)$ coincide with the Guerrero seismic gap. We note that the widths of the elements along the down-dip direction have been chosen to reflect our current knowledge of the seismic behavior of the plate interface along the Mexican subduction zone. Quite generally, large, shallow thrust earthquakes in Mexico do not occur between the trench and a distance of ~50 km towards the coast. The seismogenic zone roughly extends from 50 km to 100 km, and the transition zone extends beyond 100 km. The element widths have been chosen to reflect this (Figure 1): 0-50 km; 50-100 km; 100-170 km; 170-350 km. Note that the division of the transition zone in two segments, 100 km to 170 km and 170 km to 350 km, is arbitrary. As Figure 1 shows there are more GPS sites in the Guerrero gap than in the adjacent regions. For this reason, we expect the slip on elements $(2,j)$ to be better resolved than those on other elements.

In the inversion, the displacement from each rectangular element is calculated using closed form expressions developed by Okada (1992). The rake of the slip vector, λ, is taken as an unknown parameter but is assumed to be the same for each element. The displacement from slip over the elements of the fault plane may be written as:

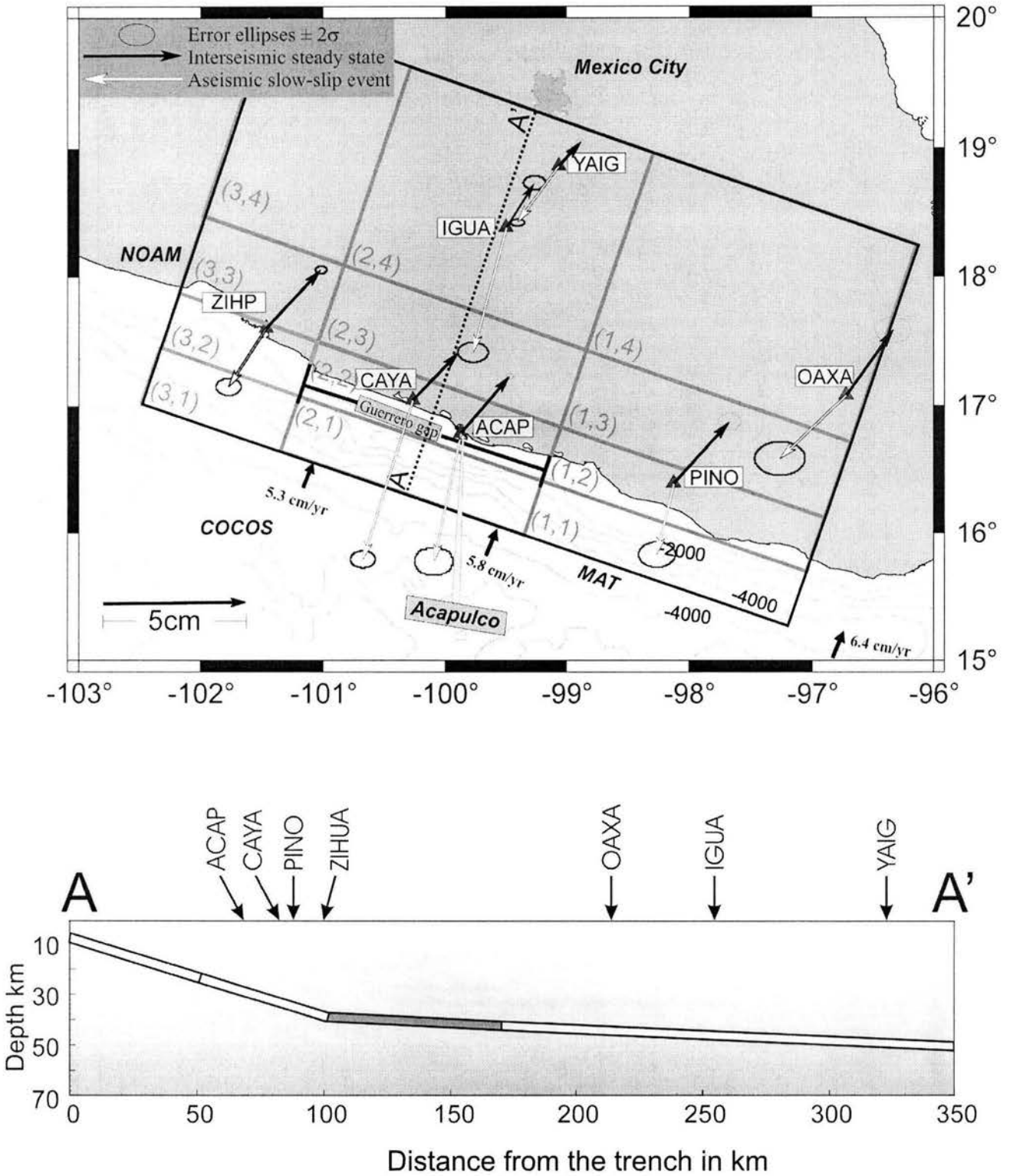

Fig. 1. (Top) Location of permanent GPS sites in and near the Guerrero seismic gap, Mexico. The vectors at the sites indicate horizontal position change for a year of interseismic, steady state strain accumulation phase (dark arrows) and during the January-April, 2002 slow-slip (white arrows). The vectors near the mid-America trench (MAT) illustrate velocity of Cocos plate relative to NOAM plate. Large rectangle is the horizontal projection of the plate interface over which the slip was inverted from the GPS data. The rectangle is divided in (3x4) elements. The element number is shown in parentheses. Guerrero gap coincides with elements (2,j). (Bottom) Idealized geometry of the Benioff zone along AA' used in the inversion. The white and the dark segments of the interface indicate the element widths.

Table 1

Position change of GPS sites in southern Mexico relative to McDonald Observatory, Texas. Z is positive upward. σ is the standard deviation.

Site	Steady-state phase (yearly)			Slow-event phase Jan-Apr 2002 (4 months)		
	$\Delta N \pm \sigma_N$ (cm)	$\Delta E \pm \sigma_E$ (cm)	$\Delta Z \pm \sigma_z$ (cm)	$\Delta N \pm \sigma_N$ (cm)	$\Delta E \pm \sigma_E$ (cm)	$\Delta Z \pm \sigma_z$ (cm)
CAYA	1.64±0.01	1.60±0.02	1.04±0.06	-5.57±0.06	-1.76±0.09	-6.12±0.27
ACAP	1.96±0.02	1.71±0.03	1.50±0.10	-4.49±0.05	-0.96±0.07	-2.05±0.22
IGUA	1.54±0.05	0.99±0.08	-0.47±0.23	-4.35±0.07	-1.18±0.11	1.98±0.34
YAIG	0.83±0.02	0.77±0.03	0.77±0.08	-1.97±0.05	-1.47±0.10	2.90±0.26
ZIHP	2.02±0.04	1.89±0.06	-0.22±0.18	-2.04±0.06	-1.33±0.09	-6.00±0.26
PINO	2.13±0.06	1.92±0.08	1.14±0.24	-2.50±0.09	-0.60±0.13	-7.20±0.38
OAXA	2.24±0.09	1.63±0.13	-1.58±0.38	-2.20±0.12	-2.34±0.18	3.28±0.50

$$u_k = \sum_{i=1}^{3}\sum_{j=1}^{4}(Gd_{i,j}^{k} * S_{i,j} * \boldsymbol{sin}(\lambda) + Gs_{i,j}^{k} * \boldsymbol{cos}(\lambda)) \quad ,$$

where u_k is the displacement vector at station k, $Gd_{i,j}^{k}$ and $Gs_{i,j}^{k}$ are the displacements at station k due to the unit pure dip slip and unit pure strike slip on the (i,j) element, respectively, and $S_{i,j}$ is the slip on the (i,j) element.

We invert for slip distribution using a simulated annealing algorithm. This algorithm allows us flexibility in imposing constraints on the misfit function and to assign weights to the data. Recently, the simulated annealing algorithm has been applied to solve some inverse problems in seismology (e.g., Hartzell and Liu, 1995; Courboulex *et al.*, 1996; Iglesias *et al.*, 2001). The method explores the whole model solution space using a procedure based on the equations that govern the thermodynamic process known as annealing (Kirkpatrick *et al.*, 1983). Several works show that this process guides efficiently the search to reach a global minimum of misfit. Some details of this inversion technique may be found in Goffe *et al.* (1994) and Iglesias *et al.* (2001).

As misfit function to minimize, we choose an L2 norm:

$$misfit = \sqrt{\sum_{L=1}^{n}\left(u_L^{obs} - u_L^{pre}\right)^2 * w_L} \quad ,$$

where n is the number of data points (n=number of components multiplied by number of stations), u_L^{obs}, u_L^{pre} are the observed and predicted displacements for the L-th component-station and w_L (weight for each component-station) is the reciprocal of standard deviation over data (σ) .

Slow-slip phase

The data set consists of 21 values. The unknown parameters are 13, corresponding to 12 slip amplitudes on (3x4) elements and 1 slip direction. First we inverted for the slip distribution without any further constraint. The results showed a large slip on the element (2,3) that lies between 100 and 170 km from the trench. The slip on this element was at least twice greater than on any other element. We then performed several tests by changing the number of elements in the down-dip direction. Basically, the solutions showed that the slip on the central strip (2,*j*) (corresponding to the Guerrero seismic gap) is well resolved. The slip on the elements (1,*j*) and (3,*j*), however, significantly changed with any change in the number of the elements, indicating that the slip distribution on these elements is not well resolved from the available data. These initial tests suggest that the solutions are unstable because of a large number of parameters (13), relatively small number of data points (21), and their spatial distribution.

Before performing additional inversions, we imposed further constraints that are physically reasonable. We required that the slip on the elements (*i*,1) be equal. The same constraint was imposed on the elements (*i*,4). These bands represent the shallowest and deepest portion of our model (Figure 1). In the initial tests, the lateral elements (1,2), (1,3), (3,2), (3,3) had shown significant instability due to lack of stations. For this reason, we constructed bigger blocks by

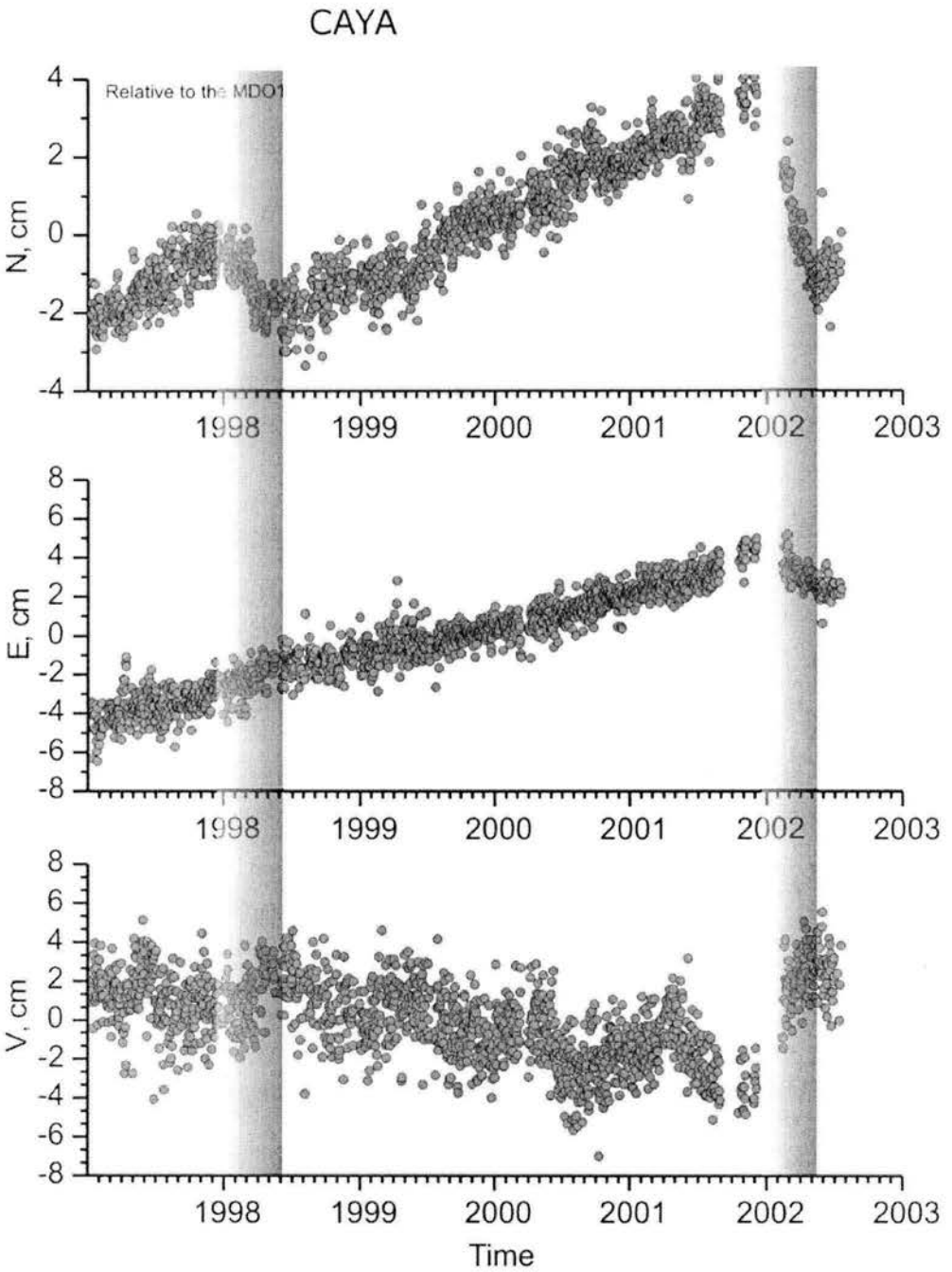

Fig. 2. Time series of the position of CAYA station for the interval from January 1997 to July 2003. Shaded rectangles show the two silent events recorded by the station. (Modified from Kostoglodov *et al.*, 2003)

setting the slip on (1,2) to be equal to that on (1,3) and the slip on (3,2) to be equal to that on (3,3). These constraints reduced the number of free parameters from 13 to 7. Physically, the slip at the boundaries of the elements must be continuous. In our inversion, however, we have not imposed this condition. The result of the inversion is shown in Figure 3 (top). We point out that the misfit resulting from this model (10.8 cm) is similar to that from the model where slip on each of the 13 elements is free (7.9 cm). The total seismic moment release, assuming a rigidity $\mu=3.5 \times 10^{11}$ dyne/cm^2, is 2.97×10^{27} dyne-cm (Mw7.6).

Figure 3 (top) shows that the slow slip was mostly confined to the element (2,3). This element extends from 100 to

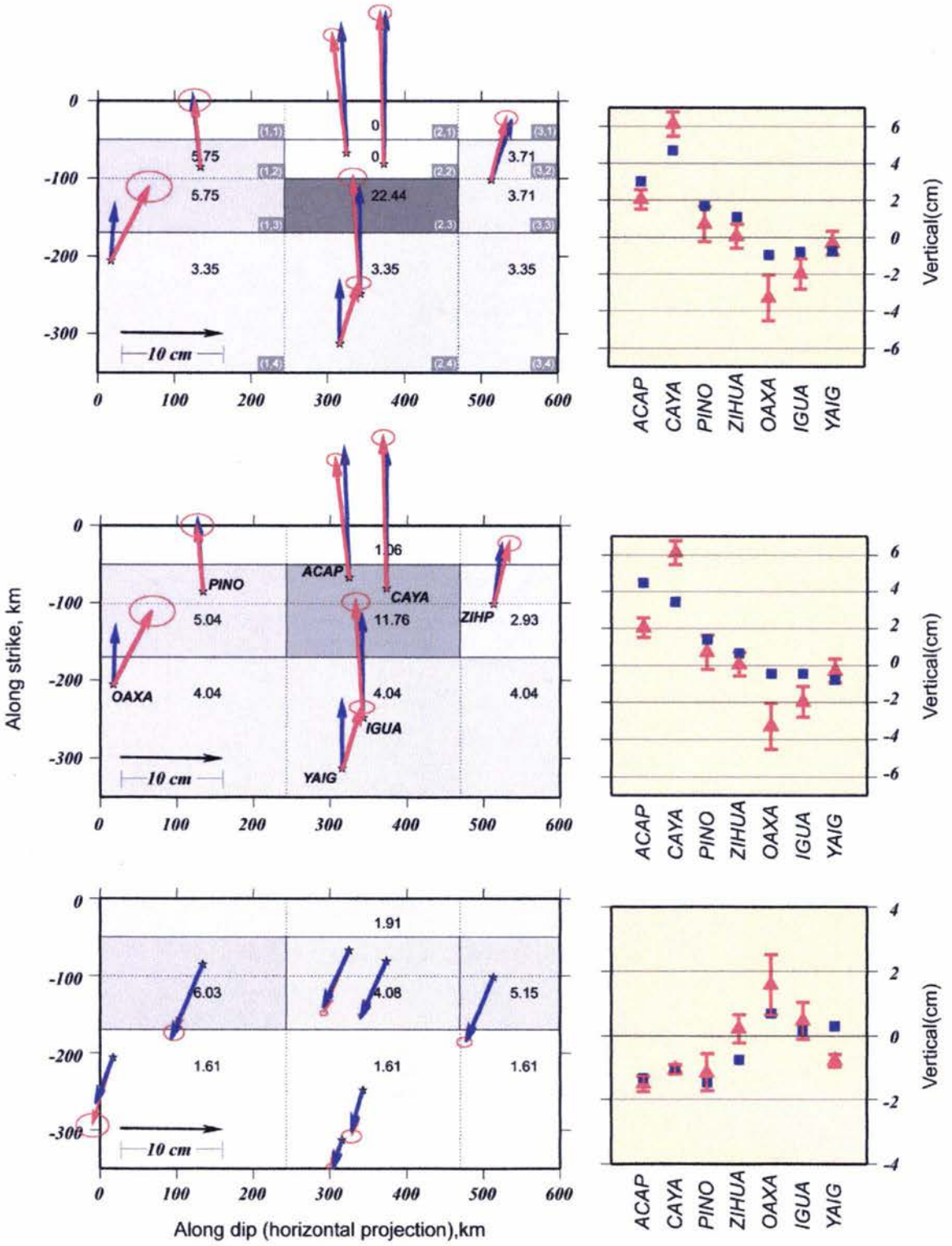

Fig. 3. (Top) Slip distribution on the plate interface obtained from inversion of the GPS data during the slow-slip phase (January-April, 2002; 4 months). The area in the figure corresponds to the rectangle shown in Figure 1. The numbers in parentheses indicate elements as in Figure 1 (top). Elements separated by dashed lines have been merged. Vectors shown by continuous and dashed lines indicate observed and calculated displacements, respectively. For clarity, vertical components are shown to the right side of the figure. (Middle) Same as top but with elements (2,2) and (2,3) merged together. (Bottom) Same as middle but for the steady-state velocities.

170 km from the trench and corresponds to the transition zone. This segment of the plate interface slipped about 22.5 cm in 4 months. The slip direction (rake) was 91°. The parameters of the slow slip on the interface can be described by the usual convention for focal mechanisms: φ = 288°, δ=2°, λ=91°. No slip occurred on the elements (2,1) and (2,2). The observed position change at sites IGUA and YAIG, however, requires a slip on the element (2,4). It is important to note that the amount of slip on elements (2,3) and (2,4) depends on the widths of the elements. A smaller width would result in a larger slip and vice versa.

As mentioned above, a critical question is whether the slow slip also extended over the seismogenic zone of the Guerrero gap (element (2,2)). To test this possibility, we merged elements (2,3) and (2,4) together. The result of this inversion is shown in Figure 3 (middle). The slip on the two merged elements is ~11.8 cm. The slip direction is 91°. The total seismic moment release (3.05 x10^{27} dyne-cm) is very similar to the previous case. The misfit (10.8 cm) is slightly greater and the fit to the vertical components is now worse than in the previous case. Thus, the results of the inversions favor a slow slip that was mostly confined to the transition zone, in the distance range of 100 to 170 km from the trench (Figure 3, top). This is our best model.

Steady-state phase

The data on yearly position change of GPS sites during the steady-state phase of the deformation (Table 1) were inverted using the same fault geometry and constraints as in the previous case. The slip distribution, shown in Figure 3 (bottom), suggests that in the Guerrero gap (elements (2,j)) the data can be explained by an average back slip (20) of ~4.1 cm on the plate interface between 50 and 170 km from the trench (elements (2,2) and (2,3)). The plate interface further down dip, in the distance range of 170 to 350 km from the trench (element (2,4)), requires a back slip of ~1.6 cm. The back slip in this element appears to be real in view of the position change of inland sites of IGUA and YAIG (Figure 1). The inversion also shows that the elements nearest to the trench (i,1) require a back slip of ~1.9 cm. The back slip on the lateral elements (1,2) and (1,3), and (3,2) and (3,3) are ~ 6 cm and 5 cm, respectively. The direction of back slip (rake) is -108°, which is consistent with the direction of convergence of Cocos with respect to NOAM of 35°.

DISCUSSION AND CONCLUSIONS

The displacement vectors at GPS sites above the subduction zone of Guerrero, Mexico, during the steady-state phase of strain accumulation are in agreement with the relative convergence of Cocos with respect to NOAM (5.6 cm/yr towards N35°E). The inversion of the GPS data, with

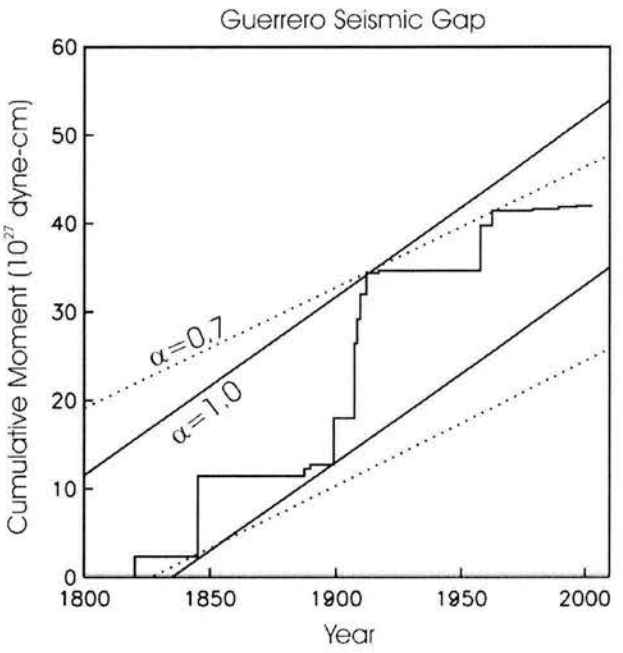

Fig. 4. Cumulative seismic moment release curve for the Guerrero region; modified from Anderson *et al.*, 1989. Slopes of the parallel lines, both of which envelop the curve, correspond to 100% seismic coupling (α=1.0, continuous lines) and 70% coupling (α=0.7, dashed lines) (see text).

physically reasonable constraints, shows an almost completely locked plate interface in the distance range of 50 to 170 km from the trench and a partially locked (~35%) interface further down dip between 170 and 350 km from the trench (Figure 3, bottom). The direction of the back slip vector, -108°, is consistent with the direction of the relative convergence vector.

The reversed motion of the GPS sites, which began in January 2002 and lasted for around four months, demonstrates the occurrence of a large silent earthquake. Our best model shows that the slow slip occurred below the Guerrero seismic gap on the plate interface that extends from ~100 to 170 km (slip ~22.5 cm) and from 170 to 350 km (slip ~3.5 cm). The direction of slow slip was 91°. In this model, the slow slip did not extend over the upper, locked portion of plate interface (~50 to 100 km from the trench). Thus the slip of 22.5 cm in four months cancelled the strain accumulated on the element (2,3) (~100 to 170 km from the trench; Figure 3, top) during about five years of steady-state loading. This is our preferred model. A consequence of this model is an increased shear stress at the bottom of the locked interface, thus enhancing the probability of rupture of the Guerrero seismic gap in the near future. Support for this model comes from slow slip on the transition zone reported in other regions where the age and relative speed of the subducting plate is similar, e.g., (Draggert *et al.*, 2001) and before 1944

Tonankai and 1946 Nankaido great earthquakes in Japan (Linde and Sacks, 2002).

The alternative model, in which slow slip extends over the seismogenic zone, results in larger misfit than in the previous case. Nevertheless, we cannot discard this model on this basis alone, since the difference in the misfit between the two models is significant at only about 85% confidence. If, indeed, this is the correct model, then the slow event liberated some fraction of the accumulated strain, thus diminishing the seismic hazard in the near future. This fraction cannot be estimated from the GPS data since they cover only a short time span.

Which of the two models is in better agreement with seismic history of the region? The cumulative seismic moment release in Guerrero gap as a function of time, for the period 1800-2003 (modified from Anderson *et al.*, 1989), is shown in Figure 4. The figure includes two sets of parallel lines both of which envelop the moment release. The slopes of these two sets of lines, 0.20×10^{27} and 0.14×10^{27}dyne-cm/yr, correspond to perfect seismic coupling ($\alpha=1.0$) and partial seismic coupling ($\alpha=0.7$), respectively. In computing these slopes, we have assumed a seismogenic zone with width=50 km, length=200 km, relative plate velocity=5.8 cm/yr, and rigidity $\mu=3.5 \times 10^{11}$ dyne/cm^2. As can be seen from Figure 4, the time series is not long enough to discriminate between a fully-coupled and a partially-coupled seismogenic interface.

It will require more extensive data to map the process of strain accumulation and release in the region. If the process is non-periodic in Guerrero, as it appears to be the case (Kostoglodov *et al.*, 2002), then a more definitive answer may require very long-term monitoring as well.

ACKNOWLEDGMENTS

Fruitful conversations with Javier Pacheco and Shoichi Yoshioka are acknowledged. This research was partially funded by CONACYT grants G25842-T, 37293-T, PAPIIT grant IN104801, and NSF grants EAR 9725712 and 0125618.

BIBLIOGRAPHY

ANDERSON, J. G., S. K. SINGH, J. M. ESPÍNDOLA and J. YAMAMOTO, 1989. Seismic train release in the Mexican subduction thrust. *Phys. Earth Planet. Int., 58*, 307-322.

COURBOULEX F., J. VIRIEUX, A. DESCHAMPS, D. GIBERT and A. ZOLLO, 1996. Source investigation of small events using empirical Green functions and simulated annealing. *Geophys. J. Int., 125*, 768-780.

DEMETS, C., R. GORDON, D. ARGUS and R. STEIN, 1994. Effect of recent revisions to the geomagnetic reversal time scale on estimates of current plate motions. *Geophys. Res. Lett., 21*, 2191-2194

DRAGERT, H., K. WANG, K. and T. S. JAMES, 2001. A silent slip event on the deeper Cascadia subduction interface. *Science, 292*, 1525-1528.

GOFFE, W., G. D. FERRIER and J. ROGERS, 1994. Global optimization of statistical functions with simulated annealing. *J. Econom., 60*, 65-100.

HARTZELL, S. and P. LIU, 1995. Determination of earthquake source parameters using a hybrid global search algorithm. *Bull. Seism. Soc. Am., 85*, 516-524.

HEKI, K., S. MIYAZAKI and H. TSUJI, 1997. Silent fault slip following an interplate thrust earthquake at the Japan Trench. *Nature, 386*, 595-597

IGLESIAS, A., V. M. CRUZ-ATIENZA, N. M. SHAPIRO, and J. F. PACHECO, 2001. Crustal structure of south-central Mexico estimated from the inversion of surface -wave dispersion curves using genetic and simulated annealing algorithms. *Geofís. Int., 40*, 181-190.

KIRKPATRICK, S., C. D. GELATT and M. P. VECCHI, 1983. Optimization by simulated annealing. *Science, 220*, 671-680.

KOSTOGLODOV, V., S. K. SINGH, W. HUTTON, O. SÁNCHEZ, K. M. LARSON and A. R. LOWRY, 2002. How frequent are subduction aseismic slip events in Guerrero, Mexico. *Seism. Res. Lett., 73*, 245.

KOSTOGLODOV, V., S. K. SINGH, J. A. SANTIAGO, S. I. FRANCO, K. M. LARSON, A. R. LOWRY and R. BILHAM, 2003. A silent earthquake in the Guerrero seismic gap, Mexico. *Geophys. Res. Lett., 30*, 1807.

LINDE, A. T. and I. S. SACKS, 2002. Slow earthquakes and great earthquakes along the Nankai trough. *Earth Planet. Sc. Lett., 203*, 265-275.

LOWRY, A. R., K. M. LARSON, V. KOSTOGLODOV and R. BILHAM, 2001. Transient fault slip in Guerrero, southern Mexico. *Geophys. Res. Lett., 28*, 3753-3756.

MILLER, M. M., T. MELBOURNE, D. J. JOHNSON and W. Q. SUMNER, 2002. Periodic slow earthquakes from the Cascadia subduction zone. *Science, 295*, 2423.

OKADA,Y., 1992. Internal deformation due to shear and tensile faults in a half-space. *Bull.Seism. Soc. Am., 82*, 1018-1040.

OZAWA, S., M. MURAKAMI and T. TADA, 2001. Time-dependent inversion study of the slow thrust event in the Nankai trough subduction zone, southwestern, Japan. *J. Geophys. Res., 106*, 787-802.

SAVAGE, J. C., 1983. A dislocation model of strain accumulation and release at a subduction zone. *J. Geophys. Res., 88*, 4984-4996.

SINGH, S. K., J. HAVSKOV and L. ASTIZ, 1981. Seismic gaps and recurrence periods of large earthquakes along the Mexican subduction zone. *Bull. Seism. Soc. Am., 71*, 827 843.

SINGH, S. K. and F. MORTERA, 1991. Source-time functions of large Mexican subduction earthquakes, morphology of the Benioff zone and the extent of the Guerrero gap. *J. Geophys. Res., 96*, 21487-21502.

SINGH, S. K. and M. PARDO, 1993. Geometry of the Benioff zone and state of stress in the overriding plate in central Mexico. *Geophys. Res. Lett., 20*, 1483-1486.

SUÁREZ, G., T. MONFRET, G. WITTLINGER and C. DAVID, 1990. Geometry of subduction and depth of the seismogenic zone in the Guerrero gap, Mexico. *Nature, 345*, 336-338.

A. Iglesias[1], S.K. Singh[1], A. R. Lowry[2], M. Santoyo[1], V. Kostoglodov[1], K. M. Larson[3] and S. I. Franco-Sánchez[1]

[1] *Instituto de Geofísica, Universidad Nacional Autónoma de México, México, D.F., México*
Email: "Arturo Iglesias" <amg@ollin.igeofcu.unam.mx>
[2] *Department of Physics, University of Colorado, Boulder, Colorado, USA*
[3] *Department of Aerospace Engineering Science, University of Colorado, Boulder, Colorado, USA*

Capítulo IV

"Los sismos de trinchera en México presentan aceleraciones máximas anómalamente bajas"

Bulletin of the Seismological Society of America, Vol. 93, No. 2, pp. 953–959, April 2003

Near-Trench Mexican Earthquakes Have Anomalously Low Peak Accelerations

by A. Iglesias, S. K. Singh, J. F. Pacheco, L. Alcántara, M. Ortiz, and M. Ordaz

Abstract It has previously been reported that regional seismograms of earthquakes that occur near the Middle America trench are relatively deficient at high frequencies. Based on this observation, an algorithm has been proposed for detecting potentially tsunamigenic earthquakes and issuing tsunami alerts. It is reasonable to expect relatively low peak accelerations during these earthquakes. In this note, we present evidence that this is indeed the case. This explains why the seismic alert system for Mexico City, with sensors located along the coast, does not trigger during some earthquakes. Low peak accelerations from near-trench earthquakes also have important implications in seismic hazard estimation.

Introduction

Shapiro *et al.* (1998) showed that earthquakes in Mexico that occur near the Middle America trench are abnormally depleted in high-frequency radiation at the broadband station CUIG, located in Ciudad Universitaria, Mexico City. This station lies about 300 km from the nearest point of the Pacific coast (Fig. 1). Shapiro *et al.* suggested that the converse may also be true, that is, all events depleted in high-frequency radiation at CUIG may be located near the trench. Because of their near-trench location, these earthquakes, if they are large enough in magnitude, are potentially tsunamigenic. Indeed, on the basis of these observations, Shapiro *et al.* proposed a fast and simple method for identifying tsunamigenic earthquakes along the Mexican subduction zone. The method relies on the ratio of the total radiated energy to the high-frequency energy ($f \geq 1$ Hz), ER, computed from the CUIG seismograms. The same seismograms are also used to compute preliminary magnitudes, M_a and M_e, of Mexican earthquakes (Singh and Pacheco, 1994). M_a is based on the amplitude of long-period (15–30 sec) waves, while M_e is based on seismic energy computed from the seismograms at CUIG. These magnitudes are related to M_w. The estimation of magnitude and ER can be accomplished in about 5 min after the origin of the earthquake, and a useful tsunami alert can be issued. A precise location of the event is not required; an ER greater than 100 is found to be sufficient evidence that the earthquake is near trench.

Since the near-trench events are depleted in high-frequency radiation, it follows that during such earthquakes the peak accelerations, A_{max}, at CUIG and other stations in the Valley of Mexico would be less than during near-coast earthquakes of the same magnitude. It also seems reasonable to expect relatively low A_{max} along the coast for near-trench earthquakes. Unfortunately, the issue of A_{max} from near-trench earthquakes was not addressed in the previous article.

The recent earthquake of 18 April 2002, 05:03 (M_w 6.7), has motivated us to look at this issue carefully. The earthquake was located about 55 km from the coast of Guerrero, Mexico (Fig. 1). This part of the coast is instrumented by the Guerrero Accelerograph Array (GAA) (Anderson *et al.*, 1994) and the Seismic Alert System (Sistema de Alerta Sismica [SAS]) (Espinosa Aranda *et al.*, 1995). The goal of SAS is real-time detection of earthquakes that may be damaging to Mexico City and alerting the population of the city of incoming strong ground motions. The magnitude and location of the earthquake of 18 April was such that it should have triggered the SAS stations. However, the peak accelerations at SAS sensors, apparently, did not exceed 5 Gal and, for this reason, the system did not trigger (J. M. Espinosa, personal comm., 2002). The GAA stations were located at $R \geq 65$ km (Fig. 1). A visit to the closest seven GAA stations (65 km $\leq R \leq$ 136 km), shown in Figure 1, revealed that none of them triggered during the event, indicating that the A_{max} was less than 3 Gal, the trigger level at these sites. The low accelerations along the coast and in the Valley of Mexico (where only a few stations in the lake-bed zone triggered) immediately raised questions about the accuracy of the magnitude and the location of the earthquake. Since this scenario is likely to recur in the future, it is important to understand the cause of this discrepancy.

In this note we show that the discrepancy arose because the earthquake was located near the trench. We find that the peak accelerations along the coast and in the Valley of Mexico from near-trench earthquakes are indeed less than those during the near-coast events. Thus, the earthquakes that are deficient in high-frequency radiation at the broadband station of CUIG (with ER > 100) are potentially tsunamigenic. This is the bad news. The good news is that they give rise to relatively low peak accelerations at the coastal and inland

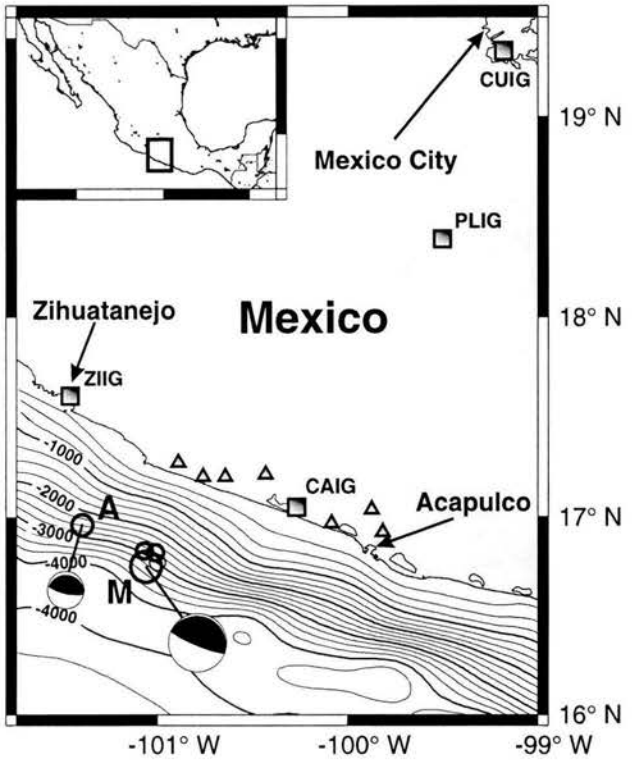

Figure 1. Locations of the events of 18 April 2002 (open circles). M, mainshock; A, principal aftershock. Broadband stations in the region are indicated by rectangles. Triangles show locations of accelerographs of GAA in the immediate neighborhood of the events. Peak accelerations at these stations were less than 3 Gal.

sites and, hence, are less likely to cause damage from strong ground motions. However, there is catch to this good news. Because of its low acceleration, the earthquake may go unfelt by the coastal inhabitants and a large tsunami may be their first exposure to the phenomenon. This was the case during the 2 September 1992 tsunami earthquake of Nicaragua (m_b 5.3; M_s 7.2; M_w 7.6). The ground motion during the earthquake was very weak along the entire coast of Nicaragua. The earthquake was lightly felt, if at all, in the coastal village of El Transito, located 85 km east-northeast of the epicenter. Yet, the village was devastated by a tsunami (Ide *et al.*, 1993). This emphasizes the importance of the implementation of a tsunami alert system on the line proposed by Shapiro *et al.* (1998).

Earthquakes of 18 April 2002

Source Parameters

Table 1 lists source parameters of the mainshock of 18 April 2002 and some of its larger, immediate aftershocks. It includes an event that occurred on the same day but a few hours later (18 April 2002, 17:57, M_w 5.9). Although this event may not strictly qualify as an aftershock, as it is located 43 km from the mainshock, in the following we will denote it as the principal aftershock. The locations given in the table are based on local and regional data. For the mainshock, the table also provides the source parameters reported in the Harvard Centroid Moment Tensor catalog. Figure 1 shows the epicenters of the events listed in Table 1. We note that the locations of the events lie near the trench. Figure 2 illustrates the locations of the earthquakes studied by Shapiro *et al.* (1998) and the two events of 18 April. Table 2 gives a list of all events.

Evidence of Deficient High-Frequency Radiation

Since the locations of the 18 April mainshock and its principal aftershock are close to the trench, we expect these events to be relatively deficient in high-frequency radiation. This can be seen in Figure 3, which shows the north–south velocity traces and the spectra of the near-coast earthquake of 15 July 1996 (M_w 6.6, event 14, Table 2) and the 18 April mainshock (M_w 6.7, event 20, Table 2) recorded at CUIG. The character of the 18 April seismogram is markedly distinct. The spectrum of the 18 April event at $f \geq 0.6$ Hz is much lower than that of the 15 July event, and ER values are 519 and 7.8, respectively (Table 2). While V_{max} is about the same for both events (~0.5 cm/sec), the A_{max} values are 0.85 and 3.7 Gal, respectively.

To quantify the relative high-frequency radiation, we computed ER defined by (Shapiro *et al.*, 1998)

Table 1
Source Parameters of the Earthquake of 18 April 2002 and Some Its Aftershocks

Date (yymmdd)	Time	Latitude (°N)‡	Longitude (°E)‡	Depth (km)	Strike	Dip	Rake	M_0 (dyne cm)	M
020418*	05:02:43.5	16.75	−101.06	6.0	291°	9°	89°	1.5×10^{26}	6.7 M_w
020418†	07:24:27.3	16.77	−101.00	2.0				2.4×10^{22}	4.2 M_w
020418	08:01:34.9	16.82	−101.01	2.0					4.3 M_c
020418	08:28:05.7	16.83	−101.07	2.0					4.3 M_c
020418*	17:57:23.9	16.96	−101.40	4.0	273°	17°	81°	8.8×10^{24}	5.9 M_w

*Moment and focal mechanism from Harvard CMT catalog.
†Moment from regional data.
‡All epicentral locations and depths are from local/regional data. Depths are poorly constrained.

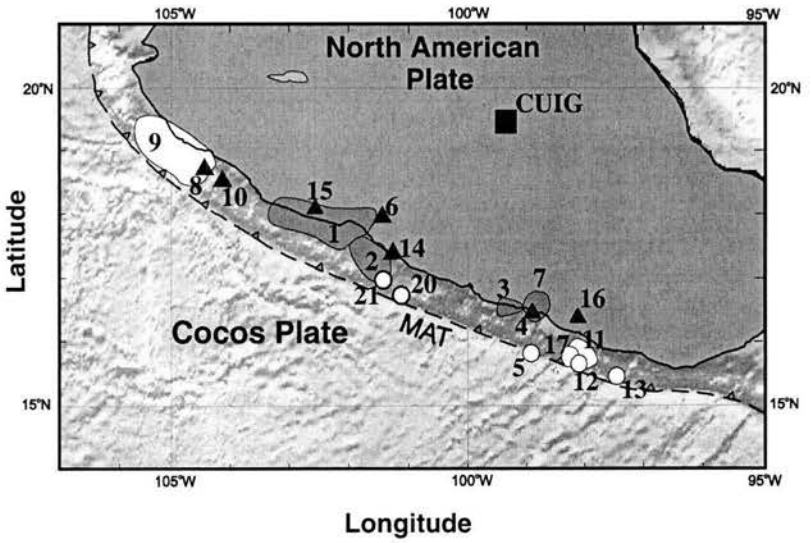

Figure 2. Location of events whose total to high-frequency energy ratio, ER, have been estimated. Event numbers are keyed to Table 2. For near-trench (open circles and white rupture areas) and near-coast events (triangles and shaded rupture areas), ER is greater than and less than 100, respectively. Modified from Shapiro *et al.* (1998).

Table 2
Earthquakes and Their Source Parameters

No.	Date (yy.mm.dd)	Latitude (°N)	Longitude (°E)	M_0 (dyne cm)	M_w	ER	E_s* (erg)	E_s/M_0
1	85.09.19	18.1	−102.7	1.1×10^{28}	8.0	45.9	8.5×10^{22}	7.7×10^{-6}
2	85.09.21	17.6	−101.8	2.9×10^{27}	7.5	35.8	2.2×10^{22}	7.6×10^{-6}
3	89.04.25	16.6	−99.5	2.4×10^{26}	6.9	53.1	2.5×10^{21}	1.0×10^{-5}
4	93.10.24	16.5	−99.0	1.0×10^{26}	6.6	31.5	1.1×10^{21}	1.1×10^{-5}
5	93.11.13	15.7	−99.0	4.1×10^{24}	5.7	173	2.3×10^{19}	5.6×10^{-6}
6	94.12.10	18.0	−101.6	5.2×10^{25}	6.4	19.5	2.8×10^{20}	5.4×10^{-6}
7	95.09.14	17.0	−99.0	1.3×10^{27}	7.3	62.4	1.2×10^{22}	9.2×10^{-6}
8	95.10.06	18.8	−104.5	5.8×10^{24}	5.8	40.8	–	–
9	95.10.09	18.8	−104.5	1.1×10^{28}	8.0	258	1.8×10^{22}	1.6×10^{-6}
10	95.10.12	18.7	−104.2	1.0×10^{25}	5.9	46.6	3.0×10^{19}	3.0×10^{-6}
11	96.02.25	15.6	−98.3	5.5×10^{26}	7.1	174	1.3×10^{21}	2.4×10^{-6}
12	96.02.26	15.7	−98.2	2.3×10^{24}	5.5	472	–	–
13	96.03.19	15.5	−97.6	6.9×10^{24}	5.8	160	–	–
14	96.07.15	17.5	−101.1	1.0×10^{26}	6.6	7.8	3.3×10^{20}	3.3×10^{-6}
15	97.01.16	18.1	−102.9	2.2×10^{24}	5.5	20.2	–	–
16	97.01.21	16.4	−98.2	2.1×10^{24}	5.5	5.6	–	–
17	97.07.19	16.0	−98.2	1.2×10^{26}	6.7	227	2.3×10^{20}	1.9×10^{-6}
18	96.02.21	−9.6	−79.6	2.2×10^{27}	7.5	1180	5.7×10^{21}	2.6×10^{-6}
19	96.11.12	−15.0	−75.7	4.6×10^{27}	7.7	10.1	2.2×10^{22}	4.8×10^{-6}
20	02.04.18	16.8	−101.1	1.5×10^{26}	6.7	519	–	–
21	02.04.18	17.0	−101.4	8.8×10^{24}	5.9	132	–	–

Modified from Shapiro *et al.* (1998).

*For all events, except 18, E_s is taken from NEIC reports. NEIC uses the method of Boatwright and Choy (1986) to estimate E_s. E_s for event 18 is taken from Venkataraman (2002).

$$\mathrm{ER} = \frac{\int_0^\infty V^2(f)df}{\int_1^\infty V^2(f)df}, \qquad (1)$$

where $V^2(f) = V_N^2(f) + V_E^2(f) + V_Z^2(f)$, and $V_i(f)$ is the Fourier spectrum of the ith component of the velocity seismogram at CUIG normalized to a distance of 400 km. For the normalization we assume that the geometrical spreading is given by $R^{-1/2}$ (surface waves) and the anelastic attenuation is given by $e^{-\pi fR/UQ(f)}$, where $Q(f) = 273 f^{0.67}$ is the quality factor (Ordaz and Singh, 1992). We take U, the group velocity of surface waves, as 3.75 km/sec. To ensure that the spectra are above the noise at CUIG, the upper limit of the integrations in equation (1) is set at 5 Hz. The ER values of the mainshock and the principal aftershock are 519 and 132, respectively. These values of ER are listed in Table 2

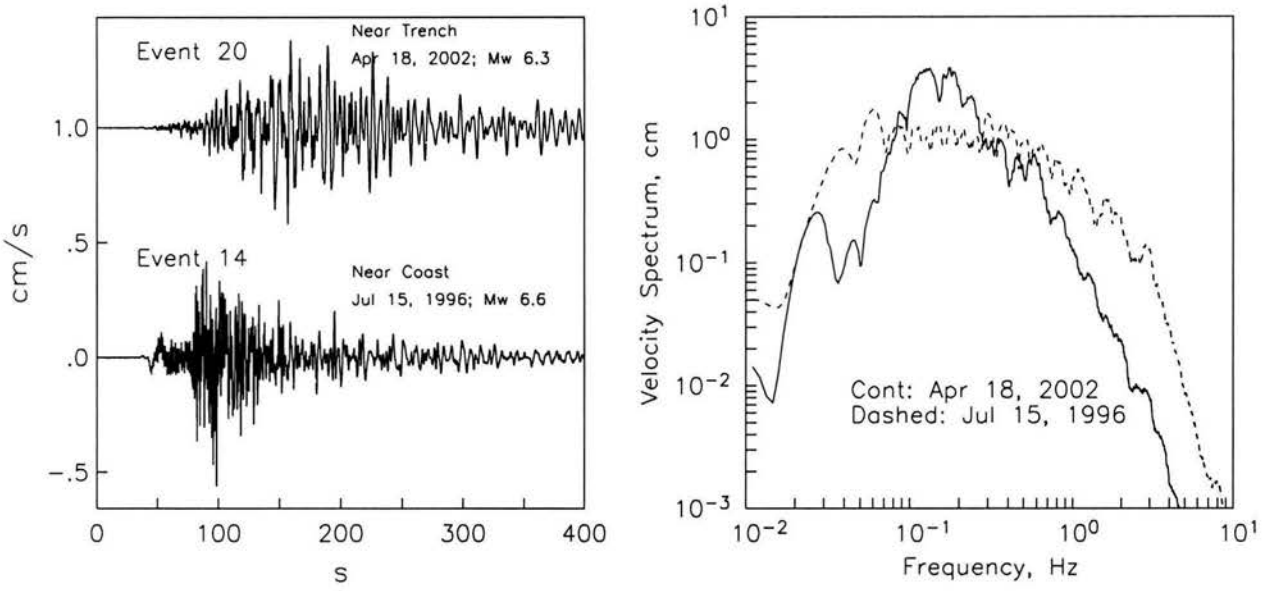

Figure 3. Left: North–South velocity traces of the earthquakes of 18 April 2002 (M_w 6.7) and 15 July 1996 (M_w 6.6) recorded at CUIG. Right: The corresponding velocity spectra.

along with the values for the events analyzed by Shapiro *et al.* (1998). Figure 4 (top) shows plot of ER versus magnitude of the events. In this plot the dashed line divides near-coast and near-trench events. We note that the ER value is greater than 100 for all near-trench events, including the two earthquakes of 18 April. Events with ER > 100 were defined as potentially tsunamigenic by Shapiro *et al.* Based on this definition, the 18 April events are potentially tsunamigenic earthquakes.

Newman and Okal (1998) reported that the radiated seismic energy–to–moment ratio, E_s/M_0, is a powerful discriminant for tsunami earthquakes. This suggests that events with high values of ER should also have low values of E_s/M_0. Table 2 lists teleseismic estimates of E_s and E_s/M_0. Note that the E_s estimates are not available for several events listed in Table 2, including the two earthquakes of 18 April 2002. Figure 4 (bottom) illustrates the E_s/M_0 versus ER plot. There is a large scatter in the data, partly due to the uncertainty in the estimated values of E_s (see Singh and Ordaz, 1994). In general, however, if ER is greater than 100 for an event, then E_s/M_0 is less than 3×10^{-6}. E_s/M_0 values for the recent tsunami earthquakes of Nicaragua (2 September 1992, M_w 7.6), Java (2 June 1994, M_w 7.8), and Peru (21 February 1996, M_w 7.5) are 1.5×10^{-6}, 0.6×10^{-6}, and 2.6×10^{-6}, respectively (Venkataraman, 2002). For these events, the expected values of ER are greater than 100 (Fig. 4, bottom). In fact, ER for the Peruvian earthquake is 1180, the largest value in Table 2.

Okal and Newman (2001) searched for a regional trend in E_s/M_0 in the subduction zones of the three tsunami earthquakes mentioned previously. They reached a negative conclusion. Our results for the Mexican subduction zone are positive: all events with ER > 100 are located near the trench.

Low Peak Accelerations

As mentioned earlier, it is reasonable to expect that the near-trench earthquakes (ER > 100) would give rise to smaller-than-expected peak accelerations. The fact that the SAS did not trigger during the two events of 18 April supports this inference. Figure 5, which shows a plot of A_{max} versus hypocentral distance R during four near-trench earthquakes of Mexico, provides a quantitative support. A reasonable number of accelerograms are available only for these near-trench earthquakes. Two of these earthquakes occurred off the coast of Pinotepa Nacional (events 11 and 17, Table 2, Fig. 2), and the other two events are those of 18 April. The observed A_{max} in all four cases is much smaller than the predicted value at a hard site for near-coast earthquakes. These predicted values are given by the relation (Ordaz *et al.*, 1989):

$$\log A_{max} = 0.3\, M_w - \log R - 0.0031R + 1.76 \quad (2)$$

with a standard deviation in log A_{max} of 0.25. In equation (2), $A_{max} = \{A_N^2 + A_E^2\}^{1/2}/2$, A_N and A_E are peak accelerations (in galileos) in the north–south and east–west directions, respectively, and R is in kilometers. As mentioned above, the SAS stations trigger at $A_{max} \geq 5$ Gal. The present trigger level of the seven closest stations of GAA (65 km $\leq R \leq$ 136 km) is set at 3 Gal. As none of these stations triggered, this provides further constraint on A_{max} during the

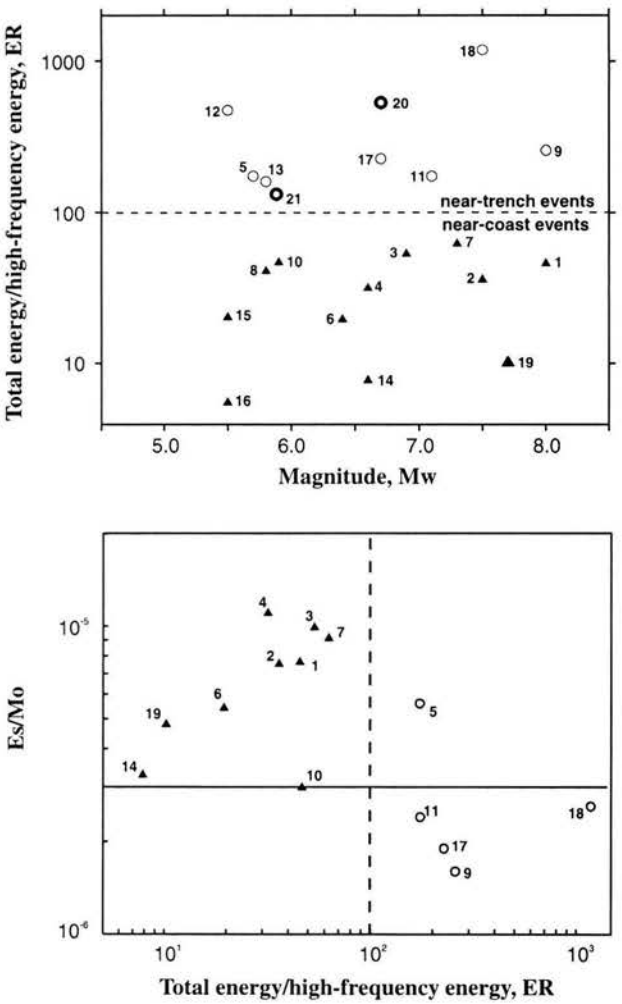

Figure 4. Top: Plot of ER versus M_w. The dashed line divides near-trench and near-coast events. Events 20 and 21 are the two 18 April 2002 earthquakes (Table 2). A_{max} versus M_w for events 11, 17, 20, and 21 is shown in Figure 5. Modified from Shapiro *et al.* (1998) Bottom: E_s/M_0 versus ER. Horizontal and vertical dashed lines indicate $E_s/M_0 = 3 \times 10^{-6}$ and ER = 100, respectively. ER is greater than 100 for events with $E_s/M_0 < 3 \times 10^{-6}$.

events of 18 April. A_{max} for the 18 April events, shown in the figure, are taken from broadband seismic stations of the National Mexican Seismological Service. The acceleration channels of these stations are triggered by the velocity channels. These stations record events with very small A_{max} values.

Based on the same argument, it is reasonable to expect anomalously low A_{max} from near-trench earthquakes at stations in the Valley of Mexico. This, indeed, was the case during the 18 April events since A_{max} exceeded 3 Gal at only a few lake-bed zone stations. The A_{max} at CUIG was 0.63 and 0.25 Gal during the mainshock and the principal aftershock, respectively. These values are about one-third of the expected ones. The expected values were computed from (Montalvo-Arrieta *et al.*, 2001)

$$\log A_{max} = 0.600\, M_w - 6.7 \log R + 0.0037R + 12.4, \quad (3)$$

a relation that is valid for Ciudad Universitaria.

Source or Path Effect?

Are the relatively depleted high-frequency radiation observed at CUIG and the low accelerations observed along the coast and in the Valley of Mexico during near-trench earthquakes a source or a path effect? The large disparity between M_s and M_w of tsunami earthquakes, which occur near the trenches (Kanamori and Kikuchi, 1993), points to a source effect, as do the relatively larger rupture duration (Bilek and Lay, 1999) and the relationship between ER and E_s/M_0 of shallow near-trench earthquakes. On the other hand, the seismic waves from these shallow earthquakes must suffer a strong path effect as they get trapped in the low-velocity accretionary prism (see, e.g., Shapiro *et al.*, 2000) and propagate in shallow oceanic layers to coastal and inland stations (Fig. 3). The complexity of seismograms of near-trench Mexican earthquakes (Fig. 3) makes it difficult to study the details of source characteristics. To study the source of the 18 April mainshock, we deconvolved the mainshock seismograms recorded at the broadband stations of ZIIG, CAIG, and PLIG (Fig. 1) by those of the aftershocks, thus minimizing the path effect. We still could not obtain a stable source time function, most probably because the aftershocks were not appropriate empirical Green's functions. While the most likely cause of depleted high-frequency radiation and low accelerations during near-trench earthquake is the source, we cannot rule out that the path plays an important role as well.

Observed Tsunami during the 18 April 2002 Mainshock

We have provided evidence that the 18 April mainshock was potentially tsunamigenic. In fact, a small-amplitude tsunami was recorded at Acapulco and Zihuatanejo. At these sites, digital sensors take one pressure reading each second, and the average value of 6 min of data is saved. In Figure 6, which shows the residual tide, a tsunami, whose amplitude is about twice the background noise, can be seen at both stations. As these sensors were not installed during previous $\sim M_w$ 6.5 earthquakes in the region, it is not possible to assert that the tsunami during the 18 April event is anomalously large.

Conclusions

It has been previously reported that the earthquakes that occur near the Middle America trench are depleted in high-

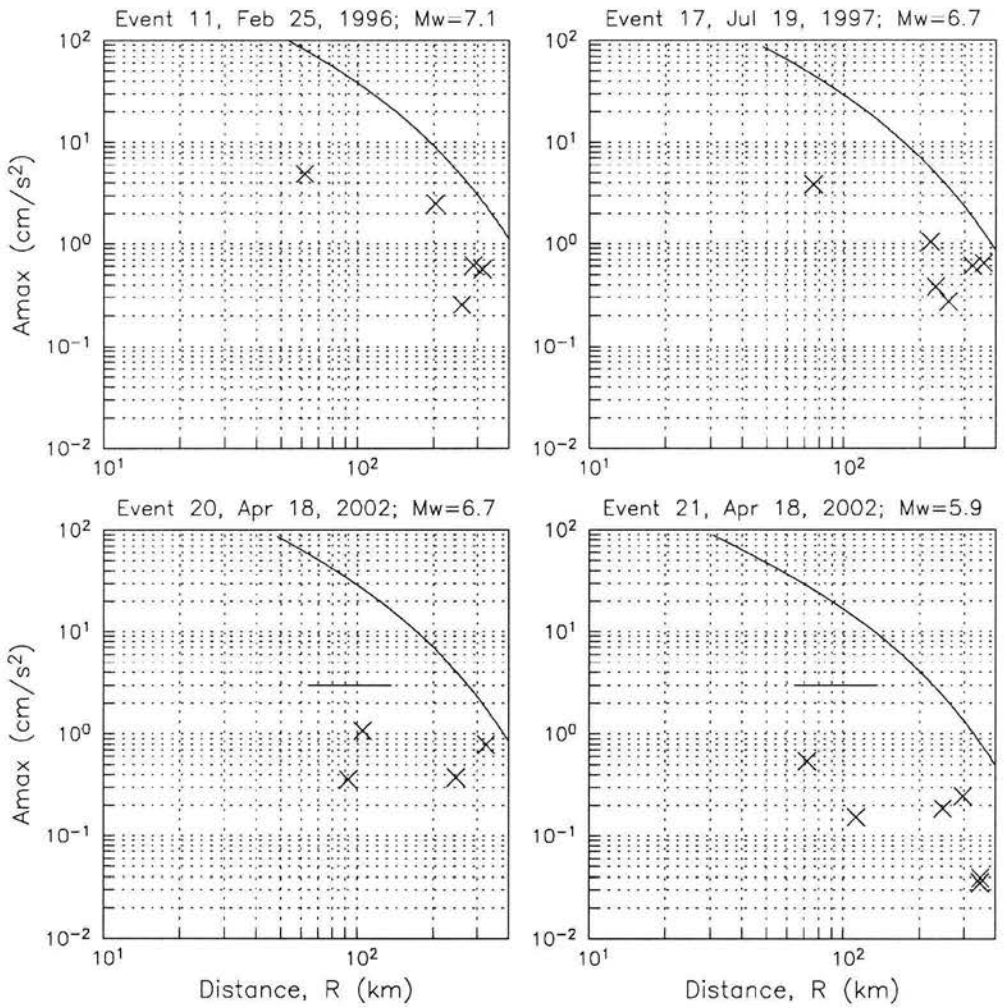

Figure 5. A_{max} versus distance for four near-trench events. The curves depict the predicted A_{max} from near-coast earthquakes. Crosses mark recorded A_{max}. The horizontal lines for the 18 April 2002 earthquakes indicate the range of distance over which A_{max} was less than 3 Gal.

frequency radiation at the broadband station of CUIG. In this note we have shown that these events also give rise to anomalously low peak accelerations along the coast and in the Valley of Mexico.

Quick detection of near-trench earthquakes may, thus, provide not only tsunami alerts for the coastal regions of Mexico but may also advise scientists and authorities that the peak accelerations may be relatively low. The importance of a tsunami alert, such as the one proposed by Shapiro *et al.* (1998), becomes clear when one realizes that ground motions from such earthquakes may be too weak to act as natural alarms for coastal inhabitants. If the CUIG seismograms yield ER $>$ 100 and a magnitude $>$7, it may be sufficient to indicate a near-trench, tsunamigenic earthquake, and, as a consequence, relatively low coastal and inland accelerations.

In the estimation of seismic hazard, it is common practice to use the same attenuation relation for all earthquakes that occur on the interface of the subducted Cocos plate and the continental North American plate. In view of the results presented in this study, it seems more reasonable to treat near-trench earthquakes distinctly. Separating these earthquakes in the existing catalogs, however, may require very careful relocation of the mainshocks and their aftershocks.

Acknowledgments

We are grateful to the technical staff that maintains the broadband seismological stations (especially Jorge Estrada, Jesus Pérez Santana, and Jose Luís Cruz) and the strong-motion networks (mainly David Almora, Miguel Torres, Ricardo Vásquez, Juan Manuel Velasco, and Mauricio Ayala). Nicolas Shapiro kindly revised the manuscript. We thank Emile Okal for his thoughtful comments. The tsunami data was provided by the sea level network of Secretaría de Marina de México. The research was partially supported by DGAPA UNAM Project IN 111601.

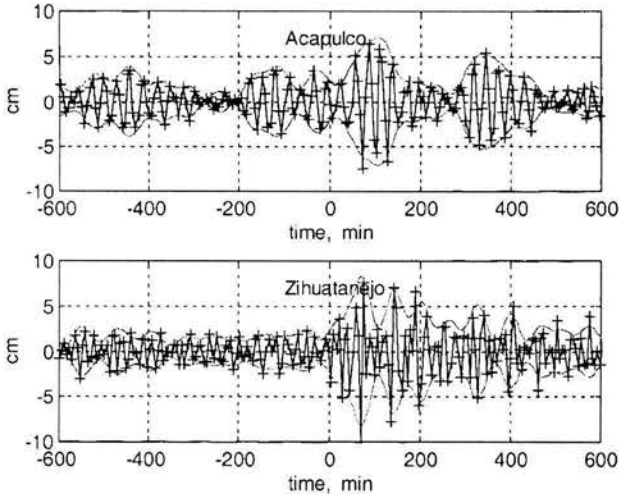

Figure 6. Residual tide at Acapulco and Zihuatanejo. Crosses indicate data (one sample per 6 min). The light curve shows the envelope. The zero along the time axis corresponds to the origin time of the mainshock of 18 April 2002 (Table 1).

References

Anderson, J. G., J. N. Brune, J. Prince, R. Quaas, S. K. Singh, D. Almora, P. Bodin, M. Oñate, R. Vásquez, and J. M. Velasco (1994). The Guerrero accelerograph network, *Geofis. Int.* **33,** 341–371.

Bilek, S. L., and T. Lay (1999). Rigidity variations with depth along interplate megathrust faults in subduction zone, *Nature* **400,** 443–446.

Boatwright, J., and G. L. Choy (1986). Teleseismic estimates of the energy radiated by shallow earthquakes, *J. Geophys. Res.* **91,** 2095–2112.

Espinosa-Aranda, J. M., A. Jiménez, G. Ibarrola, F. Alcantar, A. Aguilar, M. Inostroza, and S. Maldonado (1995). Mexico City seismic alert system, *Seism. Res. Lett.* **66,** 42–53.

Ide, S., F. Imamura, Y. Yoshida, and K. Abe (1993). Source characteristics of the Nicaraguan tsunami earthquake of September 2, 1992, *Geophys. Res. Lett.* **9,** 863–866.

Kanamori, H., and M. Kikuchi (1993). The 1992 Nicaragua earthquake: a slow tsunami earthquake associated with subducted sediments, *Nature* **361,** 714–716.

Montalvo-Arrieta, J. C., E. Reinoso, F. J. Sánchez-Sesma, S. K. Singh, J. Pacheco, and M. Ordaz (2003). The seismic response of the hill zone in Mexico City: a review and new findings (in preparation).

Newman, A. V., and E. A. Okal (1998). Teleseismic estimate of radiated seismic energy: the E_s/M_0 discriminant for tsunami earthquakes, *J. Geophys. Res.* **103,** 26,885–26,898.

Okal, E. A., and A. V. Newman (2001). Tsunami earthquakes: the quest for a regional signal, *Phys. Earth Planet. Interiors* **124,** 45–70.

Ordaz, M., and S. K. Singh (1992). Source spectra and spectral attenuation of seismic waves from Mexican earthquakes, and evidence of amplification in the hill zone of Mexico City, *Bull. Seism. Soc. Am.* **82,** 24–43.

Ordaz, M., J. M. Jara, and S. K. Singh (1989). Riesgo sísmico y espectros de diseño en el estado de Guerrero, in *Mem VIII Congreso Natl. de Ingeniería Sísmica y VII Congreso Nac. de Ingeniería Estructural* **2,** D40–D56, Acapulco.

Shapiro, N. M., K. B. Olsen, and S. K. Singh (2000). Wave-guide effects in subduction zones: evidence from three-dimensional modeling, *Geophys. Res. Lett.* **27,** 433–436.

Shapiro, N. M., S. K. Singh, and J. Pacheco (1998). A fast and simple diagnostic method for identifying tsunamigenic earthquakes, *Geophys. Res. Lett.* **25,** 3911–3914.

Singh, S. K., and M. Ordaz (1994). Seismic energy release in Mexican subduction zone earthquakes, *Bull. Seism. Soc. Am.* **84,** 1533–1550.

Singh, S. K., and J. Pacheco (1994). Magnitude of Mexican earthquakes, *Geofis. Int.* **33,** 189–198.

Venkataraman, A. (2002). Investigating the mechanics of earthquakes using macroscopic seismic parameters, *Ph.D. Thesis*, California Institute of Technology, Pasadena.

Appendix

Note Added in Proof

G. L. Choy (personal comm., 2003) reports $E_s = 2 \times 10^{20}$ ergs for the 18 April 2002 (M_w 6.7) event. Thus $E_s/M_0 = 1.5 \times 10^{-6}$ for this event. Since ER = 519 (Table 2), this event agrees with our expectation that if ER > 100 then E_s/M_0 is less than 3×10^{-6}.

Instituto de Geofísica
Universidad Nacional Autonoma de México, C.U.
04510 México, D.F.
México
(A.I., S.K.S., J.F.P.)

Instituto de Ingeniería
Universidad Nacional Autonoma de México, C.U.
04510 México, D.F.
México
(L.A., M.Ord.)

Departamento Oceanografía Fisica
Centro de Investigación Científica y de Educación Superior de Ensenada
Ensenada, B.C.
México
(M.Ort.)

Manuscript received 1 August 2002.

Capítulo V

"El sistema de alerta sísmica para la ciudad de México: La evaluación de su desempeño y una estrategia para mejorarlo"

The Seismic Alert System for Mexico City: An Evaluation of its Performance and a Strategy for its Improvement

A. Iglesias[1], S. K. Singh[1], M. Santoyo[1], J. Pacheco[1], and M. Ordaz[2]

[1]Instituto de Geofísica, UNAM, CU, 04510 México, DF
[2]Instituto de Ingeniería, UNAM, CU, 04510 México, DF

Abstract

The seismic alert system (SAS) for Mexico City, an impressive technological feat, has now been in operation for more than 10 years. The SAS takes advantage of the fact that the city is located more than 300 km from the foci of potentially damaging earthquakes. The system consists of 15 accelerometers located along the coast of the State of Guerrero, above a segment of subduction plate boundary that is a mature seismic gap. An algorithm estimates magnitude of an event from the near-source accelerograms, and issues public and restricted alerts for $M \geq 6$ and $5 \leq M < 6$, respectively. An evaluation of the SAS's performance during 1991-2004 reveals a surprisingly high failure rate. This poor performance results from an inadequate detection algorithm and the limited areal coverage by the SAS. These two factors render the alert system of limited use.

In this paper we propose an alternative strategy for detecting potentially damaging earthquakes to Mexico City that differs substantially from the one presently implemented by the SAS. It is developed from the analysis of near-source recordings of Mexican earthquakes since 1985 and the corresponding ground motions recorded in Mexico City. In our proposed scheme, the alerts are based on the relationship between root-mean-acceleration (*Arms*) in the near-source region and the expected peak acceleration *Amax* at a reference site in Mexico City, CU. Tests are performed using unfiltered and band-pass filtered (0.2-1.0 Hz) accelerograms. The choice of the filter corresponds to the frequency band of amplification of seismic waves in the lake-bed zone. The results suggest that only a single level of general public alert may be the best option. This alert would be issued when the near-source *Arms* computed over a window of 10s exceeds 5 gal for unfiltered records or 1.0 gal for the filtered ones. The corresponding values of expected $(Amax)_{CU}$ are 3.5 and 2.0 gal, respectively. We find that the use of band-pass filtered accelerograms leads to a lower failure rate of alerts. The data since 1985 suggests that such an alert, on average, would occur about once a year. It would include the majority earthquakes felt by most persons in the lake-bed zone and, better yet, not miss any damaging event. The proposed strategy, along with deployment of about 40 sensors in three concentric rings centered at Mexico City, would considerably improve the performance of SAS and, potentially, save thousands of lives.

Introduction

About 20 million persons inhabit the metropolitan area of Mexico City. Although the city is located more than 300 km from the Pacific coast where most large earthquakes originate, it still suffers frequent earthquake disaster. Normally, the amplitudes of seismic waves at such distances must be sufficiently diminished so that even large earthquakes do not cause any damage. The principal cause of this unexpected phenomenon is well known: an extraordinary amplification of seismic waves in the frequency band of 0.2 to 1.0 Hz resulting from the soft clays that underlie the lake-bed zone of the Valley of Mexico (e.g., Singh et al., 1988a,b). The most recent example was the Michoacan earthquake of 1985 (Mw8.0) which originated at a distance of about 350 km from the city. The collapse of buildings during the earthquake killed about 10,000 and injured 30,000 persons.

Relatively large distances (>300 km) between the foci of most of the potentially damaging earthquakes and the city provides a unique opportunity for a seismic alert system (SAS). The large amplitude S waves reach Mexico City more than 85 s after the earthquake origin. A quick earthquake detection occurrence and an estimation of its potential damage to the city are possible by deploying sensors above the epicentral region. This can provide about 60 s of alert time to Mexico City and, potentially, an important seismic mitigation risk will occur.

In fact, a SAS for Mexico City has been in operation since August 1991(Espinosa-Aranda et al., 1995; Espinosa-Aranda and Rodriguez, 2003). It is an impressive technological achievement. The sensors deployed by the SAS presently cover a 300 km-long segment of the Guerrero coast (Figure 1), a known mature seismic gap (Singh et al., 1981). It consists of 15 accelerometers located ~25 km apart. The system detects P and S waves at the nearest sensor to the focus, and computes the energy in the accelerogram over a time window beginning with S wave and lasting twice the (S-P) time (generally about 6 to 8 s). It also computes the rate of accumulation of energy during this window. These two parameters are used to estimate the magnitude, M, of the earthquake (Espinosa-Aranda et al., 1989). The system issues restricted alert for $5 \leq M < 6$. This alert is

sent only to authorities and some special radio receivers. Public alert is issues for M>6 and is sent to mentioned before and broadcast radio stations. At least two stations must confirm the occurrence of the event before the warning is automatically broadcast by SAS.

In this study, we evaluate SAS's performance so far, and, based on the analysis of strong motion data in Mexico, suggest modifications that may improve its effectiveness.

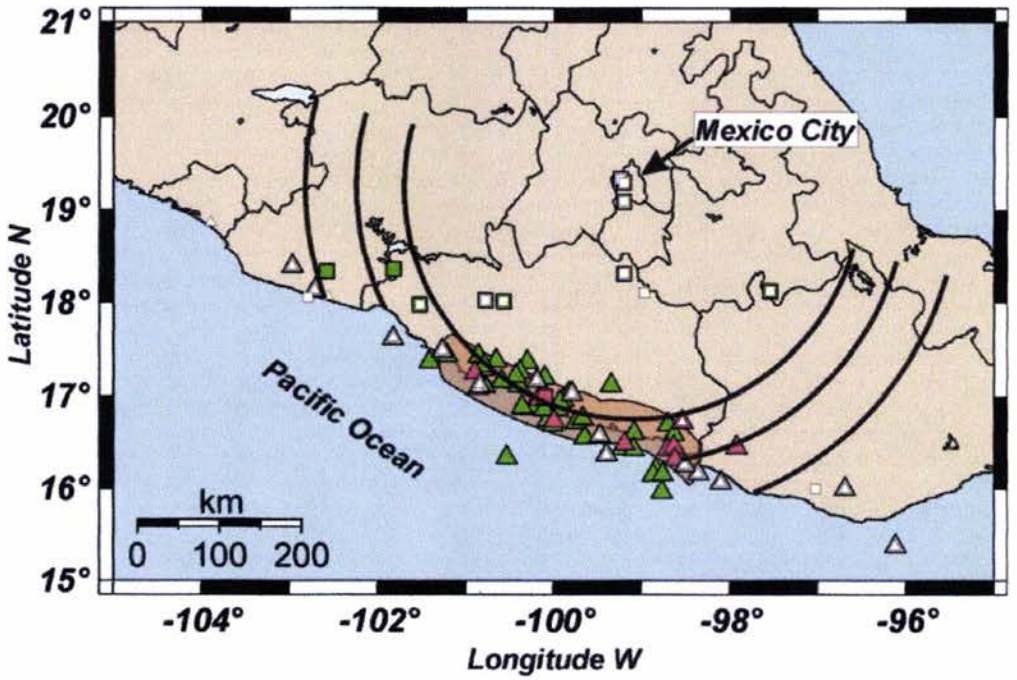

Figure 1. Map of Mexico showing, in orange, the area covered by Mexico City's seismic alert system (SAS). Triangles and rectangles indicate interplate and non-interplate events. Green and red symbols show locations of events for which the SAS issued restricted and public alerts, respectively during the period August 1991-August 2004. Symbols with white interior are events which generated $(Amax)_{CU} \geq 5$ *gal. Gray symbols with white interior: events before the SAS coverage (1964-July 1991) with* $(Amax)_{CU} \geq 5$ *gal. Events with* $(Amax)_{CU} \geq 5$ *gal during the SAS coverage but with no alert are shown by white symbol. The three concentric semi-circles show the geometry of a proposed array which would provide a more adequate coverage by the SAS. Sensors would be located about 60 km apart in each of the semi-circular rings (for a total of about 40).*

An Evaluation of the SAS

Table 1 summarizes SAS's performance since August 1991 when the system became operational. During this period, SAS issued 46 restricted and 11 public alerts (J. M. Espinosa-Aranda, personal communication, 2004). Figure 1 shows epicenters of these earthquakes. As Table 1 illustrates, a restricted alert ($5 \leq M < 6$) was justified only in 15 of the 46 cases, in 27 cases no alert should have been given, and in 4 cases (with $M \geq 6$) a public alert should been issued. Only three of the 11 public alerts actually fulfilled the requirement of $M \geq 6$. During this period the SAS also gave one false public alert when no earthquake occurred and, in one case, it failed to give any alert when it should have issued a public one. As Table 1 shows, the SAS's failure rate is high.

Table 1. Performance of Seismic Alert System for Mexico City
(August 1991-August 2004)

Type of alert issued	Magnitude estimated by SAS as the basis of the alert	Number of alerts issued	'True' magnitude distribution of the events		
			$4 \leq M < 5$	$5 \leq M < 6$	$M \geq 6$
Restricted	$5 \leq M < 6$	46	27	15	4
Public	$M \geq 6$	11	2	6	3

In reality, we do not need an estimate of the magnitude for issuing a seismic alert for Mexico City. The performance of the SAS may be better evaluated by associating alerts with recorded ground accelerations in Mexico City. For this purpose, we analyze recordings at a reference station in the city where accelerographs have been in continuous operation since the mid sixties. This station, CU, is located on basaltic lava flows. The peak horizontal acceleration, *Amax*, in the lake-bed zone of the city, where much of the damage occurs during earthquakes, is 4 to 5 times greater than at CU (Singh et al., 1987, 1988c).

We define *Amax* at CU by

$$(Amax)_{CU} = \left[a_N^2 + a_E^2 + a_Z^2\right]^{\frac{1}{2}} \qquad (1)$$

where a_i is the maximum acceleration in the i^{th} direction. Figure 1 shows epicenters of 28 events since 1964, which produced *Amax*≥ 5gal at CU (see Tables 2 and 3 for events during 1964-1984 and 1985-2004, respectively). Eleven of these events occurred in the period covered by the SAS (August 1991-August 2004). Of these 11 events, two were local earthquakes in the Valley of Mexico and another two occurred within a distance of 140 km from CU (Figure 1). The local events do not cause damage to the city even when they give rise to large *Amax* at CU. A useful seismic alert for events at a distance of 100 to 150 km from CU is possible only if the detection is made in the epicentral region during the first seconds of P waves train. This may, however, require a large number of high-quality stations, which is, presently, lacking in Mexico. For the remaining 7 events, SAS issued 4 restricted and 2 public alerts. As Figure 1 shows, the four events with restricted SAS alert and one event with no alert were all located outside the region of SAS coverage. Of the 11 public alerts issued by the SAS (Table 1), only four resulted in *Amax*≥ 5gal at CU. Figure 2 gives histogram of SAS alerts *versus* $(Amax)_{CU}$. We conclude that the SAS alerts have been not truly indicators of *Amax* at CU.

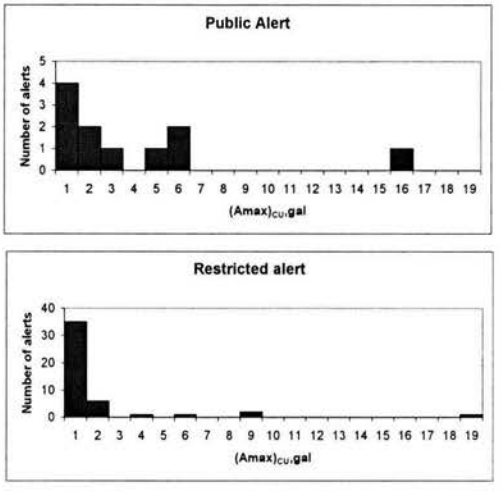

Figure 2. Histogram of public and restricted alerts issued by the SAS (August 1991-August 2004) versus $(Amax)_{CU}$.

Table 2. Earthquakes during 1964-1984, which produced $Amax \geq 5$ gal at CU

Date	Lat	Long	H (km)	M	$(Amax)_{CU}$ (gal)	Type[1]
07/06/1964	18.03	-100.77	55	7.2	26.95	IS
23/08/1965	15.38	-96.12	12	7.4	9.15	T
03/02/1968	16.37	-99.4	33?	5.6	12.14	T
02/08/1968	16.6	-97.8	16	7.3	20.00	T
07/12/1974	19.29	-100.77	<5?	3.5	60.57	L
01/02/1976	17.17	-100.19	52?	5.6	6.42	T
07/06/1976	17.406	-100.682	57	6.3	15.50	?
19/03/1978	17.03	-99.79	44	6.6	8.37	?
29/11/1978	16.00	-96.69	23	7.6	8.99	T
14/04/1979	17.49	-101.26	25	7.4	27.32	T
07/06/1982	16.17	-98.36	6	6.9	14.34	T
07/06/1982	16.26	-98.51	19	7	14.55	T

[1]IS: Inslab earthquake; T: Shallow-dipping interplate thrust earthquake; L: Local earthquake

Analysis of Near-Source Recordings to Estimate Ground Motions in Mexico City

To develop a more appropriate strategy for issuing reliable seismic alerts for Mexico City, we analyzed accelerograms recorded at CU and the corresponding near-source recordings of the same events. Extensive near-source recordings in Mexico began in 1985 with the installation of the Guerrero Accelerographic Array (Anderson et al., 1994). Although the free-field accelerographic networks operated by the Institutes of Engineering and Geophysics, UNAM have steadily grown, the near-source recordings are not available for many significant earthquakes.

Table 3 lists 45 earthquakes, which gave rise to the largest *Amax* at CU during 1985-2004. The events are listed in descending order of *Amax* at CU. The table indicates the event type: shallow thrust-faulting interplate earthquake along the Pacific coast ($10<H<30$ km), steeply-dipping thrust or normal-faulting inslab earthquake ($35<H<120$ km), and shallow local earthquake near Mexico City. We note that six of the first 10 events in the table are inslab, normal-faulting earthquakes. In Mexico, these events occur

below the coast as well as below the altiplano. These earthquakes are known to be relatively enriched in the high-frequency radiation (García et al., 2004). As mentioned above, the present SAS is designed only for events occurring near the coast of Guerrero.

In Table 3 we do not assign a number to the local earthquakes and to those events recorded at CU but did not produce a near-source recording. For events 18, 28, 30, and 35, the epicentral distance to the closest station, Δ_S, was greater than 100 km. Although we analyze these four events, we do not include them in the statistics. The first two events in Table 3 devastated Mexico City and the third and fourth events were strongly felt but resulted in only minor damage to the city. *Amax* at CU exceeded 8 and 7 gal during the first 7 and 10 events, respectively.

Our goal is to design an algorithm, using near-source accelerograms that can reliably and quickly provide an estimate of *Amax* at CU and, based on this value, issues an appropriate alert. For this purpose, we shall explore two alternatives: (1) estimate the magnitude, M, of the event, which can then be used *via* an attenuation relation to estimate $(Amax)_{CU}$ (e.g., Singh et al., 1987b; Ordaz et al., 1994), and (2) estimate directly $(Amax)_{CU}$. We note that the SAS uses the alternative (1) which, as shown above, leads to a high alert missing. We, nevertheless, explore alternative (1) further to investigate whether a modified version of the SAS algorithm can lower the alert missing rate.

From previous studies, it is well known that the peak acceleration, *Amax*, in the near-source region, as a function of M shows large scatter and is, essentially, independent of M for M greater than about 5.5 (e.g., Singh et al., 1989). Both the source and the site effects are responsible for the large scatter. It follows that near-source *Amax* as a measure of M is unsatisfactory. Since larger earthquakes last longer, such earthquakes cause sustained high acceleration over longer duration. This suggests that root-mean-square acceleration, *Arms*, computed over an adequate time window, t_d, may be a more useful measure of the size of the earthquake. The window t_d should be sufficiently small to provide as much warning time as possible and, yet, large enough to provide information about the size of the earthquake.

Table 3. Events with largest *Amax* in CU, Mexico City (1985-2004).

Event No.	Date	Lat	Long	H (km)	M	$(Amax)_{CU}$ (gal)	Station	Δ_s[1] (km)	Δ_{CU}[2] (km)	Type[3]
1	19/09/1985	18.14	-102.71	22	8	42.156	CALE, VILE, UNIO	9,98,56	402,314,350	T
2	21/09/1985	17.62	-101.82	22	7.6	19.669	AZIH, PAPN	39,89	307,297	T
3	15/06/1999*	18.13	-97.54	60	6.9	18.072	CHFL, RABO	51,107	215,115	IS
4	25/04/1989	16.58	-99.48	17	6.9	17.042	SMR2, CPDR, VIGA	23,27	284,288	T
5	21/07/2000	18.11	-98.97	50	5.9	15.381	TNLP, RABO, TEAC	63,76,78	142,115	IS
6	14/09/1995**	16.73	-98.54	22	7.3	14.587	COPL, PNIG, VIGA	48,74,58	303,285,344	T
	19/10/1985	19.09	-99.2			11.022				L
7	30/09/1999	16.03	-96.96	40	7.4	10.932	LANE, RIOG, JAMI	26,96,51	431,367,411	IS
	27/10/1991	18.32	-99.2			10.695				L
	18/08/1991	19.33	-99.24			7.863				L
8	10/12/1994*	17.98	-101.52	50	6.4	7.687	BALC	33	259	IS
9	11/01/1997*	18.34	-102.58	40	7.1	7.181	CALE	35	401	IS
10	23/05/1994*	18.02	-100.57	50	6.2	7.036	COMD	13	193	IS
11	30/04/1986	18.4	-102.97	21	6.9	6.614	CALE	43	401	T
12	31/05/1990	17.12	-100.84	21	6	6.001	SLUI	18	291	T
13	22/01/2003	18.86	-103.9	26	7.5	5.904	MZ02	52	474	T
14	09/08/2000	18.07	-102.56	32	6.5	5.042	CALE	20	401	IS
15	15/07/1996*	17.44	-101.21	27	6.6	4.892	AZIH	31	307	T
16	24/10/1993**	16.63	-98.97	35	6.6	4.796	COPL	3	303	T
	07/11/1991	?	?			4.353				L
17	08/10/2001**	17	-100.09	8	5.9	4.268	COYC	7	279	N
18	15/05/1993**	16.45	-97.92	16	6	4.149	SMR2	163	284	T
19	09/10/1995	19.34	-104.80	15	8	3.960	MZ01	50	543	T
20	21/06/1999	18.15	-101.70	53	6.3	3.883	AZIH	66	307	T
21	08/02/1988	17.45	-101.19	22	5.8	3.735	AZIH	32	307	T
22	11/05/1990	17.12	-100.87	21	5.3	3.631	ATYC	47	270	T
23	01/01/2004	17.36	-101.44	21	6	3.450	AZIH	77	297	T
24	14/06/2004	13.23	-98.16		5.9	3.199	PNIG	19	344	T
	09/05/2002	?	?			2.830				L
25	19/11/2003	17.91	-99.03	69	5.2	2.547	TNLP	31	307	IS
26	22/05/1997*	18.37	-101.82	54	6.5	2.428	ZIIG	93	307	IS
27	03/04/1997	18.02	-98.02	42	5.2	2.298	CHFL	52	214	T
28	27/09/2002*	17.44	-100.10	36	5.1	2.063	TNLP	151	142	T
29	03/02/1998	15.90	-96.25	27	6.3	2.033	HUIG	29	512	T
30	15/05/1993**	16.43	-98.74	39	5.3	1.968	SMR2	163	284	T
31	20/04/1998	18.35	-101.19	64	5.9	1.916	ZIIG	89	307	T
32	01/01/2004	17.46	-101.35	15	6.0	1.768	PET2	77	297	T
33	22/12/1997**	17.14	101.24		5.1	1.699	SLUI	40	291	T
34	27/03/1996	16.36	-98.30	18	5.4	1.565	PNTP	25	351	T
	23/02/1994	17.82	-97.3			1.539				?
35	16/12/1997	16.43	-98.73	16	5.9	1.520	SMR2	126	284	IS
36	31/03/1993	17.19	-101.01	6	5.5	1.454	SLUI	17	291	T
37	18/07/1996*	17.44	-101.21	25	5.4	1.245	AZIH	7	297	T
38	19/07/1997*	15.86	-98.26	15	6.7	1.208	PNTP	62	351	T
	21/10/1995	16.92	-93.62			1.200				?
39	19/05/1990	17.21	-101.33		5.9	1.190	PAPN	34	297	T
40	21/01/1997	16.42	-98.21	28	5.5	1.185	JAMI	39	367	T
41	29/07/1993*	17.38	-100.65		5.0	1.161	ATYC	30	270	T
42	11/07/1998	17.35	-101.41	29	5.4	1.130	PET2	41	300	T
	04/07/1994	14.83	-97.9	17	6.4	1.110				?
	14/03/1994	15.67	-93.01	168	6.8	1.055				?
43	11/03/1993	15.35	-98.25		4.2	1.029	UNIO	37	314	T
44	17/07/1998**	16.98	-100.16		4.6	1.012	VNTA	37	275	T
45	30/10/1995	16.55	-98.13	16	5.6	1.012	PNTP	47	351	T

[1] Δ_s Epicentral distance

[2] Δ_{CU}: Distance between the near-source station and CU

[3] ?: Unknown. All other symbols are the same as in Table 2

* : Events which triggered SAS-restricted alert; **: Events which triggered SAS-public alert

For our analysis of the near-source accelerograms, we compute $I(t_d)$, $Arms(t_d)$, and $\alpha(t_d)$, where

$$I(t_d) = \int_0^{t_d} \{a_N^2 + a_E^2 + a_Z^2\} dt \qquad (2)$$

$$Arms(t_d) = \frac{1}{3}\left[\frac{I(t_d)}{t_d}\right]^{\frac{1}{2}} \qquad (3)$$

$$\text{and, } \alpha(t_d) = \frac{I(t_d)}{I(t_d - 2)} \qquad (4)$$

$$\text{where, } I(t_d - 2) = \int_0^{t_d - 2} \{a_N^2 + a_E^2 + a_Z^2\} dt$$

We perform the analysis using both unfiltered as well as filtered near-source accelerograms. The reason for using filtered records stems from the fact that the damage to Mexico City, at least from coastal earthquakes, is related to the ground motion in the frequency band of 0.2 to 1.0 Hz. It is in this frequency range that the ground motion is amplified in the lake-bed zone. This suggests that an alert based on bandpass filtered (0.2-1.0 Hz) near-source and CU accelerograms may be more reliable and robust, since the filter should eliminate random high-frequency ground motion arising from source and site effects.

Figures 3a and 3b illustrate what we may expect from using filtered records. They also help to understand the results that follow. In Figures 3a, the left frames are near-source accelerograms (NS component) of 6 selected events from Table 3, and the center and right frames are the plots of $I_N(t)$ using unfiltered and filtered accelerograms, respectively. Here

$$I_N(t) = \int_0^t \{a_N^2(t)\} dt$$

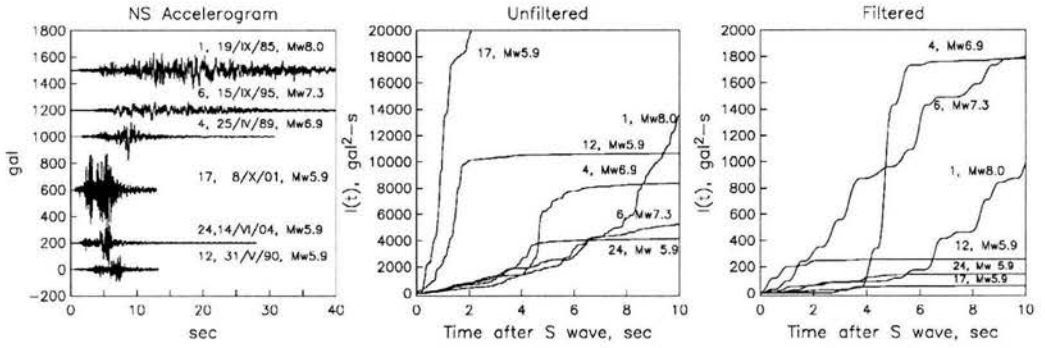

Figure 3a. (Left): NS component of near-source accelerograms of 6 events (5.9≤Mw≤8.0) from Table 3. (Middle): plots of $I_N(t) = \int (a_N^2(t))dt$, *where the integration begins with the S-wave arrival. Unfiltered accelerograms are used in computing* $I_N(t)$. *(Right):* $I_N(t)$ *plots using band-passed filtered (0.2 -1.0 Hz) accelerograms.*

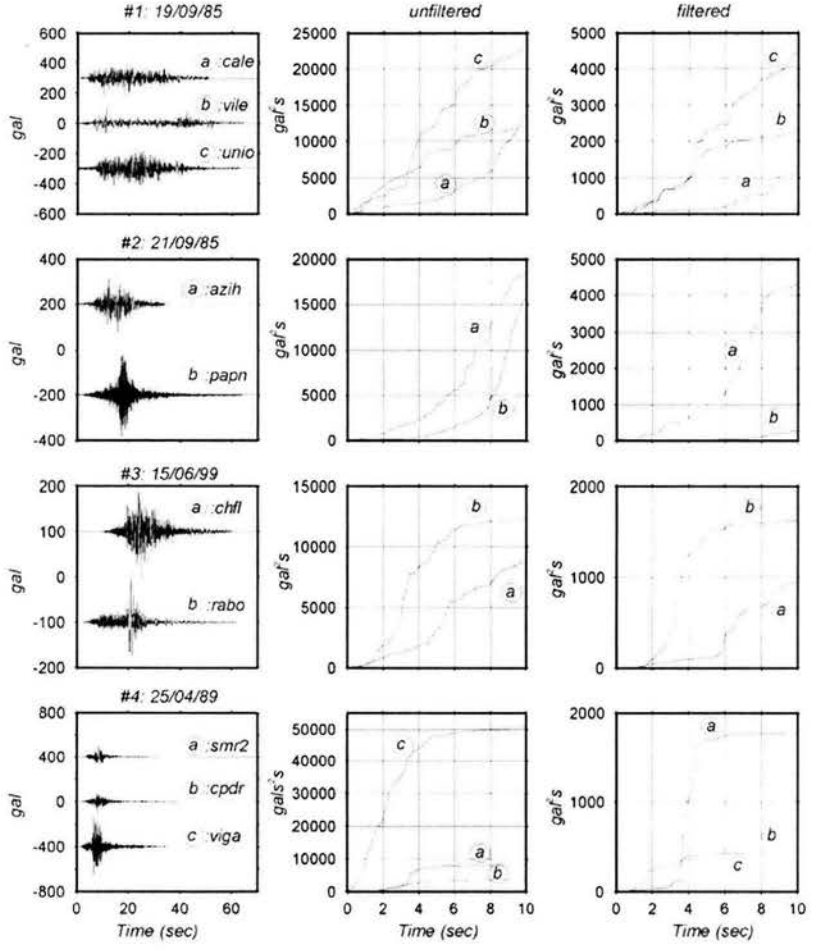

Figure 3b. (Left): NS component of near-source accelerograms of the first four events of Table 3. For each event more than one near-source trace is shown. (Middle). $I_N(t)$ *plots using unfiltered accelerograms. (Right):* $I_N(t)$ *plots using band-passed filtered (0.2 -1.0 Hz) accelerograms.*

Several points may be noted from Figure 3a: (1) Near-source *Amax* is independent of M in the magnitude range 5.8 to 8.0. (2) $I_N(10)$, computed from unfiltered record, does not scale with M. The largest $I_N(10)$ corresponds to the smallest event 17 (M5.8). (3) When computed using filtered records, $I_N(10)$ of the smaller events (M~5.9) are much smaller than for the larger events. (4) For M~5.9 events, $I_N(t)$ is nearly flat 4 to 5s after the arrival of S wave and, hence, $\alpha_N(10) = I_N(10)/ I_N(8) \sim 1$. For large earthquakes (events 1 and 6), $I_N(t)$ keeps increasing up to 10s, thus $\alpha_N(10) > 1$.This suggests that $\alpha_N(10)$ in Equation 4 could be used to discriminate between small and moderate earthquakes, and large earthquakes. Unfortunately, $\alpha_N(10)$ for event 4 (M6.9) is about 1, which would classify it as a small or moderate earthquake. As mentioned earlier, this earthquake was strongly felt in Mexico City and gave rise to the fourth largest *Arms* at CU (Table 3). Any useful algorithm must classify this event for a public alert.

Figure 3a may suggest that for earthquakes with multiple near-source recordings, $I_N(10)$ at different stations will show more dispersion when computed using unfiltered accelerograms than when using filtered ones. Figure 3b, which shows recordings and plots of $I_N(10)$ for first four events in Table 3, contradicts this. It seems that the complexity of the sources, at least of large earthquakes, becomes more important when using filtered traces.

Before we present results of the analysis, we note that the distance between the near-source station, which recorded an event, and CU, Δ_{CU}, varies between 142 and 543 km (Table 3). The three events in the distance range of 142 and 220 km are inslab, normal-faulting earthquakes (H~40 to 60km). Since detection based on S waves for this type of earthquake results in less alert time, it may be more useful to develop an algorithm based on P waves (e.g., Tsuboi et al., 2002; Allen and Kanamori, 2003). In this study, however, we only consider alerts based on S-wave. We reduce computed *Arms* values of all events at a common distance of 275 km by multiplying *Arms* by $(275/\Delta_{CU})$. Δ_{CU} for each station is known. Here we are assuming that the attenuation with distance is reasonably well approximated by $(1/\Delta_{CU})$. As Table 3 shows, the distance between the epicenter and the closest station, Δ_S, varies, as does the depth of the focus. In the present

analysis, we do not apply any correction to reduce the computed *Arms* to a common source-to-station distance. Δ_S is greater than 100 km for events 18, 28, 30, and 35. Although we show these events in the figures, we do not include them in the statistics.

Analysis based on unfiltered accelerograms

Figure 4 shows results from the analysis of unfiltered accelerograms with $t_d=10s$. It includes plots of M versus *Arms(10)*, M versus $\alpha(10)$, $(Amax)_{CU}$ versus *Arms(10)*, and $(Amax)_{CU}$ versus $\alpha(10)$. The figure includes more than one near-source station for the first 7 events in Table 3. As expected, the scatter in M versus *Arms(10)* plot is large: M ranges up to two units of magnitude for a given value of *Arms(10)*. We note that if $Arms(10)\geq 10$ *gal*, then M≥5.9 with two exceptions; however, for several events M≥5.9 even though $Arms(10)<10$ *gal*. Thus, if we were to set a public alert threshold at M≥5.9 and require $Arms(10)\geq 10$ gal to accomplish this, then several events with M≥5.9 would go unreported. We would have to set the threshold at $Arms(10)\geq 1$ gal to include all M≥5.9 events but, in this case, the alert will also be issued for almost all M<5.9 events as well. The value of $\alpha(10)$ is not a reliable discriminator between M≥5.9 and M<5.9 events. For large earthquakes $\alpha(10)$ is expected to be greater than 1. However, for many M≥5.9 events, $\alpha(10)$ is about 1. Quite generally, if $\alpha(10) \geq 1.35$ then M≥6.9. There are, however, two earthquakes for which $\alpha(10)$ is about 1 although M≥6.9. One of these events is the earthquake of 25 April 1989 (event 4, Table 3), which gave rise to $(Amax)_{CU}$ of 17 gal and was very strongly felt in Mexico City. It follows that a reliable estimation of M is not possible from *Arms(10)* and $\alpha(10)$. This partly explains the high failure rate of the SAS.

As discussed before, an estimate of the magnitude is not needed for issuing a seismic alert for Mexico City. We now pursue the more logical approach of directly relating *Arms(10)* from the near-source recording with $(Amax)_{CU}$ and consider alerts based on the expected value of $(Amax)_{CU}$.

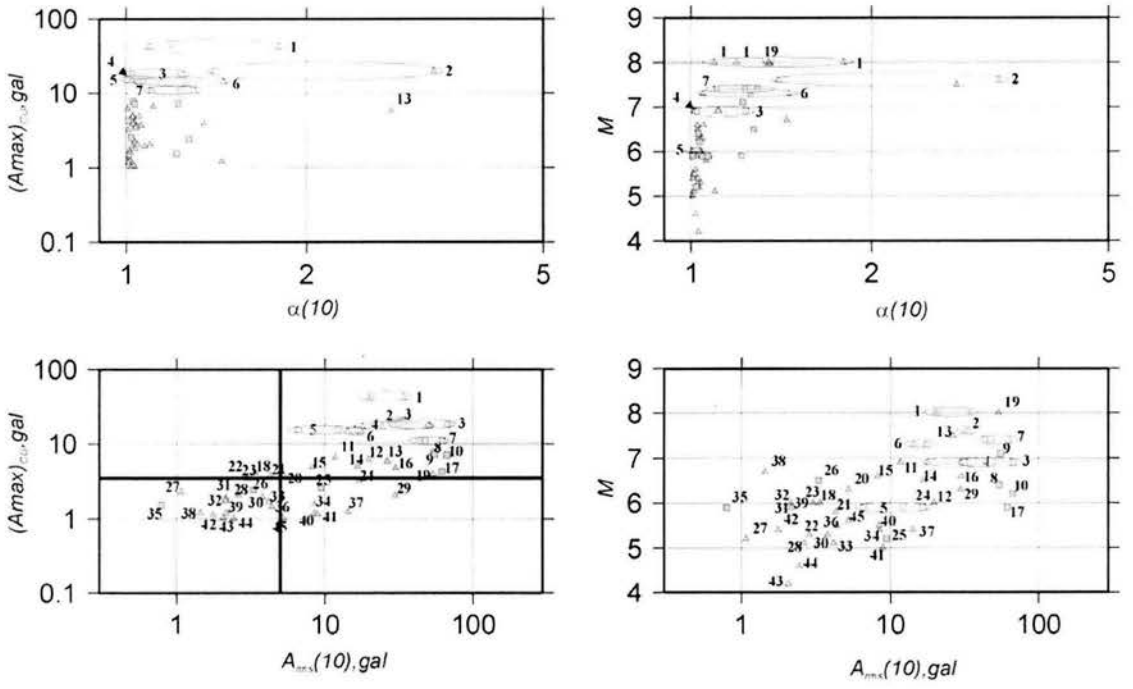

Figure 4. Analysis of unfiltered accelerograms with t_d=10s. Bottom right: M versus Arms(10)*; Top right: M versus* α(10)*; Bottom left:* $(Amax)_{CU}$ *versus* Arms(10)*; Top left:* $(Amax)_{CU}$ *versus* α(10)*. Results from more than one near-source recording are shown for first seven events in Table 3.*
Arms(10) *value is normalized for a station located at 275 km from CU. Triangle: interplate event; rectangle: non-interplate event.*

The relationship between an alert and expected *Amax* at CU is a decision, which needs a thorough public debate. Should an alert be issued only when some damage is expected? Do we need an alert for each earthquake that may be felt by some residents of the lake-bed zone, or only when most persons in the city are likely to feel it? Do we need two levels of alert, as currently implemented by the SAS? We search for a reasonable answer based on Table 3 and $(Amax)_{CU}$ versus *Arms(10)* plot in Figure 4. We first note that events 1 to 7 must qualify for a general alert. Events 1 and 2 devastated the city while events 3 to 7 were very strongly felt and also have caused some damage. Thus any credible alert system must flag these events for general alert. From Table 3 and Figure 4 it follows, then, that a general alert must be issued if *Arms(10)* $\geq$*5.0 gal*. This threshold for *Arms*, however, qualifies for a general alert not only events 1 to 7, but all first 19 events in Table 3 (excluding event 18 which is ignored from the statistics since Δ_s >100

km). We note that for these events the *Amax* at CU was greater than 3.5 gal. Although we do not have the statistics, it is most likely that all of these events were felt by many in the lake-bed zone and by some in the hill-zone of the city. A general alert would also be issued for eight other events that gave rise to smaller *Amax* at CU. These may be considered "false" alerts. No alert would have been issued for two events, however *Amax* at CU during these events was only slightly greater than 3.5 gal. Setting up a lower, second level of alert is very problematic (Figure 4), unless we require that this level of alert be issued if $1.0 \leq Arms(10) < 5.0$ gal corresponding to $1 \leq (Amax)_{CU} < 3.5$ gal. This alert, however, would include all remaining events but one which did not qualify for the general alert.

We think that only one level of alert, a general alert if $Arms(10) \geq 5.0$ *gal*, is the best option. This would include most earthquakes that would be felt by many of the inhabitants of the city. On average, about one alert/year will be issued which should make the system credible to the society. Most importantly, no potentially damaging earthquake would be missed. The fact that some weaker events [$(Amax)_{CU} < 3.5$ gal] will also qualify for general alert is inevitable. Fortunately, this is an error in the preferable, conservative direction.

Analysis based on filtered accelerograms

We now consider the consequences of using band-pass filtered (0.2-1.0 Hz) near-source and CU accelerograms. The results for $t_d = 10s$ are shown in Figure 5. The scatter in plots of M and $(Amax)_{CU}$ *versus* $Arms(10)$ plots is somewhat less than the corresponding plots with unfiltered accelerograms (compare Figures 4 and 5). We now require $Arms\ (10) \geq 1.0$ gal for a general alert. This ensures the alert for events 1 to 7. This threshold on *Arms* flags most events with $(Amax)_{CU} \geq 2.0$ gal. Only three weak events, $(Amax)_{CU} < 2.0$ gal, are also flagged for a general alert and one earthquake (event 23, Figure 5) is missed. It is interesting to note that if $Arms\ (10) \geq 1$ gal then $M \geq 5.9$.

Setting up a lower, second level of alert presents the same difficulty as in the previous case. For reasons mentioned earlier, we prefer just one level of alert: a general alert.

We find that the performance of the alert based on filtered traces is superior to that based on unfiltered traces as it decreases the number of false alerts. Table 4 compares the performance of the proposed general public alert with unfiltered and filtered accelerograms.

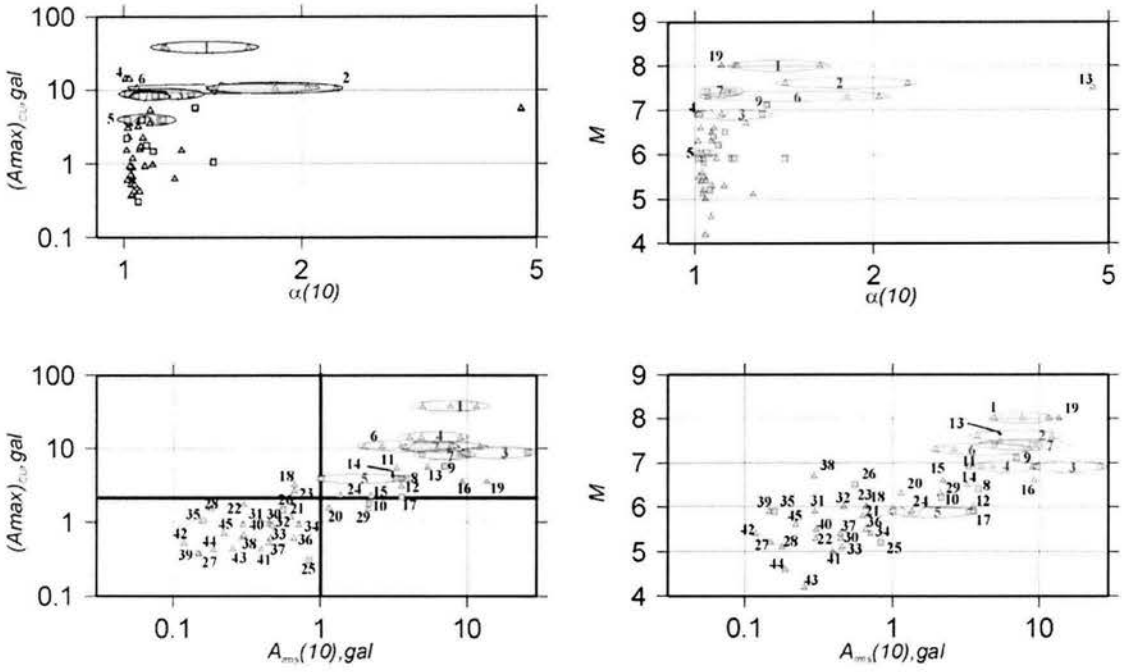

Figure 5. Same as Figure 4 but with band-pass filtered (0.2-1.0 Hz) accelerograms.

Table 4. Performance of proposed public alert for Mexico City for events in Table 3 based on expected $(Amax)_{CU}$ estimated from *Arms* computed from near-source accelerograms.

Accelerograms	t_d	Proposed near-source *Arms*, gal	Expected *Amax at CU*, gal	No. of events to be flagged	Correctly flagged events	Missed events	Excess events
Unfiltered	10s	>5.0	>3.5	21	19	2	8
Filtered (0.2-1 Hz)	10s	>1.0	>2.0	18	17	1	3

Automated Processing of the accelerograms

The results of the previous section were obtained by processing the raw and filtered near-source accelerograms using a window of 10s beginning with the arrival of the S wave. In practice, the detection algorithm will perform continuous analysis of the signal in a sliding window of 10-s duration. If at any time *Arms(10)* equals or exceeds a pre-established threshold (5.0 and 1.0 gal for unfiltered and filtered traces, respectively) at any sensor, and a nearby sensor confirm the occurrence of an earthquake, then the system would issue a general public alert. Let us test this algorithm on the dataset of Table 3.

The results are shown in Figure 6 for unfiltered data. In this figure, the events for which $Arms(10) \geq 5.0$ gal at any time over the duration of the accelerogram are shown by a colored symbol (triangle: interplate events; rectangles: non-interplate events). If *Arms(10)* remains less than 5.0 gal then the symbol is left blank and no alert is flagged. The colors are keyed to the time difference between the beginning of the window and the arrival of the S wave, at the instant the *Arms* threshold is first reached. In the figure, the *Arms(10)* is the maximum value obtained during the processing of the accelerogram. The results are roughly the same shown in Figure 4: a general alert is issued for all first 19 events in Table 3, nine false alerts [$(Amax)_{CU}<3.5$ gal] and two missed alerts [$(Amax)_{CU}>3.5$ gal]. As seen from the color code, for many events a general alert would have been issued for time windows less than 10s after S-wave arrival, thus increasing the available warning time for Mexico City.

The result from processing the filtered data is shown in Figure 7. The *Arms* threshold for a general alert is now set at 1.0 gal. All events with $(Amax)_{CU}>2.0$ gal, but one, are flagged for a general alert and there are three false alerts [$(Amax)_{CU}<2$ gal]. Again, in real-time processing, for many events the alert is flagged in less than 10s after the S-wave arrival.

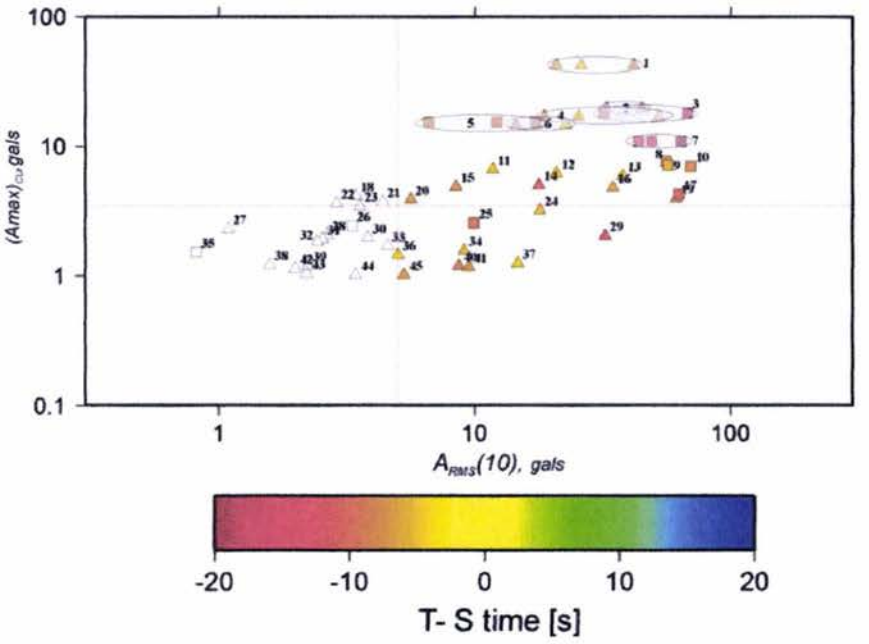

Figure 6. $(Amax)_{CU}$ versus Arms(10) plot obtained by processing accelerograms of events in Table 3 in the same manner as the alert algorithm would operate in the field. Continuous analysis is performed on signal of 10s-long window. When Arms(10)≥5 gal then a general alert is issued (colored symbol) for expected $(Amax)_{CU}$≥3.5 gal. The colors are keyed to the beginning of the window with respect to the arrival of the S wave. If Arms(10) is less than 3.5 gal then the symbol is left blank.

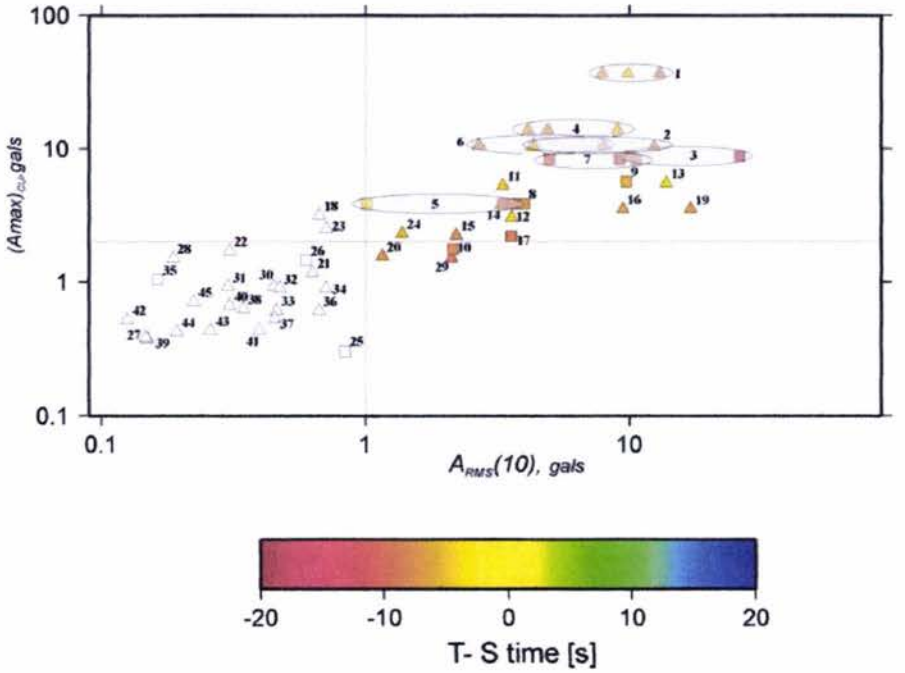

Figure 7. Same as Figure 6 but with band-pass filtered (0.2-1.0 Hz) accelerograms. In this case, a general alert is flagged when Arms(10)≥1 gal. Expected $(Amax)_{CU}$≥1.0 gal.

A possible configuration of an improved SAS array

As mentioned above and shown in Figure 1, the present SAS array consists of 15 accelerometers located ~25 km apart. The array covers a 300 km-long segment of the Guerrero coast, known as the Guerrero seismic gap. The limited areal coverage of the SAS excludes the possibility of issuing alerts for earthquakes, which occur on the adjacent segments of the subduction plate boundary and for inslab earthquakes. In fact, the present coverage of the SAS might not issue an alert if the 1985 Michoacan earthquake were to recur. As Figure 1 shows there are several inslab earthquakes which have given rise to $Amax \geq 5$ gal at CU since 1964. For such events the sensors of the present array will either provide no alert or a lower level of alert.

The deployment of an array consisting of three concentric half rings of radii 275, 335, 395 km centered at CU (Figure 1), with sensors located about 60 km apart in each ring (for a total of 40 sensors for the entire array), could provide an adequate coverage for all coastal and inland earthquakes which may occur at a distance between 245 and 425 km south of Mexico City. For such earthquakes, the location of the nearest station will be less than about 30 km from the epicenter. The depth of the coastal earthquakes ranges between 20km (interplate events) to about 35 km (inslab events). Thus, the hypocentral distance of the closest sensor for coastal events will be less than about 46 km and the S wave will arrive in less than 13s after the origin. If we allow about 10s for on site processing and transmission of relevant parameters to the central station in Mexico City, then the alert can be issued in less than about 23s from the origin. Since the intense S-wave will arrive in Mexico City after about 80 s from the origin, there will be more than 55s of warning time for coastal earthquakes. For inslab events, which occur below the Mexican altiplano at depths of ~50 to 80 km, the alert time will be somewhat less but still more than ~ 45s.

There still remains the problem of inslab earthquakes, which are known to occur as close as 140 km from Mexico City (Iglesias et al., 2002) and crustal events. Useful alerts for such events would require additional, closer, half rings of sensors, and a

detection algorithm based on P waves (e.g., Tsuboi et al., 2002; Allen and Kanamori, 2003). We have ignored such earthquakes in the present study.

Discussion and Conclusions

The challenge facing any seismic alert system (SAS) resides in the estimation of the damaging potential of an earthquake from the analysis of only a few seconds of near-source ground-motion recordings. The daunting task is made simpler for an alert system for Mexico City since the city is located more than about 300 km from the locations where most of the potentially damaging earthquakes occur. This provides reasonable warning time even when the detection in the near-source region is based on S-wave.

The present SAS for Mexico City has been in operation since August 1991. We find two basic flaws with the present seismic alert system (SAS) for Mexico City: (1) The system covers only a part of the region where damaging earthquakes to Mexico City originate (a well-known limitation of the SAS). (2) The algorithm used by the SAS to detect potentially damaging earthquakes from the analysis of the near-source ground-motion recordings is inadequate. As a consequence of these two shortcomings, alert missing rate of SAS is high (Table 1).

In this paper, we have proposed a strategy that differs substantially from that presently implemented by the SAS. It is based on the analysis of near-source recordings of Mexican earthquakes since 1985 and the corresponding ground motions recorded in Mexico City. Our approach differs from that of the SAS in one basic aspect: We relate the near-source ground motion directly to the expected motion in the city, without the intermediate step of estimating the magnitude of the event. In our proposed scheme, the alerts would be based on the relationship between root-mean-acceleration (*Arms*) in the near-source region and the expected *Amax* at a reference site in Mexico City, CU. We test the use of unfiltered and band-pass filtered (0.2-1.0 Hz) accelerograms from near-source region and Mexico City in the analysis. The choice of the filter is based on the fact that

the amplification of seismic waves in the lake-bed zone of the Valley of Mexico occurs in this frequency band. We find that the use of band-pass filtered near-source accelerograms of 10-s duration, beginning with the arrival of S-wave, leads to alerts with a much lower failure rate (Table 4).

The relationship between the level of alert and *Amax* at CU is a decision that needs thorough debate by the society. Should public alert be issued only when some damage is expected in the city? How often should restricted alerts be issued?

We find a single level of alert, a general public alert, as the best option. Our results suggest that this alert should be issued if *Arms* at a near-source station, computed over a 10s-window, exceeds 5.0 gal using the unfiltered signal. For events in Table 3, this threshold flags all events with *Amax* at CU greater than 3.5 gal but two, and gives 9 false alerts (Figure 6). When using the filtered accelerograms, the general public alert should be issued when *Arms* exceeds 1 gal. For the events in Table 3, this threshold flags all events with *Amax* at CU greater than 2.0 gal but one, and gives only 3 false alerts. For this reason, we suggest the use of filtered accelerograms in the alert algorithm. In real-time implementation of the algorithm, the alert for many events will be issued in some seconds after the arrival of S-wave at the station.

To ensure that no important alert to the city is missed and the public credibility in the system is maintained, it is essential to increase the coverage by the SAS. We suggest an array consisting of three concentric half rings of radii 275, 335, 395 km (Figure 1), with sensors located about 60 km apart in each ring (for a total of 40 sensors for the entire array). Such an array could provide an adequate coverage for all coastal and inland earthquakes, which may occur at a distance between 245 and 425 km south of Mexico City. If an alert is desired for crustal and inslab earthquakes that may occur nearer to the city, then an additional closer ring of stations and an algorithm based on P-waves would be required.

Acknowledgements

We express our thanks to Juan Manuel Espinosa and other colleagues at CIRES for many fruitful discussions and for providing us with information. The goal of this research is to make the SAS, a technical achievement without parallel in Mexico and a fruit of years of effort by the personnel of CIRES, as useful as possible. The opinion expressed here may or may not be shared by CIRES and it is entirely the responsibility of the authors. The research was partially funded by CONACyT project 42671-F.

References

Allen. R. M., and H. Kanamori (2003). The potential for earthquake early warning in southern California, *Science* **300**, 786-789.

Anderson, J.G., J.N. Brune, J. Prince, R. Quaas, S. K. Singh, D. Almora, P. Bodin, M. Oñate, R. Vásquez, and J.M. Velasco (1994). The Guerrero accelerograph network, *Geofísica Intern.* **33**, 341-372.

Espinosa-Aranda, J.M., A. Uribe, G. Ibarrola, V. Toledo, and C. Rebollar (1989). Evaluacion de un algoritmo para detectar sismos de subducción, Mem. VIII Congreso Nacional de Ingenieria Sismica y VII Congreso Nacional de Ingenieria Estructural, Acapulco, Mexico, Vol I, A199-A211.

Espinosa-Aranda, J.M., A. Jiménez, G. Ibarrola, F. Alcantar, A. Aguilar, M. Hinostroza, and S. Maldonado (1995). Mexico City seismic alert system, *Seism. Res. Lett.* **66**, 42-53.

Espinosa-Aranda, J.M. and F. H. Rodríguez (2003). The seismic alert system of Mexico City, in International Handbook of Earthquake and Engineering Seismology, Vol. 81B, Academic Press, Chapter 76, 1253-1259.

García D., S.K. Singh, M. Herraíz, J.F. Pacheco and M. Ordaz (2004). Inslab earthquakes of Central Mexico: Q, source spectra, and stress drop. *Bull. Seism. Soc. Am.*, **94**, 3.

Iglesias, A., S.K. Singh, J. Pacheco, J.F. Pacheco, and M. Ordaz (2002). A source and wave propagation study of the Copalillo, Mexico earthquake of July 21, 2000 (Mw=5.9): Implications for seismic hazard in Mexico City from inslab earthquakes, *Bull. Seism. Soc. Am.* **92**, 885-895.

Ordaz, M., S.K. Singh, and A. Arciniega (1994). Bayesian attenuation regressions: and application to Mexico City, *Geophys. J. Intern.* **117**, 335-344.

Singh, S.K., J. Havskov, and L. Astiz (1981). Seismic gaps and recurrence periods of large earthquakes along the Mexican subduction zone, *Bull. Seism. Soc. Am.* **71**, 827-843.

Singh, S.K., E. Mena, R. Castro, and C. Carmona (1987). Empirical prediction of ground motion in Mexico City from coastal earthquakes, *Bull. Seism. Soc. Am.* **77**, 1862-1867.

Singh, S .K., E. Mena y R. Castro (1988a) Some aspects of source characteristics of 19 September 1985 Michoacan Earthquake and ground motion amplification in and near Mexico city from the strong motion data, *Bull. Seism. Soc. Am.* **78**, 451-477.

Singh, S.K., J. Lermo, T. Domínguez, M. Ordaz, J.M. Espinosa, E. Mena y R. Quaas (1988b). A study of relative amplification of seismic waves in the valley of Mexico with respect to a hill zone site (CU), *Earthquake Spectra* **4**, 653-674.

Singh, S. K., E. Mena, R. Castro, and C. Carmona (1988c). Prediction of peak, horizontal ground motion parameters in Mexico city from coastal earthquakes, *Geofisica. Intern.* **27**, 111-129.

Singh, S.K., M. Ordaz, M. Rodríguez, R. Quaas, E. Mena, M. Ottaviani, J.G. Anderson, and D. Almora (1989). Analysis of near-source strong motion recordings along the Mexican subduction zone, *Bull.*
Seism. Soc. Am. **79**, 1697-1717.

Tsuboi, S., M. Saito, and M. Kikuchi (2002). Real-time earthquake warning by using broadband P waveform, *Geophys. Res. Lett.* **29**, 2187-2190.

Conclusiones

Como se ha mencionado reiteradamente, la brecha símica de Guerrero es una de las regiones con mayor potencial sísmico del país por lo que existe un interés constante en los procesos relacionados con esta región. En este contexto, el estudio de cada uno de los eventos que ocurren en la zona o en sus alrededores representa un nuevo aporte para el entendimiento de la sismotectónica regional. Es de suponerse que algunos de los sismos reportados en el pasado contengan errores importantes en su localización, lo que pudo haber acarreado interpretaciones sobre-simplificadas tanto de la situación sismotectónica de la zona, como de la estimación del peligro y riesgo sísmico asociados a ella.

La situación actual de la instrumentación sísmica del país, especialmente en el sur, permite determinar con mayor precisión la localización de los temblores. Aunado a esto, la calidad de los datos actuales posibilita los análisis detallados de la fuente sísmica y de la propagación de las ondas generadas. Los recientes modelos numéricos y una impresionante evolución de las capacidades de cómputo durante los últimos años, son herramientas que contribuyen a un mejor entendimiento de los procesos sísmicos. Con todos estos elementos, hoy en día, se sabe con certeza que la actividad relacionada con la brecha sísmica es compleja ya que abarca una gran variedad de sismos con características muy diferentes.

Por ejemplo, el capítulo 1 muestra el análisis de un sismo intraplaca de fallamiento normal (sismo de Copalillo). Este sismo fue situado dentro de la placa de Cocos subducida; su mecanismo focal indica un régimen extensivo seguramente gobernado por la fuerza que causa la placa al "hundirse" por su propio peso. La inversión cinemática de los desplazamientos sobre el plano de la falla muestra un mejor ajuste para el plano que buza al noreste (ϕ=305°,δ=32°,λ=-80°). Si bien la incertidumbre es grande, la solución para este plano muestra que la ruptura se propagó en dirección del echado de la falla. Esta característica parece ser común a otros sismos de fallamiento normal estudiados anteriormente. Análisis de futuros temblores podrán mostrar sí esta característica persiste en todos ellos y sí está relacionada con fenómenos como el doblamiento de la placa subducida. El temblor de Copalillo parece marcar el límite de la actividad sísmica intraplaca ya que más al norte no hay registro de sismos de este tipo por lo que la placa

subducida pierde su identidad sísmica. Esta observación puede ayudar a restringir los modelos térmicos de la placa.

Por su localización, el sismo de Copalillo representó, también, un buen ejemplo para estudiar las implicaciones que tendría un temblor similar pero de mayor magnitud en el análisis del peligro símico previsto para la Ciudad de México. Este interés proviene de que solo en la década pasada ocurrieron dos temblores de este tipo (15-06-1999, Mw=6.9 y 30-09-1999, Mw=7.4) que causaron daños en ciudades importantes del Altiplano Mexicano.

En el capítulo II se presenta el análisis del sismo de Coyuca (08-10-2001, Mw=5.8) el cual también está asociado a un régimen extensivo pero, su localización y profundidad, lo sitúan dentro de la placa cabalgante de Norteamérica. De manera intuitiva es razonable pensar que encima de la zona acoplada debería dominar un régimen compresional, sin embargo el sismo de Coyuca demuestra que, aún cerca de la costa, el estado de esfuerzos está asociado a un régimen extensional.

El sismo de Coyuca generó una larga secuencia de réplicas y a través de un proceso de relocalización de ellas fue posible delimitar con precisión el plano de la falla.

Otro fenómeno asociado a la "brecha sísmica de Guerrero", son los deslizamientos asísmicos registrados por las estaciones GPS en gran parte del sur del país. Un evento de este tipo es analizado en el capítulo III, donde se muestra que lo más probable es que en este caso, los deslizamientos hayan ocurrido en la interfase entre las placas de Cocos y Norteamérica, justo debajo de la zona acoplada, en una zona denominada de "transición". Estos deslizamientos parecen ser frecuentes, en esta y otras zonas del mundo (P.ej. Cascadia y Japón), sin embargo, aparentemente, en cada región tienen características diferentes.

El capítulo IV muestra el análisis del sismo del 18 de Abril del 2002 (Mw=6.8). Este sismo ocurrió muy cerca de la línea de la trinchera Mesoamericana y presentó una deficiencia de energía a altas frecuencias provocando que las aceleraciones, tanto en la

costa como en el resto de las estaciones que lo registraron, fueran especialmente bajas. Siguiendo un método propuesto anteriormente se clasificó al sismo del 18 de Abril como un "sismo de trinchera". El análisis de otros sismos de la misma naturaleza permitió establecer que los sismos de trinchera, al menos en México, presentan bajas aceleraciones, y por lo tanto, el peligro sísmico asociado es considerablemente menor que para sismos costeros de magnitud similar. Sin embargo, un resultado previo muestra que estos sismos tienen alto potencial tsunamigénico, lo que establece una doble condición: por un lado este tipo de sismos puede no causar daño significativo a las estructuras pero su potencial tsunamigénico representa un peligro para la población que habita en las regiones cercanas a la costa.

Finalmente, en el capítulo V se presenta la evaluación del Sistema de Alerta Sísmica para la Ciudad de México, que desde 1994 opera de manera continua para alertar ante temblores importantes que se generan en la región de la brecha sísmica de Guerrero. En un análisis de las aceleraciones producidas en la ciudad de México por los sismos que causaron algún tipo de disparo en el sistema, se encontró que las alertas son un indicador poco adecuado de la aceleración registrada en el Valle de México.

Analizando registros de aceleración de las diferentes redes sísmicas que operan en el sur del país, fue posible determinar que a través del cálculo de unos segundos de RMS de estos registros, filtrados entre 0.2 y 1 Hz., es posible separar, de manera exitosa, aquellos sismos que provocaron aceleraciones mayores a 2 gales en la estación CUIP localizada en la zona de roca del Valle de México. Estos resultados sugieren que una red de ~40 estaciones, distribuidas en tres semicírculos concéntricos a la Ciudad de México, sería suficiente para alertar ante prácticamente cualquier sismo costero importante así como también ante un buen número de sismos de fallamiento normal que, como se mencionó anteriormente, también representan un peligro para esta ciudad.

En función de los eventos estudiados es razonable pensar que una gran cantidad de fenómenos sísmicos de diferente naturaleza pudieron haber sido ignorados o simplificados en el pasado. Este trabajo representa un pequeño esfuerzo para poner en el mismo papel

diferentes aspectos de la sismicidad asociada a la brecha sísmica de Guerrero. Sin embargo, no se puede dejar de reconocer que la tarea, aún pendiente, de "compilar" todos los trabajos, pasados y futuros, es indispensable para entender de mejor manera el ciclo sísmico y la sismotectónica de la región.

Sin poder extrapolar del todo, es viable pensar que en el resto de regiones sísmicamente activas del país, la sismicidad esté caracterizada por la ocurrencia de temblores de diversa naturaleza, tal como ocurre en la brecha de Guerrero. La única manera de entender mejor los procesos tectónicos que originan dichos temblores así como el riesgo sísmico asociado a ellos, es a través de una mayor instrumentación y esfuerzo científico, tarea, que desde luego, requiere mayores recursos materiales y humanos.

Agradecimientos

Agradezco:

A mi familia por haber puesto en mí su confianza y apoyo

A los doctores Shri Krishna Singh y Javier Pacheco Alvarado
por su amistad,
por haberme empapado de sismología y
por un sin fin de razones más.

A mis maestros y amigos: T. Mikumo, Nicolai S., Vladimir K., Carlos V., Raúl V.,
Luis Q., Bruno H., Juan Martín G.

A Sara Ivonne Franco y a Miguel Santoyo
por su amistad, apoyo
y por compartir juntos la aventura del doctorado

A mis amigos: Daniel G., Bea G., Víctor C., Carlos O., Rocío A., José Luis L.,
Manuel V., Lily P., Ricardo G., Alma T., Carles C., Mario I.,
Marina M., Vlad M., Xyoli P., Aline C., Cyn M., Alan L.,
Israel M., Raúl E., Moisés G.

Al Posgrado en Ciencias de la Tierra de la UNAM, especialmente a Araceli Chamán y a Mónica Salgado por que, con su eficiencia, aligeraron enormemente la carga burocrática.

Se debe mencionar que este trabajo fue posible, en gran medida, gracias al apoyo del Consejo Nacional para la Ciencia y Tecnología (CONACyT), pero sobretodo, gracias al esfuerzo de la Universidad Nacional Autónoma de México (UNAM), debido a que en los momentos en los que el CONACyT decidió dejar de apoyar el proyecto por "detalles" burocráticos, la UNAM lo sostuvo.

Ciudad Universitaria, Ciudad de México, Octubre del 2004

"POR MI RAZA HABLARÁ EL ESPIRITU"